Hindawi
Wireless Communications and Mobile Computing
Volume 2020, Article ID 8881305, 46 pages
https://doi.org/10.1155/2020/8881305

Review Article

Indoor Visible Light Communication: A Tutorial and Survey

Galefang Allycan Mapunda,[1] **Reuben Ramogomana**,[1] **Leatile Marata**,[2] **Bokamoso Basutli**,[1] **Amjad Saeed Khan**,[3] **and Joseph Monamati Chuma**[1]

[1]*Department of Electrical, Computer and Telecommunication Engineering, Botswana International University of Science and Technology, Private Bag, 16 Palapye, Botswana*
[2]*Center for Wireless Communication, University of Oulu, Finland*
[3]*School of Computing, Electronics and Mathematics, Coventry University, CV1 5FB, UK*

Correspondence should be addressed to Bokamoso Basutli; basutlib@biust.ac.bw

Received 11 March 2020; Revised 8 October 2020; Accepted 10 October 2020; Published 11 December 2020

Academic Editor: Daniel G. Reina

With the advancement of solid-state devices for lighting, illumination is on the verge of being completely restructured. This revolution comes with numerous advantages and viable opportunities that can transform the world of wireless communications for the better. Solid-state LEDs are rapidly replacing the contemporary incandescent and fluorescent lamps. In addition to their high energy efficiency, LEDs are desirable for their low heat generation, long lifespan, and their capability to switch on and off at an extremely high rate. The ability of switching between different levels of luminous intensity at such a rate has enabled the inception of a new communication technology referred to as visible light communication (VLC). With this technology, the LED lamps are additionally being used for data transmission. This paper provides a tutorial and a survey of VLC in terms of the design, development, and evaluation techniques as well as current challenges and their envisioned solutions. The focus of this paper is mainly directed towards an indoor setup. An overview of VLC, theory of illumination, system receivers, system architecture, and ongoing developments are provided. We further provide some baseline simulation results to give a technical background on the performance of VLC systems. Moreover, we provide the potential of incorporating VLC techniques in the current and upcoming technologies such as fifth-generation (5G), beyond fifth-generation (B5G) wireless communication trends including sixth-generation (6G), and intelligent reflective surfaces (IRSs) among others.

1. Introduction

Optical wireless communication (OWC) over the past decade has acquired a highly substantial interest. OWC is perceived as both an alternative and an auspicious interdependent communication technique for the conventional radio frequency (RF) technique which has a regulated and licensed electromagnetic spectrum band, spanning from 30 kHz to 300 GHz. Due to an exponential increase in the wireless data traffic and advanced mobile devices, there are calamities that are emerging within the RF band. This increase leads to spectral crisis such as congestion and maximum data rates that are low relative to OWC. Recent developments and standardization of various RF technologies are not able to overcome these looming crisis. Numerous potential RF technologies such as massive multiple-input multiple-output (MIMO), terahertz communication, new antenna designs, reactive impedance surface (RIS), and non-orthogonal multiple access (NOMA) are still inadequate or under investigation. OWC is one candidate technology, which has proven to expand wireless technology capabilities.

OWC spectral band is between 300 GHz and 30 000 THz (wavelength between 1 mm and 10 nm) of the electromagnetic spectrum, covering the infrared (IR), visible light, and ultraviolet (UV) light bands. This being said, OWC systems utilize the free-space optical (FSO) links between the transmitter and the receiver to transmit data. OWC technology has an edge over the RF technology due to various factors. These factors include but are not limited to high energy efficiency, widely spread bandwidth which is free from

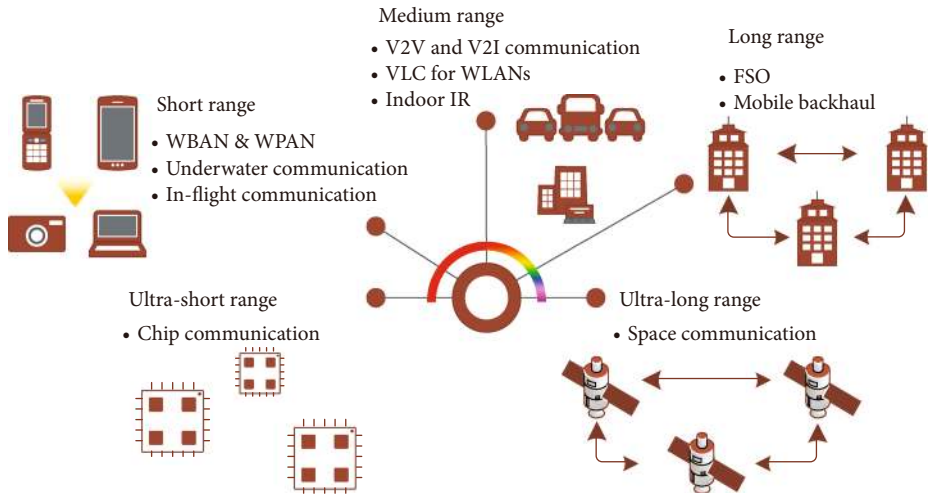

Figure 1: Classes of OWC.

regulation, intrinsic security, and low economical costs. OWC may be classified into five categories based on the scope of communication links [1–3]. A representation of these categories is shown in Figure 1.

The categories are briefly explained by giving examples of OWC applications. In the ultrashort range category (typically about a range of 100 or less), OWC is used for optical communication between and within chips of integrated circuits (ICs). For the short-range category (typically within a distance of about 1 m), OWC is used to create communication links between the ever-present electronic equipment for daily use. The said equipment form the wireless personal area networks (WPANs). Such networks wirelessly interconnect electronic devices that are used around an individual's personal work space. Moreover, the short range is used for the establishment of wireless body area networks (WBANs). WBAN is a network, which continually monitors the health of a patient by means of embedding one or more electronic devices within the body or surface mounting the device at a specific body part. The medium-range category (typically up to 10 km) is concerned with, but not limited to, indoor infrared and communication within the visible light spectrum band which is commonly known as visible light communication (VLC). FSO communication which is also referred to as outdoor intrabuilding links is found as an application of OWC in the long-range category (typically 10). Lastly, the ultralong range category (typically 4500 km to 10 000 km) is concerned with laser communication in space for intersatellite links.

A number of different research outputs on OWC technology has been presented either for integration with existing technologies or for operating purely on OWC technological competence. Tsonev et al. [4] presented the development of light-fidelity (Li-Fi) systems to be incorporated in cellular networks using orthogonal frequency division multiplexing (OFDM). Potential uplink schemes that could be utilized for these systems were also discussed. The basic aspects of VLC and power line communication (PLC) systems were surveyed by Ma et al. [5]. The main objective was to find the possibility of integrating PLC and VLC for indoor communication. PLC is a technology that paves way for the existing power cables to be utilized for sending data. MIMO techniques for the integrated system were also discussed. It is possible to directly modulate the LEDs using the data which is being transmitted by the power-line [6], and this makes VLC fit in very well with PLC. Demers et al. [7], from the networking perspective, presented a paper, which was fixated on FSO. Their work pointed out ways in which an implementation of FSO in cellular networks can be executed in order to elevate the capacity of the network.

In [8], various issues that exist in wireless RF networking technologies were investigated. Studies were done with a perspective on how these issues may be rectified using VLC systems. Furthermore, a discussion on applications, solutions to the existing VLC challenges, and future improvements was presented. Heterogeneous systems, using both VLC and wireless RF, were proposed and implemented by Shao et al. [9]. One system is a hybrid WiFi-VLC network, and the other system is implemented by the parallel aggregation of VLC and WiFi using the Linux operating system bonding technique. For the hybrid network, a VLC channel which is designed only as a unidirectional channel is used as the downlink. To create a complete bidirectional hybrid system, the uplink is established by a WiFi back-channel. The results of this study demonstrated that the hybrid system performs better than the standard WiFi with regards to throughput and the time taken to load web pages for congested areas. One of the promising techniques to address the key challenges in 5G wireless networks, known as optical NOMA (O-NOMA), was presented by Marshoud et al. [10]. A state of the art integration of O-NOMA into VLC networks was overviewed and analyzed in detail. Current challenges and anticipated opportunities to allow the designs and integration of O-NOMA into VLC systems were also provided.

Zafar et al. [11] focused on the dimming techniques that can be designed and realized for VLC systems. These techniques are anticipated to enable energy-saving and pave way for the provision of illumination control. The study presented a motivation behind the need for dimming control mechanisms, current challenges, driver circuitry, current

developments, and the envisioned prospects. A demonstration of a 3×3 imaging MIMO VLC system was presented by Hsu et al. [12]. The authors extended the bandwidth of the LED transmitter using the preequalization technique. With this technique, the power of components of high frequency such as LEDs can be significantly enhanced while attenuating the low frequency [13]. The authors employed the OFDM and bit-loading algorithm [14] for their modulation scheme. Using the proposed system, it was demonstrated that the 1 bandwidth of the phosphor-coated LED is capable of achieving a data rate of 1 Gbps over a transmission distance of 1 in free-space. In [15], the authors outlined and presented a user-centric design of VLC for heterogeneous networks (HetNets). The authors focused on identifying and elaborating a couple of aspects including service provision, system control, and signal coverage quality.

Authors in [16] outlined a framework that presents the viability of using deep-learning (DL) techniques as components for the design of optical communication systems. The authors designed a multicolored VLC system using RGB LED lamps for the realization of multidimensional color modulation as per the outlined color and illumination specifications. The aim of the system is to identify a pair of multicolor modulation transmitter and receiver that yields an efficient symbol recovery performance. An unsupervised DL technique referred to as autoencoder was used to train the recovery process from the receiver to the transmitter. A VLC transmitter-receiver pair and the characterization of the optical channel using the channel layer as well as extra LED intensity control features form part of the recovery process. The transmitter and the receiver are designed together and then optimized. The author's results demonstrated that the designed VLC DL system is better than other proposed techniques with regards to average symbol error probability.

1.1. Related Works. Currently, there is limited substantial literature survey available on OWC. However, there have been several papers detailing the state of the art techniques which have been developed over the past years up to the present day. Some published articles are aimed at pinpointing and solving the predicaments that are associated with the existing techniques whereas some are focused on designing novel approaches in order to fully acquire the full potential of OWC technologies such as VLC.

A thorough and advanced description of VLC is given in one of the most recent surveys [17]. The authors provided an overview of VLC technology that entails the physical attributes, system architecture, predominant applications, and recent research challenges. Besides, current research platforms as well as the predicted advancements of the field are detailed. A survey of OWC which provides an overview and review of VLC, Li-Fi, optical camera communication (OCC), and FSO among others is provided in [18]. This survey looks into crucial technical knowledge for understanding OWC and presents cutting edge standards for classification of OWC systems, system architecture, spectrum use, and OWC applications. The difference between the up-and-coming OWC technologies is also rendered. An all-inclusive study of innovative positioning systems technology based on visible light LED devices was furnished in [19]. A well-rooted discussion of the principal components and conventions of the said systems as well as an elaborate explanation of positioning designs and algorithms is given. Existing LED-based indoor positioning systems were explored, analyzed, and characterized according to their performance with regards to accuracy, test environment, and cost. The study in [19] also presented hybrid indoor positioning systems of VLC and other technologies such as RF and inertial sensor systems. The authors in [19] wrapped up their study by providing a classification of outdoor VLC positioning systems. They concluded by surveying the primary advances, open issues, and research outlook of VLC positioning systems.

Another survey in [20] presented the incorporation of VLC technologies with WiFi technologies towards fifth-generation (5G) technologies. The authors detailed the concepts, technologies, and challenges of the aforesaid incorporation. A thorough survey for indoor VLC has been provided in [21] with a focus on its novel applications of VLC and diverse practical aspects of the system design. These aspects include channel modeling propagation characteristics, and modulation techniques as well as their capability to provide dimming with minimal flicker to avoid degradation of spectral efficiency.

An insight focused on the literature for the development of the VLC physical layer for an indoor setting is given in [22]. A related paper discussed the potential of VLC for 5G systems [23]. The aspects of outdoor VLC in the form of FSO with the main focus on IR are covered in [1]. Diverse elements of FSO for immobile and mobile settings were presented in [24]. These elements included the propagation models and directionality within the context of FSO and a discussion on channel modeling multiplexing, solid-state lighting (SSL) management, noise, dimming techniques, and drivers. The application of VLC for both indoor and outdoor settings was surveyed in [25]. The authors went on further to look into the architecture of VLC systems, bit error rate (BER) performance measurement, light-emitting diode (LED) theory, the development of LEDs luminous efficacy, and the required power for VLC systems.

In this paper, we focus on VLC applications which are in the visible light-frequency band of 385789 (from 780 nm to 380 nm). This band falls within the medium range category of OWC as seen in Figure 1. In particular, this survey is for the design, development, and evaluation of VLC with regard to indoor scenery. This treatise also delves into the potential of integrating VLC with burgeoning wireless technological trends.

1.2. Paper Structure. The remaining part of this article is structured as follows. Section 2 gives an overview of VLC in general, why it is required together with its applications. Section 3 provides a brief theory of illumination, light sources, and photometry fundamentals. A brief background on photodetectors (PDs), photodetection schemes, noise, and optical statistics with regard to them being constituents of VLC system receivers is presented in Section 4. Section 5 provides a discussion of VLC system architecture. Section 6 presents various elements for the structure of an indoor

VLC system. Section 7 gives an overview of the constraints, open challenges, and the current developments of indoor VLC. In Section 8, we investigate the potential of incorporating VLC technology into a number of emergent and future wireless techniques such as 5G, IRSs, and 6G, specifically in sectors where VLC is applicable. Finally, in Section 9, we conclude the article based on the technical findings of the preceding sections.

2. Analysis of VLC

VLC constitutes optical links, which enable visible light sources to be employed for transmission of data using air as the transmission medium. For indoor application, the idea is that the existing illuminating devices are utilized to transmit data using the same energy which is being used for illumination. As stated in Section 1, VLC is considered to be a medium-range communication technique. This is by virtue of propagation distance which is limited by the luminaries which in most cases are white light-emitting diodes (WLEDs).

As of present, there is a swift expansion in the lighting and illumination sector. The developments in this sector have led to the commissioning of solid-state sources operating within the visible range. These sources are gradually phasing out the incandescent sources in many applications and are predicted to become predominant illumination sources [22, 26]. In addition to general illumination using the solid-state sources, a very high data-rate transmission can be achieved. The ability of the optical source's intensity to be modulated at a rapid speed greater than the human eye's response paves way for the provision of a data transmission channel.

2.1. Requirement of VLC. In RF wireless communication systems, the scramble for spectrum is increasing by a very high magnitude yearly [3, 21, 23, 27, 28]. This problem is mainly driven by an exponential increase in communication devices leading to an increase in data traffic. As of Cisco visual networking index for global mobile data traffic prediction [29], in 2016, global mobile data traffic grew at an estimated rate of 63% from 2015. Progressively, in 2017, global mobile data traffic grew at an estimated rate of 71% from 2016 which is 8% greater than that of the previous year. From 2017 to 2022, it is predicted that the global mobile data traffic will grow sevenfold to 77 exabytes per month at a compound annual growth rate (CAGR) of 46% over this forecast period [30].

The major contributors to the growth of the global mobile data traffic are fueled by the growth of various kinds of wireless devices worldwide. Every year, there is an introduction of a significant number of devices with diverse form factors, improved and increased capabilities, and intelligence to the market. Global mobile devices and connections grew from 7.6 billion in 2015 up to 8.0 billion in 2016 [29]. In 2017, global mobile devices grew from 7.9 billion in 2016 to 8.6 billion in 2017 [30]. In [29], it is predicted that there will be 11.6 billion mobile devices and connections by 2021 at a CAGR of 8% globally. On the other hand, a recent forecast in [30] shows that by 2022 there will be 12.3 billion mobile devices and connections globally at a CAGR of 7.5%.

Despite the constant development and standardization of wireless RF technologies, the efforts are falling short in meeting the demand for the limited RF band. This shortfall leads to a bottleneck which deprives meeting the needs such as high data rates and the required capacity. Over several decades, the RF band has been exploited to a point that there is very little potential to exploit further. However, there are various research efforts on RF technological advances that are currently ongoing in order to improve the spectral efficiency. Such technological advances include but not limited to millimeter-wave (mm-Wave) [31–34], massive MIMO [35–40], NOMA [41–43], and network densification [40]. In comparison to OWC, there is extreme power consumption in RF communication systems despite the innovative countermeasures such as low-power ICs. The above complications call for an urgent need for alternate and complementary wireless techniques to be developed and implemented. To resolve the RF impediments, researchers in the field are shifting their focus to new research areas of wireless communication.

One of the solutions that have been proposed with an aim to complement the conventional RF wireless communication systems is to explore other frequency bands in the electromagnetic spectrum, specifically the visible light band. This shift has led to the discovery of a potential and favorable wireless communication technique commonly referred to as VLC [4, 22, 44]. This technique is anticipated to reduce a huge amount of traffic on the conventional wireless RF technology which is heavily congested. A comparison between VLC and RF technologies can be found in [22].

VLC comes with its own pros and cons just like any other existing innovation. Nevertheless, the pros overcome the cons and some of the cons have a possibility of being mitigated. The most predominant drawback of VLC is that an increase in the link distance sharply decreases the maximum achievable data rate as VLC is a noncoherent communication technique. Relative to RF, firstly, VLC is based on part of the spectrum band which is regulatory-free from international and local authorities as the visible light spectrum is under the industrial, scientific, and medical (ISM) band. By this virtue, VLC offers a wireless communication service with an enormous bandwidth capable of transmitting at very high data rates with no requirement for a license. The VLC bandwidth is approximately ten thousand folds that of the entire RF bandwidth.

Secondly, the luminaires used for VLC systems are energy efficient as they use less power despite their high light intensity, and they also come at a very low cost. This makes the VLC systems more economical as they are used for both illumination and data transmission. Thirdly, the VLC systems are much safer compared to RF systems in the sense that there are minimal or no medical health complications caused by visible light. Emissions from RF equipment and devices may be harmful to humans and medical equipment if the radiation power exceeds a particular measure. See [45–49] for more details on the effects of RF radiation on human beings.

In VLC systems, there is no requirement for sophisticated antennas to transmit data from the light source through air. One more factor that makes VLC systems attractive over RF systems is that they have intrinsic security. The control of transmitted data in the physical layer is simple as communication is commonly in line of sight (LoS). This avoids invasion of the communication system by passive eavesdroppers. Moreover, in contrast to RF, visible light is not capable of penetrating solid surfaces such as walls. The incapability of wall penetration enables the creation of small cells to transmit without interference between cell locations (i.e., intercell interference).

VLC technology is at an early stage with merely a small fraction that has been explored. However, there are substantial research efforts that are currently ongoing leading to rapid developments as needed to set forth the deployment of VLC into vast practical applications.

2.2. Applications of VLC. VLC can be applied in many sectors ranging from household level to factory level. It is however worth mentioning that with VLC, the intention is not to supersede the existing technologies. Such technologies include RF mobile networks, RF WLANs, and PowerLANs. Relatively, it is explored as an augmentation of these existing technologies [4, 5, 15, 20, 21, 23, 44, 50, 51]. VLC offers an extra data layer at higher rates in diverse network environments. This presents a provision for an alternate wireless data link in areas where there is no desire, or no possibility, or less sufficiency for wireless radio transmission. Some of the applications where VLC may be a preference over wireless RF include as follows.

2.2.1. Community Sectors. As a consequence of expansive network traffic in various modern-day institutions such as governmental organizations, universities, and firms, the existing networking technologies are being overwhelmed. VLC systems may be used to help reduce the data traffic load from the existing RF and optical fiber technologies. This technique will offer higher data rates in such institutions. The deployment of VLC will be realized without the need for resource-intensive connections such as that of optic fiber. Facilitation of tasks such as monitoring and surveillance will consequently be easy for public safety.

2.2.2. Healthcare Facilities. Radio wave transmission is known to interfere with some health care equipment such as magnetic resonance imaging (MRI) scans and electrocardiograph (ECG) machines. To alleviate this problem of electromagnetic wave interference (EMI), VLC can be utilized to offer data and monitoring services in areas where radio waves are not desirable due to their interference with RF sensitive procedural equipment.

2.2.3. Aviation Sector. Currently, there is demand and desire for the provision of flight safe and high-speed data transmission from passengers and aviation service providers during flight. Some service providers offer aircraft-to-earth data links whereas some provide WiFi solutions that are compatible with flight equipment. These provisions are well-founded and safe. However, they are not economical to implement, and the baud rate per individual user is exceedingly low [52].

The provision of VLC would be an ideal alternative for the aviation industry to provide outstanding wireless data services that are economical. Consequently, this will eliminate or reduce the effects of RF signals that are well known to interfere with the cockpit communication systems. This provision will allow the illuminating WLEDs in flights to provide both reading lights and optical data transmitters with a different approach but with minor similarities as seen in [53]. This provision could also be used for broadcasting using the VLC system as the downlink. The uplink may be modeled using the infrared link to allow passenger connectivity during the flight [52].

2.2.4. Vehicular Communication. In modern-day lives, vehicles have come to be a vital asset to humans. In addition to quality and reliable transportation services, human beings desire more ad hoc features. The most crucial features are in relation to communication and safety. These include in-vehicle internet access, forward collision warning, emergency electronics brake lights, blind-spot warning and lane change warning, control loss warning, intersection movement assist, and do not pass warning [22, 54].

It is envisioned that by 2025, 90% of vehicles being sold will have the capability of communicating with each other and infrastructure [55]. With these demands and developments, it means that vehicles will generate higher data rates thanks to the number of sensors they are equipped with. RF technologies will fall short because of the current impediments. There is a requirement for a large bandwidth and low latency for reliable reach-ability. High-speed VLC technology can be easily adapted because of the ever-present vehicular lights and traffic light infrastructure.

2.2.5. Homeland Security. Quick and flexible reactions in situations of dismay such as unforeseen natural events, terror attacks, and emergencies are essential. In such situations where some RF communication infrastructures may not be dependable as a consequence of damage or attack, VLC may be momentarily deployed to provide secure and rapid data services. This will allow for critical tasks such as safe evacuation and counterattack measures to be carried out in a timely manner despite the malfunction of the conventional infrastructure used for data transmission.

2.2.6. Industrial Factories. Under certain conditions and circumstances, RF transmission may possibly cause explosions in hazardous areas such as petrochemical plants, mines, and explosive devices plants [56, 57]. Thus, it is very imperative that the installation of wireless RF networks be planned and executed with expertise in order to reduce the potential risk. However, it is very rare for instances of ignition to occur [56–58]. RF techniques such as leaky wave antennas have been found to be very useful in spatially constrained environments such as underground mines [59]. Nonetheless, equipment for such technologies require separate deployments. In these areas, factories may find VLC as the most suited form of wireless communication as it will be embedded in the

Figure 2: Evolution of illumination [62].

already existing illuminating infrastructure providing both illumination and high data rate transmission.

VLC technology has already been commercialized by various entities. Acuity Brands (formerly known as ByteLight) offer indoor localization based on VLC technology to some retail stores [60]. Philips Lighting also has a similar system to that of Acuity brands featuring LEDs and smartphones. A system for retail stores developed by Fujitsu which mimics the quick response (QR) code technology features the VLC technology to embed product data for customers to scan the invisible data using their smartphones [61].

3. Light Sources and Illumination

Different types of illumination sources exist. These sources evolved from back in the days when illumination was mainly achieved by the utilization of fire and wax candles. Illumination evolution is shown in Figure 2. The figure depicts the improvements at each stage of the evolution.

Through the years, since the moonlight, fire, and candle era, illumination has substantially developed and we have seen developments that have led to the inception of solid-state LEDs. During the evolution, fluorescent lamps have been used with efforts to replace the most widely used incandescent lamps which consume a lot of energy. Currently, the illumination industry is shifting towards the use of solid-state LED lamps. This is owing to a variety of factors such as higher power conversion efficiency and higher luminous efficacy [63], capability to be components required for the realization of a VLC system due to their durability, safety, size, and flexibility [5, 51], longer mean time to failure (MTTF), and free from dangerous elements like mercury. This is relative to the conventional illumination technologies. In this paper, only a brief theory of light sources, operation of an LED lamp, operation of a photodetector (PD), and selected aspects of photometry are given. All of the above elements and aspects are evaluated with regards to their significance as elements of VLC systems are covered.

3.1. Light Sources. Light sources which are suited for communication systems based on optical technology are adamantly required to possess various and appropriate properties in relation to wavelength, linewidth, numerical aperture, high radiance with a small emitting surface area, long life, high reliability, and a high modulation bandwidth. There exists an assortment of light sources, but the most widely used sources for optical communication systems are LEDs and laser diodes (LDs). Both the LEDs and LDs depend on the semiconductor material's ability to be electronically excited in order to radiate light [64]. Relative to the incandescent sources, during optical radiation, the LEDs and LDs do not exhibit thermal radiation because of the low temperatures of the semiconductor materials. Furthermore, LEDs and LD light sources come in smaller sizes with low forward voltage, low drive current, and higher brightness which is within the visible wavelengths, and light can be emitted at one wavelength or variable wavelengths. Different applications and their features including but not limited to optical power versus current attributes, speed, and the beam profile dictate the choice of the appropriate source.

The light emitted by the LEDs and LD light sources can be outspread in a range of various wavelengths depending on how it was fabricated. The said ranges are from the IR to the visible sections of the electromagnetic spectrum. Human eyes are only capable of visualizing the light with a wavelength from 780 nm to 380 nm. In OWC, all of the aforementioned wavelengths are of high interest and very significant as they pave way for the design and implementation of various systems of optical technology. The emission of light, generally, is caused by electrons, which are transitioning from an excited state to a lower energy state. The transition of an electron creates an energy difference, and this brings about a radiative or a nonradiative process. The latter leads to the production of heat, whereas the former leads to the production of light hence optical sources. With regards to light conventional sources, the photon flux is provided by means of the recombination of the carrier. As for solid-state sources, there are three distinguishable ways in which the photon interrelate with an electron and these are as follows [64]; the first way is whereby the electron in a filled valence band attains the energy transferred by the photon. The electron then transits to the conduction band which is an empty state. The solar cell is fundamentally associated with this kind of photon-electron interaction. One other way is that from a filled conduction band, an electron can spontaneously go back to the valence band which is an empty state and this releases a photon during this process of recombination. This is termed radiative recombination (see Figure 3), and it is the process associated with the light produced by LEDs. The third way is an instance whereby a photon can be used to invigorate the radiative recombination process. The incident photon makes the emission of a second photon with the same

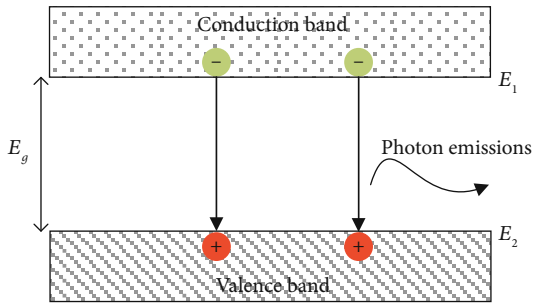

FIGURE 3: Spontaneous radiative recombination.

phase as the incident photon, i.e., the photons are coherent. The fundamental functioning of a laser is based on this type of photon interaction.

For radiative recombination, it is conventionally assumed that the emitted photon has the same energy as the band-gap energy of the material. Nevertheless, the additional thermal energy due to temperatures beyond the absolute zero makes the electrons in the conduction band to reside just above the band edge and the holes in the valence band to reside just below the band edge. This phenomena lead to the photon energy level that is a bit higher than the band-gap energy. The generated photon's frequency and wavelength are related to the energy level E which is given as

$$E = E_2 - E_1 = hf = \frac{hc}{\lambda}, \tag{1}$$

where, E_2 and E_1 are the two energetic states, $h = 6.626 \times 10^{-34}$ J s is the Planck's constant, $c = 3 \times 10^8$ m/s is the speed of light, and λ is the wavelength of the emitted or absorbed energy.

3.1.1. Light-Emitting Diode. A solid-state device comprising of a semiconductor, directly capable of converting electrical energy into light energy, is referred to as an LED. The said conversion is made possible by the radioactive recombination process as illustrated in Figure 3. Depending on the energy of the band-gap of the semiconductor material, the light emission could fall in the UV, visible, or IR part of the electromagnetic spectrum. The semiconductor chip is the main component of an LED under the condition that the chip forms a p-n junction. The p-n junction is formed by adding impurities to the intrinsic semiconducting chip. Applying the voltage in such a way that the LED is forward biased makes the free electrons and holes to flow back and forth across the junction. As they move across the junction, the free electrons combine with the free holes. As the electrons recombine with the holes in the valence band, they result in energy bursts which are released as photons; this is referred to as spontaneous radiative recombination. Human eyes perceive the emitted photons as visible light; this phenomenon is referred to as electroluminescence [65].

The energy of the released photon is equivalent to the energy that results as the difference of energy levels between the conduction and valence bands, i.e., the band-gap energy.

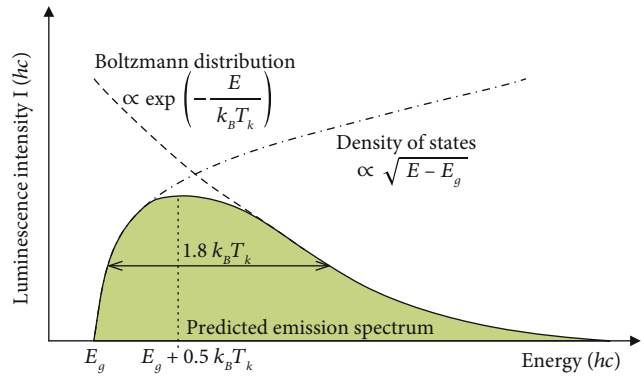

FIGURE 4: Photon emission spectrum.

The rate at which photons are emitted together with its wavelength is given by equations (2) and (3) [64], respectively.

$$I(E = h\nu) \propto \sqrt{E - E_g}\ \exp\left(-\frac{E}{k_B T_k}\right), \tag{2}$$

$$\lambda = \frac{hc}{E(eV)}\mu\text{m}, \tag{3}$$

where, E_g is the band-gap energy, ν is the radiation frequency, k_B is the Boltzmann's constant, and T_k is the absolute temperature in kelvins (K).

As depicted in Figure 4, for the photons to be emitted, the energy should be at least equal to the band-gap energy with a half-power width of $1.8 k_B T_k$. The wavelength spectra width of the half-power width is given by [64].

$$\Delta\lambda = \frac{1.8 k_B T_k}{hc}. \tag{4}$$

The spectral width $(\Delta\lambda)$ is wide as a result of electron transition from numerous levels of conduction and valance bands. The transition and the resulting photon emission occur randomly without a mutual phase relationship between the radiated photons. This consequently leads to what is commonly known as an incoherent light source [3, 64]. Typical LEDs operating at wavelengths of 850 nm and 1300 nm have $\Delta\lambda$ of approximately 60 and 170, respectively [64]. Higher temperatures cause a decline in the band-gap energy. Since the photon energy emission is directly proportional to the band-gap energy, it means that an increase in temperature decreases the peak photon energy.

There are different types of LEDs; each type has distinct characteristics that make it suited for a specific application. Different LEDs, their properties, and applications are summarized in Table 1. This survey will only cover a brief discussion of the phosphor-converted LED (PC-LED) and multichip LED (RGB LED) types. For the realization of VLC transmitters, RGB LEDs and PC-LEDs are the most preferable candidates to be utilized as luminaires for both illumination and data transmission for VLC systems since they are capable of producing white light.

Table 1: Characteristics of LED types.

	Intricacy	Efficacy	Bandwidth	Cost	Application
RGB LED	Moderate	65 lm/W	10-20 MHz	High	Illumination
PC-LED	Low	130 lm/W	5-3 MHz	Low	Illumination
OLED	High	45 lm/W	≤1 MHz	Lowest	Display
μ-LED	Highest	—	≥300 MHz	High	Biosensors

PC-LEDs are made up of a blue Indium Gallium Nitride chip. Illuminating this chip produces Yttrium Aluminum Garnet phosphor coating. Part of the blue light is converted into a yellow segment of the spectrum by the phosphor layer coating. Appropriately mixing the remaining blue light and yellow light produces white light. The color temperatures being neutral white, cool white, and warm white are dependent on the thickness of the phosphor layer.

On the other hand, RGB LEDs conventionally consist of three or more LED chips which typically emit the red, green, and blue light. White light is produced when the wavelengths of the three individual chips are selected and mixed properly. The suitable wavelengths for white light production are 625 nm for red, 525 nm for green, and 470 nm for blue.

By reason of a simplified implementation and cost-effectiveness of PC-LEDs, in contrast to RGB LEDs, they are the most preferred type for producing white light. Nonetheless, they have a low response time due to the phosphor coating leading to a provision for the narrow bandwidth only. This poses a limitation for communication as this will negatively affect the modulation speed. This makes RGB LED more suitable for communication because of their ability to provide data modulation through three different color wavelengths. This property of having more than one wavelength leads to a total throughput three times higher than that of a single-chip LED. This is achieved through wavelength division multiplexing (WDM) using color shift keying (CSK) and metameric modulation (MM) schemes. The use of CSK intrinsically forms a color space MIMO (CMIMO). In [66, 67], data rates of 1.2 Gbps and 3.4 Gbps using RGB LEDs were achieved, respectively. For both of the abovementioned achievements, all the three channels of the RGB LED were utilized. Both experiments were carried out using the acceptable illumination intensities for the human eye as the LED is used for both illumination and communication.

WLED luminaires used for illumination are lighting units, which are mainly made up of housing, ballast, and an LED lamp which may have single or more LEDs. Additionally, there is a driver circuit used to alter the brightness intensity by controlling the current that flows through the LED. Normally, for VLC communication, an amendment of the driver circuitry is required so as to allow for modulation of data using the light being emitted [21].

3.2. Radiometry and Photometry. Radiometry is concerned with the measurement of optical radiation for a wider optical spectrum from UV to IF. On the contrary, photometry involves the examination of optical radiation which is only visible to the human eye as opposed to radiometry which does not consider the human eye's sensitivity. The parameters of photometry only look into and evaluate the alterations for various wavelengths of the visible light band [68]. Stereotypical parameters of radiometry include radiant power flux, irradiance, radiant intensity, and radiance. VLC is a wireless communication technology that relies on the conversion of light energy into electricity; therefore, it is a necessity to convert between radiometric and photometric parameters. This conversion takes into consideration the relative visibility of light for a specific wavelength. The relative visibility of light is given by the eye sensitivity curve which is interchangeable with the luminous efficiency curve [3]. This curve represents the ratio of all photometric parameters to their equivalent radiometric parameters. The correlation between photometric and radiometric parameters is given by

$$[1\text{lx}] = [1\text{W}] \times 683 \left(\frac{\text{lm}}{\text{W}}\right) \times V(\lambda), \tag{5}$$

where V is the relative spectral sensitivity function at wavelength λ. Typical aspects of photometry to be understood with regard to VLC systems are luminous flux, luminous intensity, illuminance, and luminance; each of these aspects is briefly described as follows.

3.2.1. Luminous Flux. The total quantitative amount of power emitted per second from an optical source and within the visual sensation of the human eye is referred to as luminous flux. SI unit for luminous flux is lumen (lm) or candela steradian $(cd{\bullet}sr)$. In general terms, luminous flux may mathematically be given as

$$\Phi_v = I_v \cdot \Omega, \tag{6}$$

where I_v is the light intensity in candela, and Ω is the angular span (in steradian) over which the light is emitted. With respect to isotropic sources, equation (6) may be rewritten as to yield

$$\Phi_v = 4\pi I_v. \tag{7}$$

The sensitivity of human eyes due to various visible light wavelengths changes notably when adjusting the luminous flux. The spectral sensitivity function depicts that the human eye is capable of comprehending colors due to variations of wavelengths between 780 nm to 380 nm. The human eye has a maximum sensitivity of 683 l m/W at 555 nm wavelength which is the yellow-green region of the visible light spectrum.

For sources that emit light through various wavelengths over the visible light spectrum, the luminous flux may be

obtained using equation (8). Integrating the radiant flux Φ_e in all directions gives the total optical power which is expressed by equation (9).

$$\Phi_v = k_m \int_{380\text{nm}}^{780\text{nm}} \Phi_e(\lambda) \cdot V(\lambda)\, \mathrm{d}\lambda, \tag{8}$$

where constant $k_m \approx 683\,\text{lm/W}$ at a wavelength of 555 nm, and Φ_e is the radiant flux at wavelength λ.

$$P_t = k_m \int_{\Lambda_{\min}}^{\Lambda_{\max}} \int_0^{2\pi} \Phi_e \, \mathrm{d}\theta \mathrm{d}\lambda, \tag{9}$$

where $\Lambda_{\max}$ and $\Lambda_{\min}$ are obtained from the sensitivity curve of the photodiode.

3.2.2. Luminous Intensity. The intensity of the power radiated per unit time from an optical source is known as luminous intensity. In simpler terms, it is the luminous flux per solid angle in a given direction. The units are lm/sr or as commonly known candela (cd). The intensity may be given as [69, 70].

$$I = \frac{\mathrm{d}\Phi_v}{d\Omega} = \frac{\mathrm{d}\left(k_m \int \Phi_e(\lambda) \cdot V(\lambda) \mathrm{d}\lambda\right)}{d\Omega}. \tag{10}$$

3.2.3. Illuminance. The amount of irradiance on a given surface, i.e., the luminous flux per unit area, is referred to as illuminance. Illuminance is measured in lm/m^2 or lx [69, 70], hence, given by

$$E_v = \frac{\mathrm{d}\Phi_v}{\mathrm{d}S} = \frac{\mathrm{d}\left(k_m \int \Phi_e(\lambda) \cdot V(\lambda)\, \mathrm{d}\lambda\right)}{\mathrm{d}S}, \tag{11}$$

where $\mathrm{d}S$ is the illuminated area. In an instance where the illuminated area is large, the illuminance is simply the ratio of the luminous flux to the total area S.

3.2.4. Luminance. The amount of radiance on a given surface area and a given solid angle in a given direction, i.e., the luminous flux per unit area per unit solid angle, is referred to as luminance. Luminance is measured in $\text{lm/m}^2 sr$ or cd/m^2. Luminance may therefore be expressed as the following equation [69, 70].

$$E_v = \frac{\mathrm{d}\Phi_v}{dSd\Omega} = \frac{\mathrm{d}\left(k_m \int \Phi_e(\lambda) \cdot V(\lambda)\, \mathrm{d}\lambda\right)}{\cos(\theta_s) dSd\Omega}. \tag{12}$$

Of all the three parameters that are based on the flux intensity, this is the most significant one. This is on account of the fact that the light energy is radiated from an extended source instead of a point source. Moreover, it is the only parameter, which is conserved during the propagation of light [70].

3.3. Lambert Radiator. An estimation of power transfer for a radiant source having a uniform radiance across its surface and uniformly emitting in an isotropic manner is very useful in optics. Such a source is said to be a Lambertian source [70, 71]. Ideally, a Lambertian source conforms to Lambert's cosine law. The law states that the luminous intensity viewed from an ideal diffuse radiator varies directly with the cosine of the angle between the surface normal and the incident light ray [3, 72]. This is graphically depicted in Figure 5 and mathematically represented by equation (13). Lambert's law is of significance in the measurement of light. In order to obtain worthwhile radiance measurements of an object that has a large or uncertain angular distribution, cosine receptors on detectors are a requirement. As a consequence, a commonly used model for radiance estimation is the Lambert radiator [73]. Take luminous intensity with an arbitrary direction of a Lambertian radiator to be denoted as

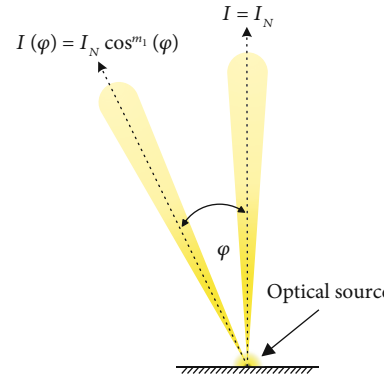

Figure 5: Lambert radiator.

$$I(\varphi) = I_{\text{N}} \cos^{m_1}(\varphi) = I_N k_d \cos^{m_1}(\varphi) = I_N k_d \left(\vec{N} \cdot \vec{L}\right), \tag{13}$$

where, φ is the angle between the surface normal and the incident light ray, I_N is the intensity of the light source in the normal direction, m_1 is the order of Lambertian emission, k_d is the diffuse reflection coefficient, $\vec{N}$ is the unit normal vector, and $\vec{L}$ is the unit light vector.

The luminance of such a radiator is independent from the orientation angle φ despite different levels of the luminous intensity at different viewpoints. Therefore, with this condition, the luminance from any point of view is equal.

VLC light sources (WLEDs) can be estimated using the Lambert radiator. The spatial distribution of LEDs is similar to a Lambert radiator. The International Commission on Illumination (CIE) states that different levels of illuminations are required depending on the type of environment. Typically, any level from 30 lx to 100 lx is adequate for visualization tasks in public places. As for residential and corporate places, a wider range with higher levels, ideally from 300 lx to 1000 lx, is indispensable. Figure 6 depicts the illumination distribution of an LED with a 30 semiangle.

4. Light Detection

One other element which is of significance to the realization of VLC systems is photodetection. Light detection is normally achieved by the use of photodetectors (PDs), which are also known as nonimaging receivers. A PD is a square-

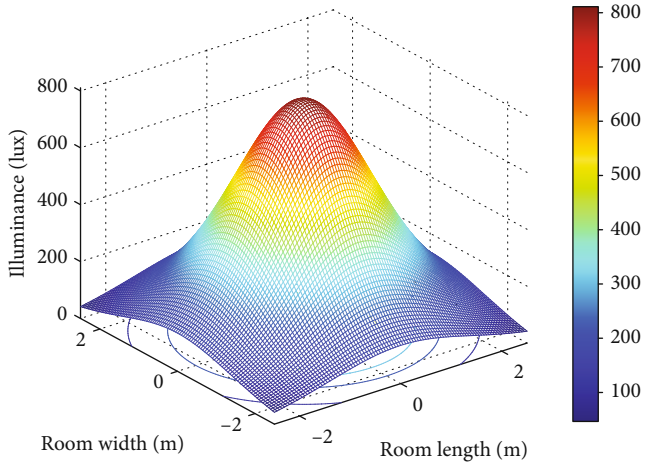

FIGURE 6: Spatial illumination distribution.

law optoelectronic transducer sensor that detects and responds to electromagnetic radiation (EMR), specifically light, which is incident to its surface. They respond to the impinging EMR signals by converting the light photons into current which is proportional to the square of the received radiation. Alternatively, photodetection can be done by the utilization of imaging sensors also referred to as camera sensors. An imaging sensor is a matrix of multiple PDs. Such sensors are found in many of the existing mobile devices including smartphones. This makes it possible for the mobile devices with imaging sensors to be easily converted and used as VLC receivers. The need for the conversion is motivated by a very high number of PDs which facilitates high-resolution imaging. Having numerous PDs notably decrease the rate at which frames are being captured by the sensor. This reduction consequently leads to the allocation of limited data rates in the range of merely a few kpbs for VLC signals due to low sampling rates of the sensor. In contrast to imaging sensors, detached nonimaging sensors are able to offer a provision of higher data rates in the range of hundred mbps. For this write-up, we will only cover the theory of PDs as VLC receivers.

In an optical communication channel, the PD must have precise and uncompromising performance requirements because the received optical signal is conventionally weak. The said performance requirements include a sufficient bandwidth to satisfy the desired data transfer rate, a very low noise level, and a very high sensitivity in the range of wavelengths that the PD operates within. Similar to the LEDs, the effects of temperature variations of the PDs must be very little, and the device must have a long MTTF. The composition of the detector's material determines the operational wavelengths at which the PD responds to light.

The quantum efficiency η_{qe}, which is defined as the ratio of electron-hole (e-h) pairs produced by the PD to the incident photons within a stipulated time, is given by [74].

$$\eta_{qe} = \frac{\text{electrons out}}{\text{photons out}} = (1 - R)\xi\left(1 - e^{\alpha d}\right), \qquad (14)$$

where R is the reflection coefficient at the interface of air and the semiconductor, ξ is the fraction of the e-h pairs, α is the absorption coefficient, and d is the distance between the transmitter and the receiver.

The most critical compatibility and performance requirements for detectors have a number of properties in which they are defined. Firstly, a large surface area to allow for a wider detection field of view (FOV) and a large collection aperture is required. In applications which require high-speed, it is more appropriate and best to have PD arrays that bear a small surface area. Secondly, the PD's sensitivity and responsivity at the desired wavelength must be high. One other property is that the PD must have a low noise which in turn yields a high SNR. Lastly, the PD must have a fast response time as well as high reliability, small size, and low cost. Performance characteristics for various PDs are given in Table 2 as adapted from [3].

4.1. Types of Photodetectors. The most common types of PDs which are used for optical receivers are the avalanche PD (APD) and positive-intrinsic-negative (PIN) PD (without internal gain), photoconductors, and metal-semiconductor-metal PD. Due to their properties, PIN and APD PDs meet all of the aforesaid requirements, hence, them being popularly and widely used for VLC system receivers.

4.1.1. PIN Photodetector. A PIN PD is made up of two semiconductor materials with p-type and n-type regions which are detached by an intrinsic region which is sparingly n -doped. For it to operate, an adequately large reverse bias voltage is applied across the device. The schematic is depicted in Figure 7. For the conversion of an impinging photon into an electric current, the energy of the incident photon has to be equal to or greater than the band-gap energy. An electron from the valance band is excited by the energy of the incident photon to the conduction band; during this excitation process, an electron-hole pair is generated. Concentration of impinging light is under conventional conditions directed to the depleted intrinsic region. After the separation of the generated charge carriers because of the high electric field in the depleted region, the charges accumulate across the reverse-biased junction. In turn, this process leads to the flow of current along the load resistor as shown in Figure 7. There is a single electron flow for each of the generated carrier pair.

The upper cut-off wavelength, which is determined by the type of semiconductor material used, may generally be computed by equation (3). PIN PDs have the capability of functioning at extremely high bit rates over 100 Gbps [75–81]. Nevertheless, in view of the constraints posed by the packaging, the PD-based devices that are available in the market only have a bandwidth not exceeding 20 GHz.

4.1.2. APD Photodetector. The APD differs with the PIN PD in the sense that the APD inherently supplies current gain using repeated electron ionization process. This leads to an elevated sensitivity of the device because of photocurrent multiplication prior to its encounter with the thermal noise of the receiver circuitry. The gain factor of the APD which

Table 2: Performance characteristics (typical) for various PDs.

Parameter	Silicon		Germanium		InGaAs	
	PIN	APD	PIN	APD	PIN	APD
Wavelength range [nm]	400-1100		800-1800		900-1700	
Peak [nm]	900	830	1550	1300	1550	1550
Responsivity $\mathscr{R}$[A/W]	0.6	77-130	0.65-0.7	3-28	0.75-0.97	
Quantum efficiency [%]	65-90	77	50-55	55-75	60-70	60-70
Gain	1	150-250	1	5-40	1	10-3
Excess noise factor	—	0.3-0.5	—	0.95-1	—	0.7
Bias voltage [−V]	45-100	220	6-10	20-35	5	30
Dark current [nA]	1-10	0.1-1.0	50-500	10-500	1-20	1-5
Capacitance [pF]	1.2-3	1.3-2	2-5	2-5	0.5-2	0.5
Rise time [ns]	0.5-1	0.1-2	0.1-0.5	0.5-0.8	0.06-0.5	0.1-0.5

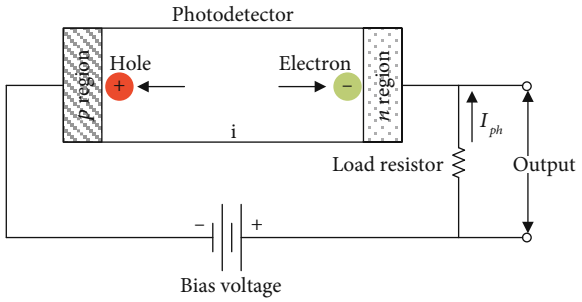

Figure 7: Schematic diagram for the PIN PD.

has an impact on the responsivity of the APD is therefore given by

$$M = \frac{I_T}{I_{ph}} = \frac{I_T hc}{\lambda \eta_{qe} q P_r} = \frac{I_T}{\mathscr{R} P_r}, \tag{15}$$

where I_T is the total output photocurrent (average) in the APD, I_{ph} is the primary photocurrent (unmiltiplied), q is the electronic charge, $\mathscr{R}$ is the PD's responsivity, and P_r is the impinging average power of the optical radiation, per time period.

Note that the value of I_{ph} is equal to that of I_T in an instance where M is unity and λ is measured in. Responsivity, $\mathscr{R}$ is given by

$$\mathscr{R} = \frac{\lambda q \eta_{qe}}{hc} = \frac{\lambda \eta_{qe}}{1.24}. \tag{16}$$

The APD's responsivity value can be higher than unity as the standard gain values are between 50 and 300. This means that the sensitivity of the APD is greater than that of the PIN PD since the PIN PD has a gain value of unity. However, it is worth mentioning that there is an omnipresent multiplication noise when it comes to the APD following the ionization process which is of a statistical nature [82]. In addition, the ionization process is highly sensitive to temperature. When an APD is used in a VLC system, it is advisable to take into account these factors as they are very significant to the performance of the system.

4.2. Intensity Modulation/Direct Detection. The process of photodetection is very crucial in OWC systems. It is used to transform an optically radiating signal which is carrying information into a corresponding electrical signal. Prior to transmission, the signal carrying information is encoded on the radiation intensity or the frequency of the optical source. On the front end of the receiver, after the encoded signal has been sent via free-space or optical fiber, the front-end equipment focuses the filtered signal (radiation) on the surface of the PD. There are several popularly known detection schemes, but the most widely used schemes in OWC are intensity modulation (IM)/direct detection (DD) and coherent detection with IM/DD being the prevalent scheme thanks to its simplicity.

In instances where a system uses IM/DD, there is only one method in which the information can be relayed from one node to the other. The said method involves the use of the radiated emissions from the light source. A local oscillator is not required for a direct detection scheme since it does not contribute to any of the processes during detection. When employing direct detection to retrieve the encoded information, it is imperative for the transmitted information to have certain attributes. These attributes associate the data with the transmitted field's intensity variations. A receiver based on DD is depicted in Figure 8. The instantaneous current of the PD, $i(t)$ for an instantaneous power $P(t)$, is defined by

$$i(t) = \frac{\eta_{qe} q \lambda M P(t)}{hc}. \tag{17}$$

4.3. Photodetection Noise. Like any other communication systems, noise source identification at the front-end of the receiver is crucial. The performance of an OWC channel is influenced by noise sources together with the frequency and distortions induced on the link. In OWC, the noise from the electronic equipment of the receiver and the shot noise

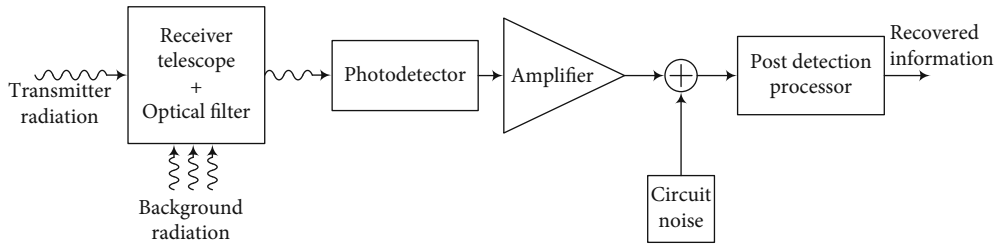

Figure 8: Direct detection receiver block diagram.

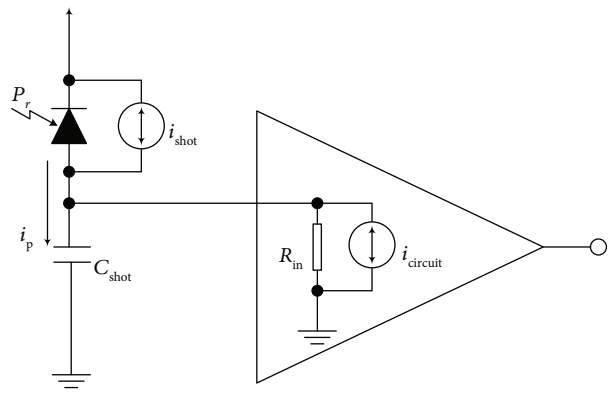

Figure 9: Diagram of an optical receiver front-end with a PD and noise sources.

induced on the received photocurrent are the most predominant noise sources at the receiver input. Depicted in Figure 9 is the diagram of the optical receiver front-end. This front-end is normally made up of a preamplifier for amplification of the electrical current produced in the PD. There exists three classes of amplifiers used for optical receivers, and they are transimpedance amplifier (TIA), low impedance amplifier, and high impedance amplifier. Speed and sensitivity are the two factors that determine the design of the front-end on account of the balance required between these two factors [83]. In the event that a high impedance amplifier is utilized, there is a great reduction of thermal noise, thus, enhancing the sensitivity, but this also reduces the bandwidth. Low bandwidth on high impedance front-end can be mitigated by the use of an equalizer. Low impedance front-end is not a practical technique for VLC systems due to the prevalence of the thermal noise. A balance between a desirable bandwidth and sensitivity is available for systems with a front-end that employs TIAs. The design of VLC systems using TIAs has been on the rise for the past few years, and some of the works on TIA can be found in [84–86].

The main source of noise in OWC channels is the photogenerated shot noise which is radically caused by the PD's discontinuous energy and charge. The resistive component of the front-end produces thermal noise. This noise is not dependent on the received signal, and it has a normal (Gaussian) distribution. Different types of noise sources in OWC are discussed as follows.

4.3.1. Photon Fluctuation Noise. For a coherent light source, the aggregate of the radiated photons is never constant for a given time. This is caused by the discrete nature of light impinging the receiver. Thus, the performance of an ideal PD is affected by nothing besides the noise. With regard to optical sources that produce continuous power, the number of actual photons produced per unit time has a Poisson distribution despite the source producing a constant mean number of photons per unit time. This phenomena lead to quantum noise which is also termed as photon noise. This type of noise is prevalent in every photon detector. Quantum noise is a shot noise with variance given by equations (18) and (19) for the PIN PD and APD, respectively.

$$\sigma^2_{q-\mathrm{PIN}} = 2q\langle i\rangle B, \tag{18}$$

$$\sigma^2_{q-\mathrm{APD}} = 2q\langle i\rangle BFM^2, \tag{19}$$

where $\langle i\rangle$ is the average current over an instance of time, B is the bandwidth (in Hz) of the filter that follows the PD, and F is the excess noise factor.

The shot noise generated by both the incoming optical signal and the OLO with reference to a coherent receiver is, respectively, given by where B_c is the bandwidth of the coherent receiver.

4.3.2. Dark and Leakage Current Noise. There is always a small amount of current at the output of the PD even when there is no incident light. This current is termed as dark current, and it conventionally bears no valuable data. Dark current is a composite current made up of the bulk and surface leakage currents. It is generated by the movement of electrons into the conduction band from the valence band. Dark current goes hand in hand with the energy band-gap of the material used to manufacture the PD. Materials which possess a large band-gap exhibit values which are tremendously low for the dark current. Conversely, materials with a small

band-gap may be significant when the device operates in ambient temperature. The variance of the surface leakage current noise and that of the bulk dark current noise are, respectively, expressed as

$$\sigma_{DS}^2 = 2qI_L B, \tag{20}$$

$$\sigma_{DB}^2 = 2qI_D M^2 B, \tag{21}$$

where I_D is the detector's dark current, and I_L is the detector's leakage current.

4.3.3. Johnson Noise. All conducting materials are susceptible to thermal noise which is also referred to as Johnson noise. This type of noise is caused by the thermal instability of the electrons in the receiver circuitry. The load resistance (R_L) and temperature (T_e), in Kelvin of the PD, contribute to thermal noise. Thermal noise has a Gaussian distribution; normally, it is assumed to have a zero mean. IM/DD and coherent receiver's variances are, respectively, defined by

$$\sigma_{\mathrm{TH}}^2 = \frac{4k_B T_e B}{R_L}, \tag{22}$$

4.3.4. Intensity Noise. The variations of the optical signal's amplitude in turn cause the intensity noise. Relative intensity noise (RIN) is normally used to express intensity noise, and it is given by

$$\sigma_{\mathrm{IN-DD}}^2 = \eta_{\mathrm{RIN}} (\mathscr{R} M \mathrm{P}_r)^2 B \text{ and} \tag{23}$$

where C is defined as the common-mode rejection ratio for a balanced receiver. Mitigation of RIN effects with regard to heterodyne receivers can be done by using a configuration in which a balanced PD is employed. This configuration is depicted in Figure 10. Cancellation of RIN is achieved by the subtraction of signals that are coming from the PDs [81]. This is very beneficial for systems where there is a requirement specification for a higher SNR. Moreover, it is a very competent technique for common-mode noise compensation for LDs. The signals from the first PD and the second PD are respectively given by equations (24) and (25), whereas the resulting signal after subtraction is defined by equation (26).

$$I_{p_1}(t) = \frac{\mathscr{R}}{2}\left[P_c + P_L + 2\sqrt{P_c P_L}\cos\left(\omega_{\mathrm{IF}} t + \theta_c - \theta_L\right)\right] \tag{24}$$

$$I_{p_2}(t) = \frac{\mathscr{R}}{2}\left[P_c + P_L - 2\sqrt{P_c P_L}\cos\left(\omega_{\mathrm{IF}} t + \theta_c - \theta_L\right)\right] \tag{25}$$

$$\Delta I_p(t) = I_{p_1} - I_{p_2} = 2\mathscr{R} 2\sqrt{P_c P_L}\cos\left(\omega_{\mathrm{IF}} t + \theta_c - \theta_L\right) \tag{26}$$

4.3.5. Signal-to-Noise Ratio. For IM/DD and coherent receivers, the SNR is expressed as

$$\mathrm{SNR} = \frac{I_P^2}{N_T} = \frac{(\mathscr{R} M P_r)^2}{\sigma_q^2 + \sigma_D^2 + \sigma_{TH}^2 + \sigma_{\mathrm{IN}}^2}. \tag{27}$$

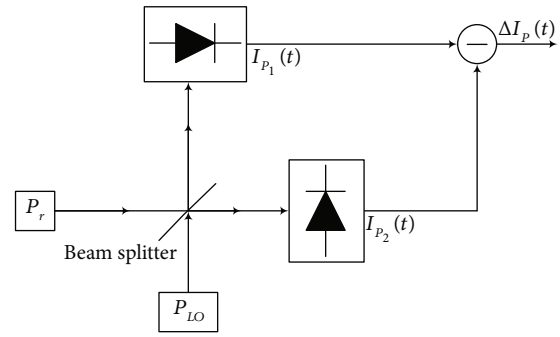

Figure 10: Configuration for a balanced PD.

Typically, different types of noise have different weights; in most cases, thermal noise and quantum noise are the most significant. In an occurrence where the power of the optical signal is quite high, the thermal noise is far much less than the shot noise. Thus, the SNR is referred to as quantum noise limited. Under the conditions where the power of the optical signal is low, the shot noise is dominated by the thermal noise, and the SNR is now termed to be thermal noise limited.

4.4. Optical Detection Statistics. The interaction of the optical radiation with the atomic structure of the detector surface is defined using semiclassical approach. The probability of a PD with aperture area A_D emitting n number of electrons from the emitted photons over a time period has a Poisson distribution defined by

$$p(n) = \frac{\langle n \rangle^n \ \exp\ (-\langle n \rangle)}{n!}. \tag{28}$$

The relationship of the mean count to the aperture area and the impinging irradiance $I(t, r)$ is given by

$$\langle n \rangle = \frac{\eta \lambda}{hc} \iint I(t, r) \mathrm{d}t \mathrm{d}r. \tag{29}$$

The variance of the mean current produced by $\langle n \rangle$ electrons is statistically denoted by

$$\sigma^2 = \left(\frac{q}{T}\right)^2 \sigma_n^2. \tag{30}$$

where T is the period of the irradiance. Since the mean and variance for a Poisson distribution are equal, and with a bandwidth of the postdetection filter as 0.5 T (Nyquist bandwidth), equation (21) can now be defined using

$$\sigma^2 = \left(\frac{q}{T}\right)^2 \langle n \rangle = \left(\frac{q}{T}\right)^2 \frac{\langle i \rangle T}{q} = \frac{q}{T} \langle i \rangle = 2q \langle i \rangle B. \tag{31}$$

5. Framework of a VLC System

Now, we look at the system architecture of a VLC system. The initial standardization for VLC was proposed in 2007 by the Visible Light Communication Consortium (VLCC)

following its formation in 2003 by major companies in Japan [87]. The consortium presented two standards being visible light communication system standard and visible light ID system standard. The Japan Electronics and Information Technology Industries Association (JEITA) later accepted these standards as JIETA CP-1221 and JIETA CP-1222, respectively [88]. The infrared communication physical layer by the International Infrared Data Association (IrDA) in 2009 was also incorporated and adapted by the VLCC. The home gigabit access (OMEGA) project [89] financially supported by the European Union (EU) also developed an optical communication network as an augmentation for RF.

In 2011, IEEE proposed a VLC standard named IEEE 802.15.7-2011 [90] which is now superseded by IEEE 802.15.7-2018 [91] to cover a wider range of OWC from 10 000nm to 190nm (IR to UV). This standard comprises of the design specifications for both the physical layer and link layer. Link capacity of over 1 Gbps has been reached over the past few years which has led to the increased research work force by various research groups to pave way for full potential of VLC. A successor for VLCC referred to as Visible Light Communication Associations (VLCA) was formed in 2014 to advance the standardization of VLC. The International Telecommunication Union (ITU) has also developed and approved their G.9991 VLC standard in 2019. The standard particularly defines three aspects for a high-speed indoor OWC transceiver based on the use of visible light. The said aspects are, system architecture, physical layer and data link layer. More details and the specifications on the G.9991 VLC standard are found in [92].

The VLC channel structure may be categorized in two main categories depending on the way in which the link configuration between the transmitter and the receiver is set up [3, 44, 71, 73, 92]. Figure 11 depicts the classes of link configurations and they are explained below.

5.1. Degree of Directionality Channels. For this category, the link may be established by means of having a directed or nondirected transmitter-receiver pair. Extending this category, there are three different feasible classes regarding directionality.

5.1.1. Directed Link. In this class, the transmitter and the receiver are directed and aimed towards each other. Moreover, the transmitter's beam angle and the receiver's FOV angle are very narrow. With this class, power efficiency and immunity to distortion due to environmental culminations such as ambient light are substantially enhanced. This is suitable for low data transfer point-to-point communication applications with no obstacles between transmitter-receiver pair. However, such a link is not capable of providing mobility in a typical indoor environment since they are easily affected by blocking/shadowing, and it does not cater for broadcast applications [71, 73, 92].

5.1.2. Nondirected Link. Another class of this category is defined by a scenario whereby the transmitter and the receiver are not specifically directed to a specific point. Transmitters with wide beams and receivers with a wide FOV are a fundamental requirement for the transmission

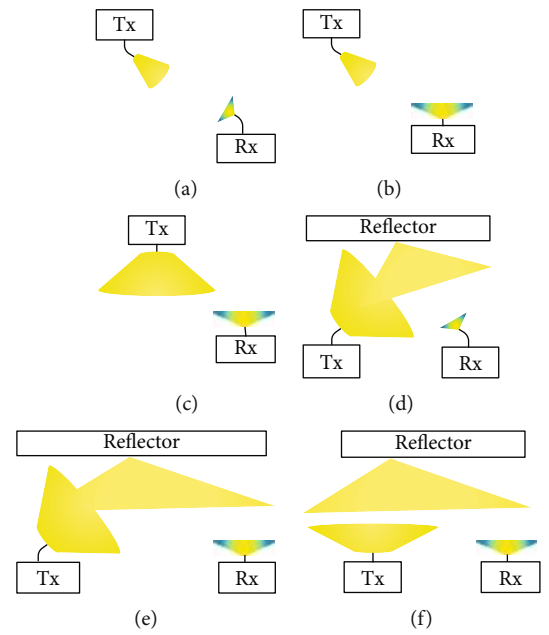

Figure 11: Link configuration classes. (a) Directed link. (b) Non directed link. (c) Hybrid link. (d) Directed non-LOS link. (e) Non directed non-LOS link. (f) Hybrid non-LOS link.

of signals for this class. The requirement of high power levels in order to strive for the reduction of elevated optical path loss and multipath-induced malformation is the major pitfalls for this second class owing to a wider beam divergence [3, 92]. On the other hand, it allows user mobility, and it also decreases the effects of shadowing as it is suited for broadcast applications.

5.1.3. Hybrid Link. A case whereby the transmitter and the receiver may assume divergent levels of directionality leads us to another class under this category. This is commonly known as a hybrid class. As an example for this class, consider a scenario whereby the transmitter with a narrow beam is directed towards a certain point and the receiver with a wide FOV is not arranged to align towards a specific direction or vice versa. Systems that are based on this class suffer from multipath propagation [3, 92].

5.2. Line-of-Sight Channels. The availability of a line-of-sight (LOS) pathway between the transmitter and the receiver yields the second category. Just like the previous category, this category may also be extended into three classes.

5.2.1. Directed Non-LOS. The directed non-LOS class features a scenario whereby the transmitter-receiver pair have a clear LOS, i.e., without any obstruction between the transmitter and the receiver. This configuration simplifies the path loss calculation owing to the fact that there is no consideration of the reflections. The power efficiency of this class is very high.

5.2.2. Nondirected Non-LOS Links. The non-LOS systems with a nondirected transmitter and receiver are also referred to as diffuse systems. For this class, the transmitter-receiver pair do not have to be directed, neither do they need to have a clear path to establish a communication link. Signals arrive

at the receiver indirectly from the transmitter due to the nearly uniform distribution of the optical signal by the reflecting panels such as walls and ceilings. Diffuse systems are considered to be the most robust, easy to design and implement, and predominantly for mobile communication systems [3, 44, 71]. This class paves way for effortless use as they allow the transmitter and the receiver to operate even when there are obstacles in between them.

5.2.3. Hybrid Non-LOS Links. In this class of configuration, the transmitted signals are reflected from various objects and are received at different time intervals. The hybrid non-LOS architecture leads to multipath distortions which creates a severe difficulty for path loss estimation which makes them complex and very costly to implement.

It is worth noting, with regard to the transmission speed only, that VLC channels may be categorized into two categories. One category is a case where the use is for a high data rate and the other category is a case where the requirement is for low data rate [50]. For utilization where there is a need for a high data rate, high-speed photodiode receivers are required. As for low data rate cases, the existing hardware found in our day-to-day lives such as mobile devices may form part of the system. A downlink communication to mobile devices in an office or flight cabin from the general omnipresent illumination lamps is one of the most promising high data rate VLC applications [93]. Other applications for high data rates include cases where files are being transferred between devices and streaming from a device to a display. Augmented reality (AR), vehicle-to-vehicle (V2V), vehicle-to-infrastructure (V2I) communication, underwater communication, and localization of indoor communication systems, just to mention a few, are examples of low data rate applications [94].

6. Design of an Indoor VLC Structure

Due to the intrinsic nature of the LEDs producing incoherent light intensity, the most prominent, convenient, and favorable modulation technology employed for indoor VLC systems is IM [4, 44, 71, 95, 96]. Moreover, this technique is easy to implement and highly cost-effective. With the IM technique, the optical power emitted by the LEDs is changed with respect to a certain attribute of the baseband signal. For demodulation, DD is employed as apposed to heterodyning as in RF and optical laser communication where coherent detection is possible [4, 44, 71, 95–97]. DD produces a photocurrent which is directly proportional to the instantaneous optical power which is incident to the photodetector. The IM/DD technique however poses a hazard to human health because of flicker which may affect the human eyes in a negative way. Nonetheless, flicker is intercepted by keeping the modulation frequencies far higher than the frequency at which the human eye blinks. This is achieved by switching LEDs on and off at a higher rate making flicker unrecognizable to the human eye [98, 99].

Optical wireless systems that are based on the IM/DD technique have an analogous baseband model which conceals the natural optical carrier's high-frequency [100]. The model

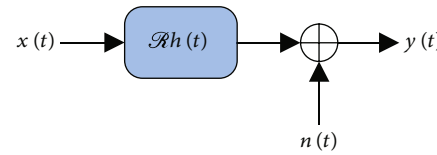

Figure 12: OWC system baseband model.

is illustrated in Figure 12. $\mathscr{R}$ is the responsivity of the photodetector, $h(t)$ is the impulse response of the baseband channel, and $n(t)$ is the shot noise which is not dependent on the baseband signal. In this article, as adapted in [3], $n(t)$ is modeled with a double-sided power spectral density (PSD) of $N_0/2$, and it is taken as the additive white Gaussian noise (AWGN).

A comprehensive general system structure block diagram based on IM/DD is depicted in Figure 13. Like any other communication system, a VLC system can be unidirectional or bidirectional. For the latter, visible light is used for the downlink, and IR is typically used for the uplink (RF can also be used for the uplink). The supremacy of using different frequencies for the uplink and downlink is that interference is greatly minimal. Furthermore, this avoids visual distress to the human eyes [21, 51].

Non-LOS indoor VLC links are subject to be negatively affected by the intersymbol interference (ISI) as a result of dispersion despite the fact that they do not suffer from multipath fading effects. Impulse response $h(t)$ taken as a linear baseband channel is used to model the dispersion. For a specified locality of the transmitter, receiver, and any other object capable of reflecting light, the channel characteristic of a VLC link does not change. The channel characteristic will only change when any of the abovementioned elements are moved by the order of a few centimeters to a different locality [3]. Simulation and analysis of the effects of dispersion can be performed by utilizing $h(t)$. Gfeller and Bapst [101] modeled the impulse response of the channel, and it is defined by

$$h(t) = \begin{cases} \dfrac{2t_0}{t^3 \sin^2(\mathrm{FOV})}, & t_0 \le t \le \dfrac{t_0}{\cos(\mathrm{FOV})}, \\ 0, & \text{otherwise} \end{cases} \tag{32}$$

where t_0 is the minimum delay. Hence, the corresponding baseband model for IM/DD VLC link is given by

$$\begin{aligned} y(t) &= \mathscr{R}x(t) \circledast h(t) + n(t) \\ &= \int_{-\infty}^{\infty} \mathscr{R}x(\tau) \circledast h(t-\tau)\mathrm{d}\tau + n(t), \end{aligned} \tag{33}$$

where the character $\circledast$ represents circular convolution. In contrast to electrical and RF systems, $x(t)$ in equation (33) is represented as a power signal instead of an amplitude signal. That being said, this inevitably yields two restrictions on the transmitted signal. One of the constraints is that $x(t)$ has to be strictly greater or equal to zero. One other constraint is with regard to human eye safety since the safety requirements restrict the amount of the transmitted optical power to a

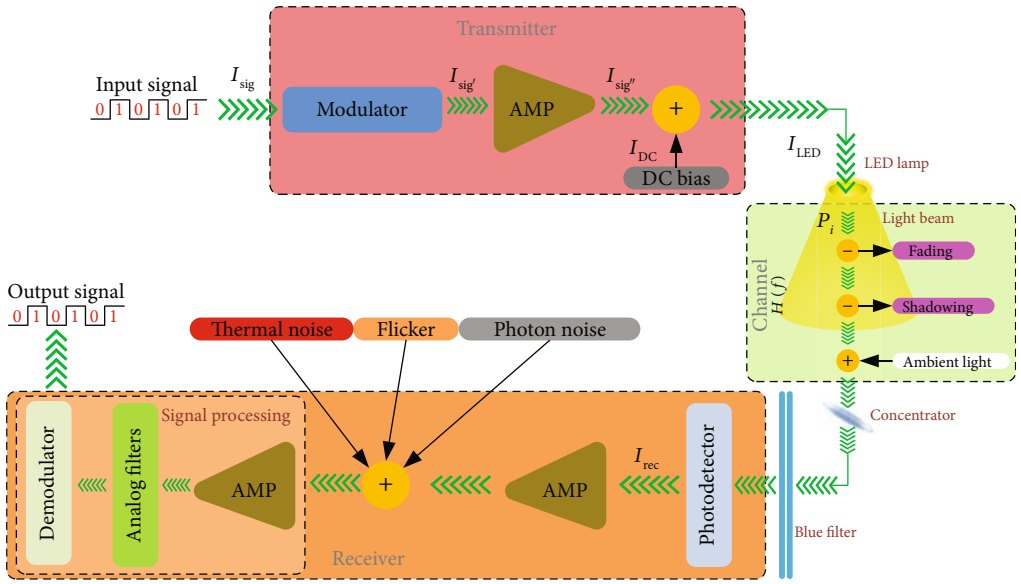

Figure 13: Indoor VLC channel propagation model.

certain level. The mean value of $x(t)$ must not be greater than the standard maximum power value given by.

$$P_{\max} = \lim_{T\to\infty} \frac{1}{2T} \int_{-T}^{T} x(t)\mathrm{d}t. \tag{34}$$

Relative to the traditional wireless communication based on RF, the signal-to-noise ratio (SNR) of VLC links is proportional to the square of the average received optical power denoted by equation (35). For RF links, the SNR is proportional to the average received RF power.

$$\mathrm{SNR} = \frac{(\mathscr{R}H(0)P_r)^2}{\sigma_T^2}, \tag{35}$$

where σ_T^2 is the overall noise variance, and $H(0)$ is the DC gain of the channel expressed as

$$H(0) = \int_{-\infty}^{\infty} h(t)\mathrm{d}t. \tag{36}$$

From equations (35) and (36), it is evident that OWC systems require a fairly high transmit power with a low tolerance of path loss. In a scenario where the dominant noise source is the shot noise, the SNR is analogous with the area of the PD as a result of the proportionality of the shot noise variance and the received electrical power to the area of the PD and to the square of the area of the PD, respectively. Thus being said, it is advantageous to have a PD that has a large area for single element receivers. However, an increase in the surface area of the detector in turn increases its capacitance which reduces the transmission capacity as a result the negative effects of capacitance on the receiver bandwidth. Therefore, there is always a trade-off between high bandwidth and high power efficiency for modulation techniques.

6.1. Propagation Models

6.1.1. Line of Sight Propagation Model. Wireless systems based on optical technology predominantly utilize LEDs and PDs with large surface area. The radiation intensity pattern for the LED's angular distribution, as depicted in Figure 14(a), is based on Lambertian approximation and is defined by

$$R_0(\phi) = \begin{cases} \dfrac{m_1+1}{2\pi}\cos^{m_1}(\phi), & \Phi \in [-\pi/2, \pi/2] \\ 0, & \phi \geq \pi/2, \end{cases} \tag{37}$$

where $\phi = 0$ is the maximum power's radiation angle, Φ is the semiangle of the LED, and m_1 is expressed in terms of semiangle at half-power by

$$m_1 = \frac{\ln\ (2)}{\ln\ (\cos\ (\Phi_{1/2}))}. \tag{38}$$

An LED's radiant intensity, defined in terms of irradiance angle and the total power of the LED, is given by

$$P_i = \frac{(m_1+1)P_t\cos^{m_1}(\phi)}{2\pi}, \tag{39}$$

where P_t is the total transmitted power of the LED. The collecting area (effective) of the receiver's PD, in terms of the active collection area A_r of the PD, which collects the incident radiation at angles ψ (less than the FOV of the detector), is mathematically expressed as

$$A_e(\psi) = \begin{cases} A_r\cos\ (\psi), & 0 \leq \psi \leq \pi/2 \\ 0, & \psi > \pi/2 \end{cases}. \tag{40}$$

Detectors with large areas of collection are preferable for indoor applications so as to allow for the collection of the

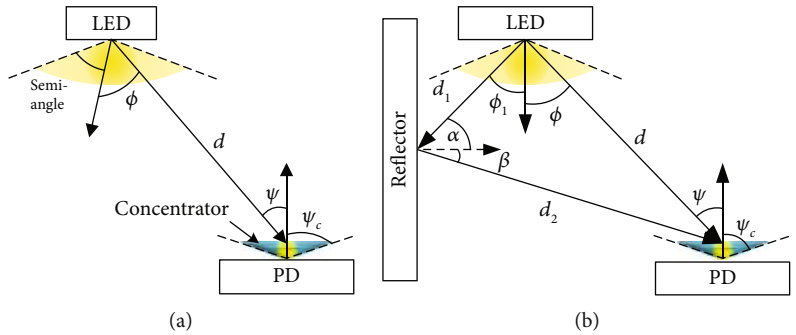

FIGURE 14: Ideal link configurations for propagation models. (a) LOS link configuration. (b) Non-LOS link configuration.

maximum available power from the source. However, practically, this poses challenges because of various economical and technical constraints such as costs, low bandwidth, and high noise. As a countermeasure, a nonimaging concentrator is put to use as a way of improving the effective collection area. Theoretically, a nonimaging concentrator has an optical gain which is given by

$$g(\psi) = \begin{cases} \dfrac{n^2}{\sin^2(\psi_c)}, & 0 \le \psi \le \psi_c, \\ 0, & \psi > \psi_c, \end{cases} \tag{41}$$

where n is the internal refractive index of the concentrator, and ψ_c is the detector's FOV. As per the constant radiance theorem [102], the relationship between the lens' collection area and the system receiver's FOV is given by equation (42). From this, it is noticeable that small FOV leads to an increased concentrator gain.

$$A_{\text{col}} \sin\left(\frac{\psi_c}{2}\right) \le A_r. \tag{42}$$

The gain of the channel between the LED and the receiver is mathematically estimated using [71].

$$H_{\text{LOS}}(0) = \begin{cases} \dfrac{A_r(m_1+1)\cos^{m_1}(\phi)}{2\pi d^2} \times T_s(\psi) g(\psi) \cos(\psi), & 0 \le \psi \le \psi_c, \\ 0, & \psi \ge \psi_c, \end{cases} \tag{43}$$

where d is the distance of the receiver from the LED, and T_s is the optical filter's gain. Thus, the received power is expressed as

$$P_{r-\text{LOS}} = H_{\text{LOS}}(0) P_t. \tag{44}$$

Multipath dispersion is sporadically a challenge in LOS links that have shorter distances between the source-receiver pair. The link is generally modeled as linear attenuation and delay [3]. The path loss of optical links is dependent on the square of the distance between the transmitter-receiver pair because the links are nonfrequency selective. The impulse response may be expressed by

$$h_{\text{LOS}}(t) = \frac{A_r(m_1+1)\cos^{m_1}(\phi) T_s(\psi) g(\psi)}{2\pi d^2} \times \cos(\psi) \delta\left(t - \frac{d}{c}\right), \tag{45}$$

where δ is the Dirac function, $\delta(t - d/c)$ is the propagation delay, $\phi < 90$, $\psi <$ FOV, and $d \gg \sqrt{A_r}$.

6.1.2. Nonline of Sight Propagation Model. Various aspects such as the orientation and positioning of the transmitter-receiver pair, room dimensions, window size, the reflectivity of the walls, ceiling, and objects in the room make the computation of optical path loss not easy to predict and analyze. The power received is conventionally given by

$$\begin{aligned} P_{r-\text{NLOS}} &= (H_{\text{LOS}}(0) + H_{\text{NLOS}}(0)) P_t \\ &= \left(H_{\text{LOS}}(0) + \sum_{\text{REFL}} H_{\text{REFL}}(0)\right) P_t, \end{aligned} \tag{46}$$

where $H_{\text{REFL}}(0)$ is the channel DC gain of the path of the reflecting object/surface and may be defined by

$$H_{\text{REFL}}(0) = \begin{cases} \dfrac{A_r \rho dA (m_1+1)\cos^{m_1}(\phi)}{(2\pi d_1 d_2)^2} \\ \times T_s(\psi)\cos(\beta)\cos(\alpha) \\ \times g(\psi)\cos(\psi), & 0 \le \psi \le \psi_c, \\ 0, & \psi \ge \psi_c, \end{cases} \tag{47}$$

where d_1 and d_2 represent the distance between and the reflecting object, respectively, d_A is the reflective area of a small region, ρ represents the reflective factor, β is the angle of irradiance to the receiver, and α is the angle of incidence to the reflecting object.

The geometrical non-LOS propagation model is as shown in Figure 14(b). Diverse factors such as the wavelength of transmission, the material used to fabricate the surface, angle of incidence, and the texture of the surface dictate the object's surface reflection attributes. The pattern of the

optical reflection is determined by the texture of the surface. To determine the texture of a surface, the Rayleigh criterion [101] is widely used. If the topmost height of the surface inconsistencies satisfies equation (48), this criterion considers the surface to be smooth.

$$h_{\mathrm{SI}} < \frac{\lambda}{8 \sinh(\theta_i)}, \tag{48}$$

where θ_i is the angle of incidence.

It is very crucial to evaluate the dispersal of the optical power for a particular setup in order to estimate the path loss for nondirected LOS and diffuse links. Several experimental attempts have been made in [73, 103–114] to precisely delineate indoor optical channels. In order to model and evaluate the power distribution of the optical power for a nondirected LOS and diffuse links, we adapted a similar approach as in [109]. For demonstration purposes, we only considered the simulation of the radiation pattern using a set of four deterministic LED lamps. The four LED lamps are assumed to be located within a room that has dimensions of $5 \times 5 \times 3$ m^3. All lamps are mounted on the ceiling. With reference to the center of the room as $(0, 0, 3)$, the lamps are positioned at coordinates $(x, y, z) = (-1.25, -1.25, 3)$, $(1.25, 1.25, 3)$, $(-1.25, 1.25, 3)$, and $(1.25, -1.25, 3)$. Each set of the three deterministic lamps have different semiangles of 15°, 30°, and 60°. The impinging power distribution pattern of each set looking from the ceiling down onto the floor is shown in Figure 15. An interesting phenomenon to note here is that the power dispersion pattern of four deterministic lamps is equal to that of a single LED that has the same illuminance level with a semiangle of 60°.

The impulse response of an OWC channel is mathematically determined by integrating the power of all the constituents that impinges their radiation on the receiver of the system postmultipath propagation [115]. The signals impinging the receiver consist of diverse elements from different paths. These elements have dissimilar path lengths with respect to the room design which leads to the broadening of the pulse. As opposed to an LOS element, which its channel satisfy a modified gamma distribution, the channele gain of NLOS channel together will all the reflections for the majority of transmitter-receiver pair distances satisfy a modified Rayleigh distribution [114]. In order to evaluate the time-dispersive characteristics for a certain multipath channel, the root mean square delay spread (D_{RMS}) based on the magnitude square of the channel's impulse response is utilized, and it can be computed using [3, 112].

$$D_{\mathrm{RMS}} = \sqrt{\frac{\int (t-\mu)^2 h^2(t) \mathrm{d}t}{\int h^2(t) \mathrm{d}t}}, \tag{49}$$

where μ is the mean delay spread and is expressed by

$$\mu = \frac{\int t h^2(t) \mathrm{d}t}{\int h^2(t) \mathrm{d}t}. \tag{50}$$

Calculations for the basic power budget can be adequately satisfied by the determination of the optical power distribution of an entire room; however, this does not take into consideration the multiple reflections. With this being said, power loss on account of multipath propagation cannot be estimated unambiguously. When a channel has more than one reflection, the optical power associated with the reflections is fairly small. The signal reaches the receiver at a later time compared to the time when there is a single reflection. Therefore, for nondirected LOS and diffuse links that operate at high-speed, this delay needs to be taken into account. In [73], the authors established a ray-tracing algorithm capable of producing an impulse response that takes into account higher-order reflections. The algorithm evaluates the path loss as well as the time delay for all the paths having a specific number of reflections. The final impulse response is given by summing all contributions. The development of the algorithm was made by considering empty rectangular rooms with an assumption that the receiver was facing the ceiling. The impulse response for a specific unique source (S) and receiver (R_x) in a room can be expressed as

$$h_{\mathrm{NLOS}}(t, S, R_x) = \sum_{k=0}^{\infty} h^{(k)}_{NLOS}(t, S, R_x), \tag{51}$$

where $h^{(k)}_{\mathrm{NLOS}}(t, S, R_x)$ is the impulse response because of exactly k reflections of light. Equation (51) can be modified to satisfy multiple (K) sources, and it can now be defined by

$$h_{\mathrm{NLOS}}(t, S, R_x) = \sum_{i}^{K} \sum_{k=0}^{\infty} h^{(k)}_{\mathrm{NLOS}}(t, S, R_x). \tag{52}$$

After the k^{th} reflection, the recursive algorithm can be used to calculate $h^{(k)}(t, S, R_x)$, and the algorithm is defined by [71, 73, 116]

$$h_{\mathrm{NLOS}}(t, S, R_x) = \frac{m_1 + 1}{2\pi} \sum_{j=1}^{K} \rho_j \cos^{m_1}\left(\phi_j\right) \frac{\cos(\Psi)}{d^2_{Sj}} \times \mathrm{rect}\left(\frac{2\Psi}{\pi}\right) h^{(k-1)}_{\mathrm{NLOS}}\left(t - \frac{d^2_{Sj}}{c}, S, R_x\right) \Delta A, \tag{53}$$

where ΔA is the area of the reflecting elements, K is the number of reflecting objects, ρ_j is the reflecting coefficient of the reflecting object, d_{Sj} is the distance between the source and a specific reflector, and $h^{(k-1)}(t, S, R_x)$ is the impulse response of order $(k-1)$ between a particular reflector and the receiver.

As the magnitude of the impulse response $\|h^{(k)}(t, S, R_x)\|$ approaches zero, k approaches infinity. Thus, "the impulse response of the channel can be approximated using only the first $\mathfrak{R}$. A very good channel estimation can be obtained by considering only the first ten (10) reflections in a case where iterative methods are employed. When evaluating

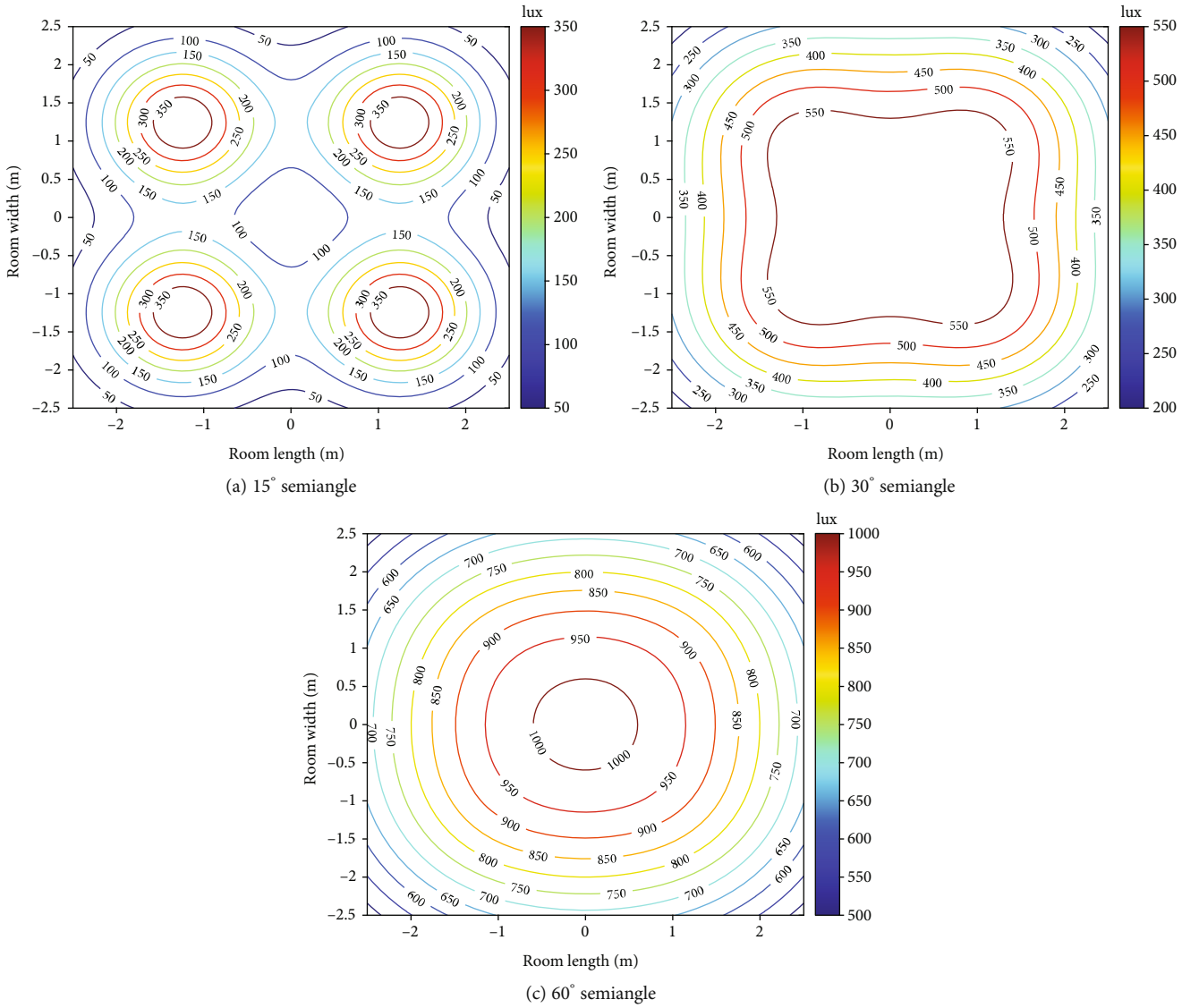

Figure 15: Optical power dispersion of four deterministic lamps with different semiangles.

the initial reflections, room surfaces are divided by $\Re$ reflecting elements having an area of ΔA" [3]. There are two components that can be used to describe the channel. For one of the components, all elements of the surface that has a surface area ΔA are considered as individual receivers. As for the other component, all of the elements are then considered to be point sources that reemits the collected signal which is scaled by the reflecting coefficient ρ_j. Now, the channel response for an individual reflection can be estimated using

$$h^1_{\mathrm{NLOS}}(t, S, R_x) = \sum_{j=1}^{\Re} \frac{(m_1+1)\rho_j A_r \Delta A \cos^{m_1}\left(\phi_{Sj}\right)}{2\pi\left(d_S d_{R_{Sj}}\right)^2} \times \cos\left(\Psi_{Sj}\right) \cos\left(\Psi_{Rj}\right) \delta\left(t - \frac{d_{Sj} + d_{Rj}}{c}\right). \tag{54}$$

For indoor OWC systems, the impulse response of the channel is dependent on the receiver's location as it varies when the receiver is moved from one position to the other. The most significant component is the first reflection since it impacts the limits of the data rates. It should be noted that this model satisfies a specific room arrangement. Shadowing and the layout of furniture are not taken into account. A modification of this model by Abtahi and Hashemi [117] took into consideration the effects of the objects (i.e., furniture and people) inside rooms of uniform and nonuniform shape. A neural network was utilized by Pakravan and Kavehrad [118] to increase the speed of the algorithm that was developed in [73]. With the neural network, just a small number of the total points that need to be calculated is computed, and then the network learns the remaining points. Lomba et al. [116, 119] considered a signal which is being reflected more than once and proposed a simulation model, which is more efficient for indoor channels. The approaches

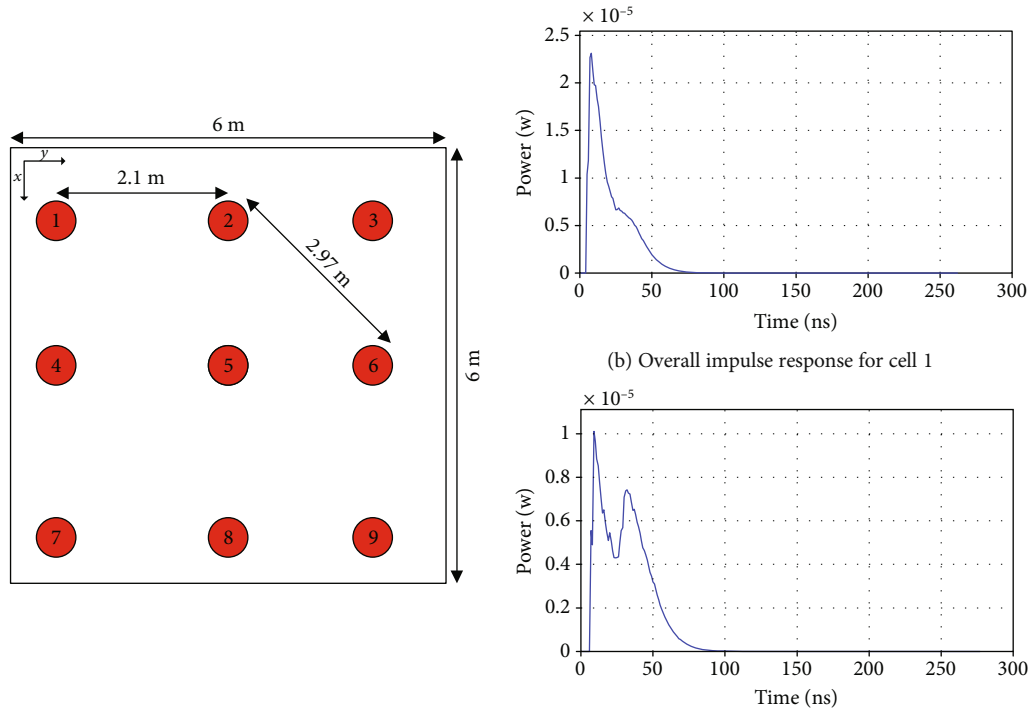

(a) Empty room setup

(b) Overall impulse response for cell 1

(c) Overall impulse response for cell 100

Figure 16: Empty room simulations for detector 5 [120].

that improve the simulation efficiency are the "time-delay agglutination" and "time and space indexed tables". The effects of multipath reflections in the receiver were simulated using the iterative site-based model suggested by Kannan et al. [113]. The author's study suggested that channels that are fully diffused and those with a LOS path must be separately modeled.

In [120], the authors modeled and simulated reference channel models for various indoor environments by considering an empty room, conference room, living room, and office space setups. The simulations for channel response for an empty space with room dimensions and LED positioning as depicted in Figure 16(a) are shown in Figure 16. The room is divided into 10×10 cells which are equally spaced by 0.6 m in both x and y directions. Using the same channel parameters, LED and PD specifications as well as user descriptions as outlined in [120], we show the impulse responses from all of the nine luminaires with the user located at cell 1 and cell 100 using the code that was developed and written by [121]. The PD is considered to be located at D5 on the user's cellphone. Figure 16(b) depicts the overall impulse response when the user is located at cell 1, whereas Figure 16(c) depicts the overall impulse response when the user is at cell 100. For both of these responses, the impact of LED response with 20 MHz cut-off frequency was taken into account.

For simulations of a conference room environment, the room dimensions, furniture arrangement, luminaire setup, and the positioning of all detectors (labeled D1-D10) are as seen in Figure 17 [120]. Using the same channel parameters, LED and PD specifications as outlined in [120], we show the overall impulse responses from all of the ten luminaires to only D1 and D6, respectively. The channel response from all luminaires to detector D1 is shown in Figures 17(b), and Figure 17(c) depicts the response for detector D6. For both of these impulse responses, the impact of LED response was not considered.

The majority of the abovementioned channel models are founded on the Monte-Carlo ray-tracing algorithm and Lambert's model of reflection. It should be noted that a different impulse response of the same channel can be obtained when using Phong's model. This is with respect to Lambert's model in a scenario where a surface depicts a high specular component [122]. Primary and higher-order reflections from the decomposed signal can be used to model the impulse response [115]. The impulse response of the primary reflections is quantified using the gamma probability density function (pdf). The spherical model is used to simulate the higher-order reflection impulse response. From analysis, the impulse response of the primary reflections dominates the bandwidth characteristics.

A practical characterization of the channel was done by Kahn et al. [112]. Using a frequency swept technique, the authors measured the frequency responses of the channel over a frequency range of 2 MHz to 300 MHz. Considering the link configurations of both LOS and diffuse channels, the authors deduced the impulse responses, RMS delay spreads, and path losses using the obtained measurements. Their study was carried out in five different rooms with variations in the location of the receiver. In [123], the authors made measurements in eight rooms which had different positioning of the photodetector. In addition, they carried out

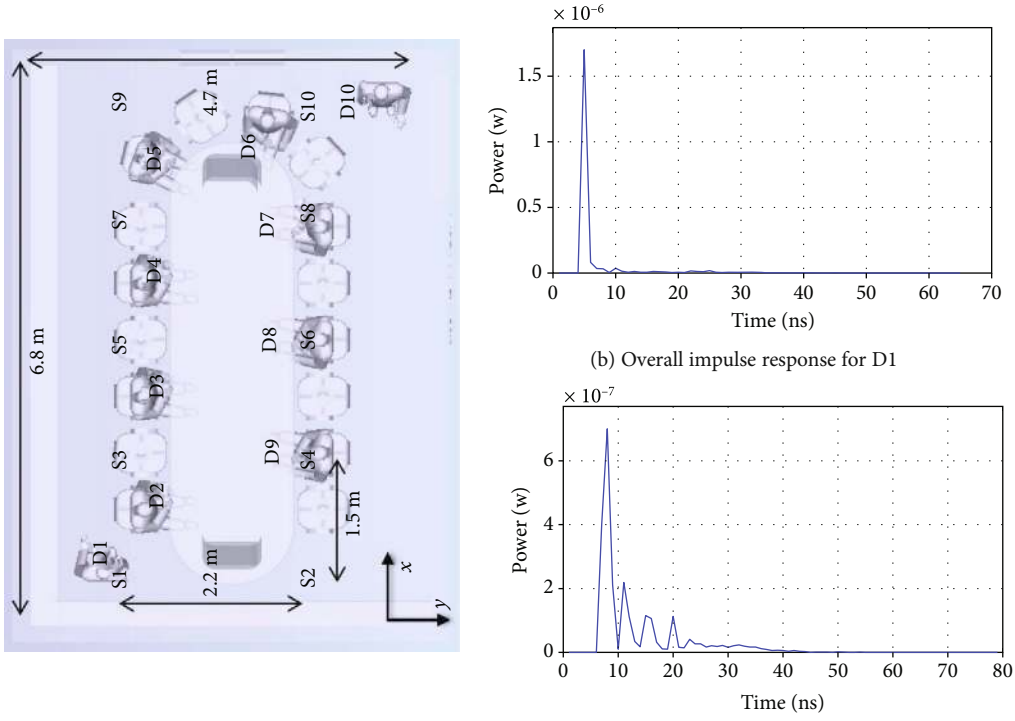

(a) Conference room setup

(b) Overall impulse response for D1

(c) Overall impulse response for D6

Figure 17: Conference room simulations [120].

measurements with varying orientation and rotation of the photodetector. The analysis of their measurements showed that the positioning of the photodetector as well as the orientation and rotation affects the sensitivity of the channel response. The authors proposed a receiver structure with a diverse angle of incidence based on the analysis of their acquired measurements.

6.1.3. Spherical Model. The spherical model is used to model higher-order reflections which is given by [121].

$$h_{\text{high}} = \frac{\eta_{\text{high}}}{\tau} \exp\left(-\frac{<t>}{\tau_e}\right), \tag{55}$$

where η_{high} is the power efficiency of the diffuse signal, τ_e is the exponential decay time, and $<t>$ is the average transmission delay.

The diffuse channel's frequency response and the higher-order reflections' 3-dB bandwidth are given by equation (56) and equation (57), respectively.

$$H_{\text{dif}} = \frac{\eta_{\text{dif}}}{1 + j2\pi f} \tag{56}$$

$$f_{3\text{dB}} = \frac{1}{2\pi f \tau_e} \tag{57}$$

6.2. Driver Circuitry. There exist various ways in which the constituents of the LED driver are arranged, and these are classified according to the LED's regulatory requirement, application, performance, power rating, and energy storage. The constituents of driver circuitry result in topologies such as buck, boost, and buck-boost. Generally, LED drivers are categorized into two main categories, viz. passive and active. The former constitutes of passive elements such as diodes and capacitors while the latter constitutes of power electronic semiconductor components [21, 22, 124]. LEDs are distinctly quick to respond to photometric, thermal, and electrical variations. Therefore, an in-depth understanding of the complex interactions of these three aspects is crucial in order to fully acquire the precise potential and exhaustive benefits of an LED for optimal design and operation of LED-based systems. The mathematical description of the interactions of the aforementioned aspects has been described in the photo-electro-thermal (PET) theory framework [125–128]. This framework paved way for analyzing the performance of LED systems. PET theory can be used for the optimization of LED-based system designs to meet practical constraints of technical specifications including but not limited to international regulations, form factors, reliability, and costs. The theory can also be used to outline the convention of an optimal thermal design of a suitable heat sink for a particular application.

In a study that was conducted by Li et al. [124], the categories of the present LED drivers have been reviewed based on their applications, costs, galvanic isolation, and output voltage ratings. The divisions contemplate the present market needs and indicate various specifications for various applications. These divisions are anticipated to continually widen as LED products for contemporary lighting markets are emerging rapidly. Based on their collected commercial data of over 1400 LEDs, the authors widely divided LED

drivers into three power range groups. The groups are low power drivers with power ratings of less than 25 W, medium power drivers with power ratings in the range of 25 W to 100 W, and lastly, high power drivers having a power rating of more than 100 W.

Typically, applications for low power LED drivers include electronic accessories and interior lighting. This makes LED technology a great substitute for incandescent and fluorescent innovations since the power rating for accessories and interior appliances is conventionally less than 25 W. Medium power LED drivers feature in applications for indoor lighting and some outdoor lighting. Application examples include downlights and flat lights. Normally, indoor lighting appliances are power rated 25 W to 50 W since the required luminous output is higher compared to low power applications. Outdoor applications which require a tremendous amount of luminous output feature high power LED drivers. The power rating for outdoor appliances which include street lighting and floodlight among others typically ranges from 50 W to over 100 W.

Other important factors that the authors in [124] studied with regard to the selection of a suitable LED driver topology for a certain application are the output dc voltage and power ratings which are load-dependent. Figure 18, which has a nonlinear scale, shows the divisions of the output DC voltage versus the DC power ratings. The depiction in the figure was computed and plotted using the power ratings of the data obtained from the 1462 LED products with a power range of 3 W to 300 W. Based on the analysis of their computations, the authors made the three most significant observations. Firstly, the authors realized that there are various power and output voltage levels between various LED products. The lack of global standards and the availability of a wide range of different LED products are the factors that lead to such variations as opposed to the stereotyped lighting products that have prevailing standardization for power and voltage levels. Secondly, with reference to Figure 18, the data points that recline on the hypotenuse of the triangular area covered by the entire data points represent samples with the maximum current rating value of 0.35 A. It is noted that this value corresponds to most of the commercial LED devices' maximum current rating. Lastly, the majority of LED products within the bounds of the low power section do not exceed 50 V as compared to the medium and high power products that have a wider range. These products conform to the 2006/95/EC directive which is an obligatory requirement for the CE Mark Scheme. The directive states that the operating voltage below 50 V is safe for human beings. Electrical isolation is not needed when designing with an output voltage below 50 V, and this simplifies the design process for LED systems both technically and economically.

Controlling and dimming of an LED are far more strenuous by reason of the LED's low dynamic resistance which is caused by the component's elevated susceptibility to subtle voltage changes and the forward current. LED drivers are used to convert the alternating current (AC) into direct current (DC), hence, allowing the operation of an LED which cannot be operated from the AC sources. The other function of the LED driver is to regulate the converted DC down to the desired operational voltage of the LED. It is adamant to maintain the operational voltage by an additional feedback controller on the driver circuitry. Simultaneous usage of LEDs for illumination and data transfer leads to various design complexities due to the very tight requirements of the LED driver design. Modern-day low power complementary metal-oxide-semiconductor (CMOS) technology has made it possible to incorporate many functions into just one chip to establish the design of driver circuits in the form of a system-on-chip. This integration may feature many elements such as control of the LED performance, data modulation, and luminance [129].

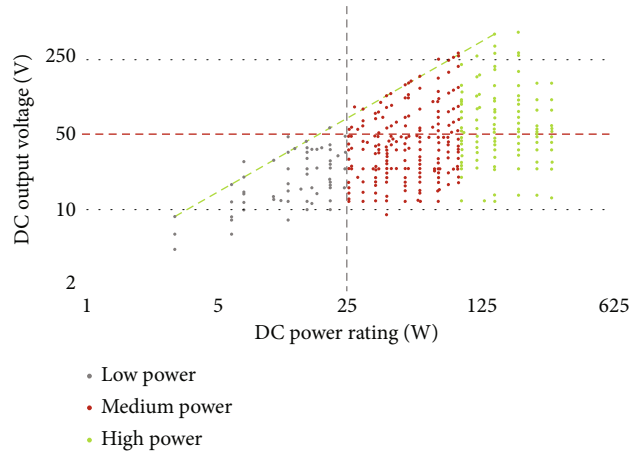

Figure 18: Voltage and power ratings of LEDs [124].

As opposed to ordinary LED drivers, VLC driver circuitry must cater for data modulation and other associated features without negatively impacting the lighting controls like dimming and flicker mitigation. Moreover, it is of vital importance that driver circuits should have longer MTTF, operate using low power, and have the ability to drive the LEDs using pulse current. In the quest to offer high data rates and various illumination levels, the advanced developments of LED driver circuits has led to the possibility of dimming LEDs to a random level as required in order to save energy. Dimming of an LED to a particular level has an impact on the light perception of the human eye. As depicted in Figure 19, various sources have shown that there is a nonlinear correlation of the perceived light and the measured light. The human eye is able to adapt to low levels of illumination thanks to the contraction of the pupil which enables supplemental light to get into the eye. The relationship between perceived and measured light is mathematically given by [130].

$$P_L = 100 \times \sqrt{\frac{M_L}{100}}, \tag{58}$$

where P_L is the perceived light in percentage form, and M_L is the measured light in percentage form.

This correlation implies that the human eye perceives the light to be dimmed to approximately 32% for an illumination source which has been dimmed to 10% of the actual measured light output. This property is very crucial for VLC

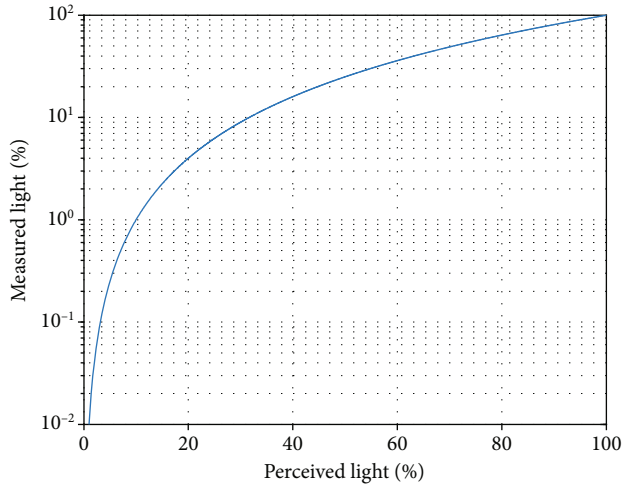

Figure 19: Human eye light perception versus measured light.

systems because the dimming level should not disturb communication even when the user selects any dimming level based on the desired application or their requirement for saving energy [98]. Simply put, all dimming levels shall be supported for any of the applicable communication.

There are numerous ongoing research efforts and attempts that are aimed at improving the performance of LED drivers in order to facilitate both dimming and data transfer. The dual usage of LED driver utilizing a single-stage buck-boost-buck converter was proposed in [131] to provide both illumination and communication as well as power factor correction (PFC). The details of the design and modeling of the converter and the variable pulse position modulation (VPPM) scheme are given in the paper. The design of the converter provides PCF by using the buck-boost section in a discontinuous conduction mode with a steady duty factor, while the buck section in continuous conduction mode with average current mode control makes a provision for a stable current source for the LED load. The state of the connected LED load is changed from high to low using a frequency of 2 MHz to concurrently enable communication and illumination. VPPM is utilized to provide data transfer. High-frequency pulse modulation (PWM) dimming is used for illumination. The experimental results of the designed converter show that VPPM scheme was able to achieve a data transfer rate of 2 Mbps at a distance of 1 from the white PC-LEDs luminaire with an output of 500 lm.

In [132], the proposed design of a LED driver that facilitates for combination of lighting and VLC was outlined. Linear current regulation is employed for the proposed driver. The driver controls both the DC current and AC current signal via just one power device using a standard 0.5 CMOS technology in order to pave way for high efficiency, high integration, and high efficiency. The driver is able to support OFDM. Moreover, a technique for impedance reduction in order to improve the bandwidth of the driver is presented. The limitation of low bandwidth of PC-LEDs is overcome by the utilization of a first-order preequalizer. Experimental results of the designed LED driver with a forward-biased LED current of 350 mA was able to yield modulation bandwidth of about 10.9 MHz and a data rate of approximately 50 Mbps.

A VLC driver circuit that has high energy efficiency based on a current-steering digital to analog converter (DAC) is demonstrated in [133]. The driver is built in a 0.8 μm CMOS technology chip having a DAC with a resolution of $4 \times 8 -$ bit. The individual channels are able to supply a full-scale current of 255 mA. When driving OFDM signals at 250 Ms/s, an electrical efficiency of 67% is attained. Two output branches of only one channel of the four channels were used to prove that the driver can optically drive two separate LEDs with an improved SNR of over 5 dB. The authors outlined that the designed chip can enable the adjustment of color temperature of the emitted light using RGB-LEDs on grounds of the chip's full digital capability to control CSK. In addition, the chip can also enable dimming and optical MIMO communication.

Mirvakili and Joyner [134] present their proposed innovation and design of a digitally controlled analog LED driver circuit on a 0.5 μm CMOS technology to advance the integration of at least one purpose for illuminating LEDs. Their invention enables both serial data transmission and illumination control. The aim of data transmission and illumination is achieved by the implementation of a two-level driving PWM scheme. This scheme paves way for data to be transmitted during the time when the LED driver current is considered to be "OFF". With this driver, the luminous intensity of the LED can be controlled from 5% to 100% using PWM dimming at a resolution of 3 – bit. Performance comparison of the designed driver using different formats of data modulation was carried out using pseudorandom binary sequences. The simulation results show that with a peak current of 33 for the PWM scheme, the maximum power consumption is at 100 mW.

6.3. Modulation Schemes and Dimming. In VLC, the modulating signals are carried by the optical intensity (power) of the illuminating source, for instance, an LED. Directly modulating the intensity of such a source carrying signal requires both a real and positive valued signal [3, 4, 135]. Therefore, amplitude and phase modulation techniques are not feasible for VLC. A provision of illumination and data transfer also poses some problems relative to dimming support and flickering [98]. Dimming support is crucial as it paves way for high energy efficiency and power saving. Moreover, dimming enables users to be able to communicate even when they require to reduce the brightness level of the occupied space. The fluctuations of the illuminance levels, termed flicker, pose a hazard to human beings. Therefore, mitigation measures must be taken into consideration when designing modulation schemes in order to constrain fluctuations within a certain time period so that the flicker is not perceivable by the human eye. Flicker frequency of over approximately 200 Hz is generally and widely considered to be safe. To safely and fully support illumination and communication, modulation techniques should reckon with issues that are associated with dimming and flickering [136]. In this paper, we will particularly discuss modulation features and properties of on-off keying (OOK), pulse modulation techniques, CSK, and

optical OFDM ($O-$ OFDM) as they are commonly used in VLC. As a way of curbing flicker, run-length limited (RLL) coding is integrated in these modulation techniques to prevent long sequences of ones and zeros. Moreover, the RLL strings are used for clock and data recovery. Error correction may be executed by the adoption of forward error correction (FEC) techniques like Reed Solomon (RS) [21, 22, 91, 98, 137].

6.3.1. On-Off Keying. OOK is one of the most straightforward modulation schemes which are easy to implement. It is fundamentally based on switching the LEDs between on and off states to modulate data. The former represents a high data bit (1) whereas the latter represents a low data bit (0). The presence of an optical pulse that takes on all or part of the bit duration corresponds to a high data bit, and the unavailability of an optical pulse corresponds to a low data bit. The nonreturn-to-zero (NRZ) and return-to-zero (RZ) techniques can both be applied for the OOK scheme as OOK-NRZ and OOK-RZ, respectively. For OOK-RZ schemes, a pulse that its period is only a fraction of the bit duration is transmitted as a high data bit, whereas in OOK-NRZ the pulse is transmitted as a high data bit if its period is equal to the duration of the bit.

During the early stages, a demonstration of 10 Mbps data rate using OOK-NRZ and WLEDs was carried out in [138]. With efforts to exhibit an improved system in terms of performance, a blue filter was used in [139] to increase the bandwidth by removing the yellow component of the phosphor-coated LED. As a result, an improved overall data rate of 40 Mbps was achieved. Consolidation of blue-filtering and equalization techniques at the receiver for OOK based systems leads to improved system data rates; this was validated by [140, 141] with each attaining a data rate of 100 Mbps and 125 Mbps, respectively.

The use of a different type of photodetector and OOK-NRZ results in higher data rates. A data rate of 230 Mbps using an APD instead of a PIN PD was demonstrated in [142]. Instead of using all of the three RGB-LED chips for data transmission, authors in [143] used only the red chip for data transfer while the other two were for the provision of illumination. The achievable data rate was recorded to be 477 Mbps using OOK-NRZ. In [144], the authors improved the data rate from 477 Mbps to 614 Mbps by making use of duobinary technique and transceiver equalization. The use of blue filtering, preemphasis circuits, and postequalization circuits based on OOK-NRZ was demonstrated in [145, 146]. The bandwidth of phosphorescent WLED-based VLC link was increased from 3 MHz to 151 MHz for the former and from 3 MHz to 233 MHz for the latter. This resulted in data rates of 340 Mbps and 550 Mbps, respectively. However, in both instances, it was observed that the increase of bandwidth resulted in a decreased wireless communication distance which may be increased by the use of a couple of convex lenses between the filter and the receiver. Authors in [147] exploited OLEDs to implement an OOK system. The maximum achievable data transfer rate for their system was 2.2 Mbps.

Using OOK-NRZ, an overall data rate of 1.5 Gbps through the realization of a GaN-based μ-LED array system inside a CMOS was accomplished by [148]. The array consisted of four μ-LEDs which were modulated concurrently with each μ-LED pixel providing a bit rate of 375 Mbps. Recently, the demonstration of a VLC system based on the exploitation of just one phosphor LD in [149] depicted data rates that are in the range of 1062.5 Mbps to 1250 Mbps. This was accomplished over a distance range of 11.5 m within an indoor setting with an illuminance level of over 500 lx. Blue filtering technique was not applied, and it is anticipated that higher data rates could be achieved if an array of LDs was to be used.

Dimming support for VLC systems that adopt OOK modulation may be facilitated in two ways as defined in [91]. One of the methods is redefining the ON and OFF levels by assigning one of the levels to have a lower intensity. Alternatively, compensation periods may be used. These periods are dependent on the desired dimming level. However, compensation periods lead to low data rates when the lights are dimmed. On the other hand, the former method is able to maintain a constant data transfer rate but decreased levels of dimming leads to a shorter communication range. Additionally, low driving currents of this method may result in color shifts of the LED light.

6.3.2. Pulse Modulation Techniques. We have seen the inception of alternate modulation techniques as a means of addressing the major shortfalls of OOK. These techniques, which their operating principle solely relies on the width and position of a pulsating signal, are described as follows.

(1) Pulse Width Modulation. The PWM technique works in such a way that the duration of pulses is altered according to the required level of brightness, and the individual pulses are used for encoding the modulated signal digitally. In PWM applications, at least one bit of data may be transmitted during longer single pulses while maintaining the exhaustive brightness of the luminaire. This property makes PWM more efficient compared to OOK where each pulse can only transmit a single bit of data during a pulse. In PWM, the data transmission rate of the system is determined by the desired level of dimming. PWM is advantageous in the sense that brightness reduction does not affect the level of intensity for the pulses. Therefore, the effects of color shifting as in OOK schemes are eliminated. A major limitation of this technique is that it has a limited data rate. Nonetheless, a combination of PWM with other techniques such as discrete multitone has promising results on increasing the data rates [21].

(2) Pulse Position Modulation (PPM). When PPM is applied in VLC, a transmitted data bit corresponds to the positioning of a pulse within one of the predetermined time frames of a symbol period. All of the frames have the same length of time. When compared with that of OOK, the PPM system's complexity is elevated since the synchronization process of the data bit and symbol at the receiver must be very accurate. On the other hand, both the average power efficiency and the signal bandwidth of PPM are higher. In spite of this good performance of PPM, there exist several variations of PPM modulation such as variable pulse position modulation, pulse

position modulation-pulse width modulation, pulse interval modulation (PIM), and the dual header PIM [21, 22, 71, 91, 136]. These variants are based on the requirement specifications in terms of performance parameters for which the standard PPM cannot satisfy, and such parameters are higher spectral efficiency and higher data rate. The VPPM technique is based on the amalgamation of PPM and PWM; this technique supports both data modulation and dimming control [91]. Varying the pulse width (duty cycle) of the transmitted data bits controls the brightness of the LED-based on the required dimming ratio. The distinction between a low data bit and a high data bit is characterized by the positioning of the pulse per symbol period. Simplicity as well as the robustness of PPM is maintained with this technique, while it allows the variation of the duty cycle to enable diversified dimming levels. This method has been widely researched in various research efforts such as those in [137, 150–152].

6.3.3. Color Shift Keying. In a CSK system, the transmitted data bit patterns are mapped into the color space of the color (wavelength) band combinations of the multicolored luminaires made up of the trichromatic LEDs (TLEDs) or the quadchromatic LEDs. TLED CSK scheme is specifically standardized by the IEEE 802.15.7 to solve problems of lower data transmission rates and restricted dimming provision faced by other VLC modulation schemes [91, 98]. CSK systems are dependent on the CIE 1931 color space chromaticity diagram which is defined by the CIE in [153]. The chromaticity diagram, which is depicted in Figure 20, is exploited to map the perceivable colors to x and y chromaticity values. Figure 20 also shows all color band centers together with a valid CSK constellation triangle for color band combination ([100], [010], [000]).

The IEEE 802.15.7 standard as outlined in [91] describes the rules and guidelines for the design and implementation of CSK symbol constellations. As seen from the transceiver architecture diagram for an M-ary CSK modulation system shown in Figure 21, a binary stream of data denoted as $\mathbf{b}$ modulates the CSK symbols, where M is the constellation size of the signal. In any of the M-ary CSK modulation schemes, one symbol is used to map one group of $N_b = \log_2 M$ incoming bits. A combination of different wavelengths of the multicolored luminaires is used to modulate the CSK symbols. For TLED CSK, a three-dimensional vector is used to represent a CSK symbol. The said vector contains the intensities of the individual constituents of the produced white light. A CSK symbol denoted by $\mathbf{s}$, can be distinctively defined by $\mathbf{s} = [s_i, s_j, s_k]$ and $\mathbf{s} \in \mathcal{S}$. Each element of $\mathcal{S}$ symbolizes the power of the matching multicolored luminaire LED chip, and $\mathcal{S} = \{\mathbf{s}_0, \mathbf{s}_1, \mathbf{s}_2, \cdots, \mathbf{s}_{M-1}\}$ represents a cluster of all the M valid symbols in M-ary CSK. Solving an optimization problem is required for the determination of the location of the symbols on the xy-plane [91]. This is owing to the dual function of providing both illumination and communication by the LEDs. Various works such as those of [154–156] have studied and evaluated this optimization problem. Describing the optimization problem, with reference to IEEE 802.15.7 standard, the output luminous intensity I of the multicolored luminaire LED chips must be restricted to $0 < s_p < I$ for

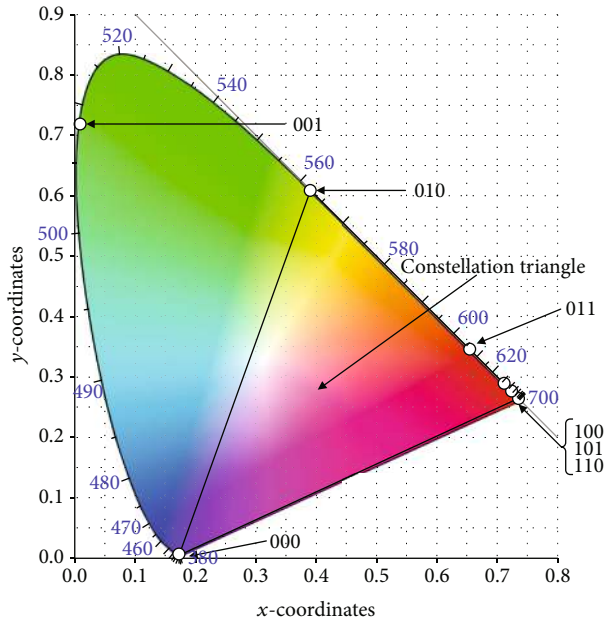

Figure 20: CIE 1931 color space chromaticity diagram, color band centers, and a CSK constellation triangle.

$p = i, j, k$, i.e., distance between the symbols must be maximized to minimize the ISI. Due to the need for a constant luminous intensity of the CSK symbol, which is expressed by.

$$\sum_{p=i,j,k} s_p = I, \tag{59}$$

valid CSK symbols in a three-dimensional space must be equally spread and confined to a triangular area on the $\sum_p s_p = I$ plane so that the combined light which transmits the symbols is perceived as white light [91]. The boundaries of the constellation plane are defined by [157].

$$\begin{cases} s_j + s_k = I \\ s_i = 0 \end{cases}, \begin{cases} s_i + s_k = I \\ s_j = 0 \end{cases} \text{and} \begin{cases} s_i + s_j = I \\ s_k = 0 \end{cases}. \tag{60}$$

The intensity boundary I is conventionally set to unity in order to normalize the symbol intensities s_p.

From equation (59), it can be seen that the three-dimensional representation of the CSK symbols can independently be represented only in two ways without violating any of the abovementioned constraints. As a result, it is then suited and desirable to represent the symbol $\mathbf{s}$ using the CIE 1931 color space which uses a two-dimensional vector denoted by $\mathbf{q} = [x, y]$. For CIE representation, the color bands of the individual LED chips for the multicolored luminaire are combined to establish the vertices of the triangular area which will have all of the valid CSK symbols. These wavelength bands are then mapped into new coordinates of $\mathbf{v}_i = [x_i, y_i]$, $\mathbf{v}_j = [x_j, y_j]$, and $\mathbf{v}_k = [x_k, y_k]$.

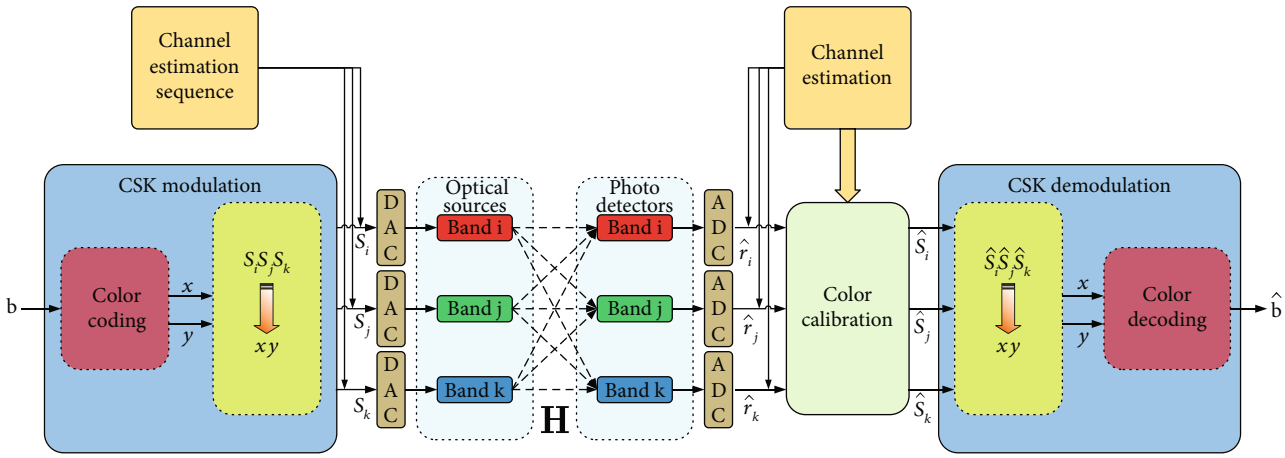

Figure 21: M-ary CSK functional system block diagram.

Table 3: M-ary CSK bands [91].

Band (nm)	Center (nm)	Color code	xy-coordinate
380 – 478	429	000	(0.169,0.007)
478 – 540	509	001	(0.011,0.733)
540 – 588	564	010	(0.402,0.597)
588 – 633	611	011	(0.669,0.331)
633 – 679	656	100	(0.729,0.271)
679 – 726	703	101	(0.734,0.265)
726 – 780	753	110	(0.734,0.265)

The new two-dimensional CSK symbols can now be defined by the following equations.

$$x = s_i x_i + s_j x_j + s_k x_k, \tag{61}$$

$$y = s_i y_i + s_j y_j + s_k y_k. \tag{62}$$

Equations (61) and (62) can be rewritten to yield

$$\mathbf{q} = s_i \mathbf{v}_i + s_j \mathbf{v}_j + s_k \mathbf{v}_k, \tag{63}$$

which subsequently paves way for all $\mathbf{s}$ vectors to be mapped into unique $\mathbf{q}$ vectors. The two-dimensional triangle vertices, $\mathbf{v}_i = [x_i, y_i]$, $\mathbf{v}_j = [x_j, y_j]$, and $\mathbf{v}_k = [x_k, y_k]$ represent the chromaticity values for the center of the wavelength bands. According to [91], there are seven wavelength bands that are used for CSK modulation. The said bands together with their chromaticity centers are as marked in Figure 21. Color codes as well as xy-chromaticity coordinates for each band are presented in Table 3.

IEEE 802.15.7 standard design rules and guidelines in [91] specify the nine-band combinations that dictate the construction of a valid constellation triangle. The standard provides the constellation design specifications for 4-CSK, 8-CSK, and 16-CSK. CSK symbols are created by modulating the intensities of various colors of the valid band combinations of the multicolor luminaire. For instance, depending on the chosen M-ary CSK modulation, the elements of each symbol are then mapped into the red, green, and blue transmitters as shown in Figure 21 using one of the mapping schemes specified in Tables 4–6. The abovementioned tables are with reference to the ([110], [001], [000]) band code combination as standardized in [91] for 4-CSK, 8-CSK, and 16-CSK.

Table 4: 4-CSK symbol mapping [91].

Band center (nm)	4-CSK		
	b	q	s
753	[00] ⇒	(0.734,0.265)	[1 0 0]
509	[01] ⇒	(0.011,0.733)	[0 1 0]
429	[10] ⇒	(0.169,0.007)	[0 0 1]
	[11] ⇒	(0.305,0.335)	[0.334 0.333 0.333]

Table 5: 8-CSK symbol mapping [91].

Band center (nm)	8-CSK		
	b	q	s
753	[000] ⇒	(0.734,0.265)	[1 0 0]
509	[001] ⇒	(0.011,0.733)	[0 1 0]
429	[010] ⇒	(0.169,0.007)	[0 0 1]
	[011] ⇒	(0.452,0.136)	[0.501 0 0.499]
	[100] ⇒	(0.188,0.237)	[0.111 0.277 0612]
	[101] ⇒	(0.470,0.366)	[0.610 0.278 0.112]
	[110] ⇒	(0.252,0.577)	[0.333 0.667 0]
	[111] ⇒	(0.064,0.491)	[0.00050.6660.333]

According to the standard, three of the symbols are mapped to the vertices of the constellation triangle while the other remaining symbols are mapped to positions within the triangle. For the three symbols positioned at the vertices, only one of the LED chips of the multiluminaire is activated for each vertex, i.e., $\mathbf{v}_i$, $\mathbf{v}_j$, and $\mathbf{v}_k$, while the other symbols are

Table 6: 16-CSK symbol mapping [91].

Band center (nm)	16-CSK		
	b	q	s
753	[0000] ⇒	(0.734,0.265)	[1 0 0]
509	[0001] ⇒	(0.011,0.733)	[0 1 0]
429	[0010] ⇒	(0.169,0.007)	[0 0 1]
	[0011] ⇒	(0.064,0.491)	[0.0005 0.666 0.333]
	[0100] ⇒	(0.493,0.421)	[0.667 0.333 0]
	[0101] ⇒	(0.252,0.577)	[0.333 0.667 0]
	[0110] ⇒	(0.305,0.335)	[0.334 0.333 0.333]
	[0111] ⇒	(0.350,0.444)	[0445 0.444 0.112]
	[1000] ⇒	(0.109,0.600)	[0.111 0.777 0.112]
	[1001] ⇒	(0.162,0.358)	[0.112 0.444 0.445]
	[1010] ⇒	(0.116,0.249)	[0 0.336 0.667]
	[1011] ⇒	(0.214,0.116)	[0.111 0.111 0.779]
	[1100] ⇒	(0.546,0.179)	[0.667 0 0.333]
	[1101] ⇒	(0.591,0.288)	[0.778 0.111 0.112]
	[1110] ⇒	(0.400,0.200)	[0.440 0.110 0.451]
	[1111] ⇒	(0.357,0.093)	[0.333 0 0.667]

activated by weighted color intensities of the symbols as seen in column three for each of Tables 4–6. As one would expect, the weighted intensities of the RGB chips, i.e., $[s_i, s_j s_k]$ of the multiluminaire sum up to unity.

The design rules as provided by [91] for 4-CSK, 8-CSK, and 16-CSK are graphically visualized in Figure 22. This visualization is for the band combination of ([100], [010], [000]) as stipulated in Tables 4–6. For 4-CSK mapping, as observed in Figure 22(a), symbols $\mathbf{s}_0$, $\mathbf{s}_1$, and $\mathbf{s}_2$ are mapped to vertices $\mathbf{v}_i$, $\mathbf{v}_j$, and $\mathbf{v}_k$ of the constellation triangle, while symbol $\mathbf{s}_3$ is mapped to the centroid of the triangle. With 4-CSK specification, the Euclidean distances of the CSK symbols are maximized. From the graphical depiction of 8-CSK mapping shown in Figure 22(b), it can be seen that symbols $\mathbf{s}_0$, $\mathbf{s}_1$, and $\mathbf{s}_2$ are mapped to vertices $\mathbf{v}_i$, $\mathbf{v}_j$, and $\mathbf{v}_k$ of the constellation triangle, while $\mathbf{s}_6$ and $\mathbf{s}_7$ are, respectively, mapped to the xy-chromaticity points that divides each of the $\mathbf{v}_i\mathbf{v}_j$ and $\mathbf{v}_j\mathbf{v}_k$ sides of the triangle into two lengths with a ratio of 1:2. Symbol $\mathbf{s}_3$ is mapped to the midpoint of side $\mathbf{v}_k\mathbf{v}_i$. Symbols $\mathbf{s}_4$ and $\mathbf{s}_5$ are mapped to the centroids of triangles $\mathbf{s}_3\mathbf{s}_7\mathbf{s}_2$ and $\mathbf{s}_3\mathbf{s}_6\mathbf{s}_0$, respectively. Figure 22(c) displays constellation mapping for the design of 16-CSK modulation. Like the previous two specifications for 4-CSK and 8-CSK, symbols $\mathbf{s}_0$, $\mathbf{s}_1$, and $\mathbf{s}_2$ are mapped to vertices $\mathbf{v}_i$, $\mathbf{v}_j$, and $\mathbf{v}_k$ of the constellation triangle, while $\mathbf{s}_4\&\mathbf{s}_5$, $\mathbf{s}_3\&\mathbf{s}_{10}$, and $\mathbf{s}_{12}\&\mathbf{s}_{15}$ are mapped to the xy-chromaticity points that divides each of the $\mathbf{v}_i\mathbf{v}_j$, $\mathbf{v}_j\mathbf{v}_k$, and $\mathbf{v}_k\mathbf{v}_i$ sides into three lengths with a ratio of 1:3. Symbols $\mathbf{s}_{13}$, $\mathbf{s}_7$, $\mathbf{s}_8$, $\mathbf{s}_9$, $\mathbf{s}_{11}$, and $\mathbf{s}_{14}$ are the centroids of the six smaller triangles that share one or two sides with the main constellation triangle. Additionally, it can be seen that joining symbols $\mathbf{s}_7$, $\mathbf{s}_9$, and $\mathbf{s}_{14}$ result in another small triangle which is congruent with 9 other small triangles as shown in Figure 22(c). With that in mind, it can be concluded that the 16-CSK constellation symbols can be mapped to the vertices and centroids of merely four small and congruent triangles that have the same design settings as those of a 4-CSK design [157].

The two-dimensional vector $\mathbf{q} = (x, y)$ of symbol $\mathbf{s}$ is created by the intensities $[s_i, s_j, s_k]$ of the three LED chips of the multiluminaire. The intensity vector $\mathbf{s}$ can be easily obtained from the two-dimensional vector $\mathbf{q}$ using any of the band combinations specified in [91]. An example of this conversion using the same band combination used in Table 5 is demonstrated as follows.

Let us consider the 8-CSK modulation. The symbols are as mapped in Figure 22(b) using the CIE 1931 color space chromaticity values. Given a band code combination of ([110], [001], [000]), the fundamental RGB coordinates to employ for deducing the elements of all the $\mathbf{s}$ vectors are given as $\mathbf{q}_R = \mathbf{v}_i = [0.734,0.265]$, $\mathbf{q}_G = \mathbf{v}_j = [0.011,0.733]$, and $\mathbf{q}_B = \mathbf{v}_k = [0.169,0.007]$. For instance, take symbol s_5 which is represented by $(x, y) = (0.470,0.366)$ in Figure 22(b), its intensity vector is determined by solving a system of linear equations given by

$$\begin{cases} 0.734s_i + 0.011s_j + 0.169s_k = 0.470, \\ 0.265s_i + 0.733s_j + 0.007s_k = 0.366, \\ s_i + s_j + s_k = 1. \end{cases} \tag{64}$$

Solving the system yields $\mathbf{s} = [0.6100.2780.112]$. All other intensity vectors of the constellation points are obtained by repeating the same procedure. Intensity vectors for 4-CSK, 8-CSK, and 16-CSK have been listed in Tables 4–6.

The conversion and mapping process for M-ary CSK modulation is summarized as follows:

(1) Define the constellation triangle with reference to the center wavelength of the chips used for the multicolor luminaire as specified in [91]

(2) Map the data stream to xy-chromaticity values using the constellation triangle to determine the positioning of the symbols

(3) Determine the intensities of the multiluminaire LED chips using equations (59) and (63) to pave way for transmission of symbols by varying the intensities of the symbol elements

In Figure 22, it is seen that the symbols are transmitted on an optical domain channel model by means of three different LED chips of the multiluminaire. These symbols are then received by three different PDs with in-built RGB filters. The PDs will in-turn convert the impinging light photons into electric signals. The optical channel depicted in Figure 22 constitutes a noisy multipath model, which characterizes the channel-instigated aggravations, some of which are the ambient light noise, device noise, multicolor

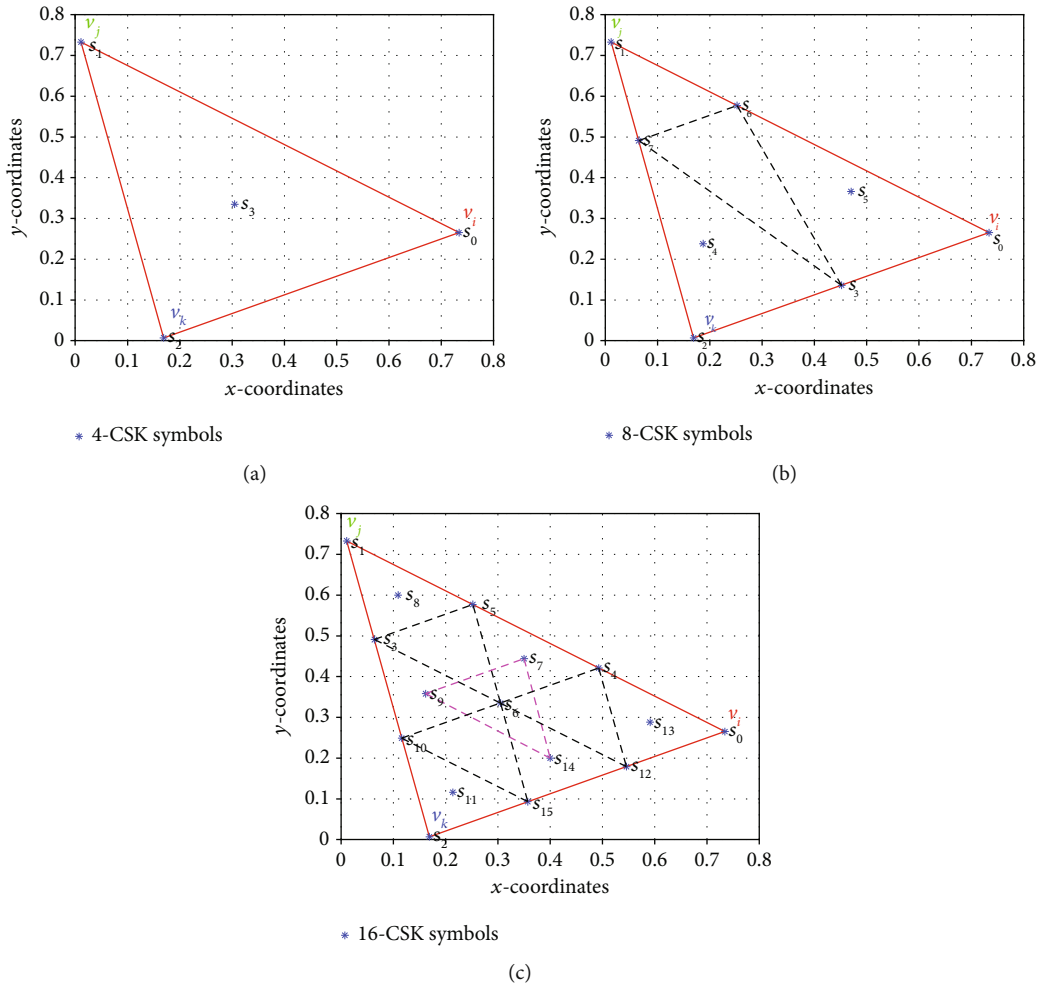

FIGURE 22: M-ary CSK constellation diagrams [91].

interference, and multicolor imbalance. The received symbol $\mathbf{r} = [\hat{r}_i, \hat{r}_j, \hat{r}_k]$, which is corrupted by AWGN, can now be expressed by

$$\mathbf{r} = \mathscr{R}\mathbf{H}\mathbf{s}^{tr} + \mathbf{n}^{tr}, \tag{65}$$

where $\mathbf{H}$ is a 3×3 element matrix denoted by

$$\mathbf{H} = \begin{bmatrix} h_{ii} & h_{ji} & h_{ki} \\ h_{ij} & h_{jj} & h_{kj} \\ h_{ik} & h_{jk} & h_{kk} \end{bmatrix}. \tag{66}$$

The individual entries of $\mathbf{H}$ define the channel gain between a certain pair of the multiluminaire LED chip and a PD. For instance, h_{ki} is the channel gain between LED chip k and PD i, which constitute for the band imposed interference. In essence, the diagonal elements (h_{ii}, h_{jj}, and h_{kk}) equate to the channel gain of the matching band, whereas the interference instituted by other bands is represented by all other elements of the matrix. For simplicity, we consider a point-to-point transmission model. By virtue of negligible propagation factors including dispersion, non-LOS components, and diffuse multipath, the channel matrix may simply be assumed to be an ideal identity matrix [158, 159]. Therefore, in this paper, we consider the CSK system to have an ideal nondispersive AWGN channel. Moreover, $\mathbf{n} = [n_i, n_j, n_k]$ corresponds to the AWGN noise vector. The noise vector $\mathbf{n}$ has a noise variance of σ^2 at the receiver, and each element has a zero mean and a variance of $\sigma_0^2 = \sigma^2 3$. The variance of the AWGN at each detector may be modeled as a summation of the shot noise and thermal noise [156] given by equations (18) and (22), respectively. The $\langle i \rangle$ in equation (18) may be split into two to denote the two components impinging the PD. The said components are the received optical instantaneous power P_r from the source and the atmospheric indoor power P_{sun} from the diffuse sunlight. According to [156], the value of P_{sun} may be approximated to only 11% of the mean value of P_r. The optical SNR of an M-ary CSK system may be expressed as $\gamma_0 = E_b\sigma^2$, where E_b is the average power of all legitimate M-ary CSK symbols and is defined by $E_b = \mathbb{E}\{\|\mathbf{s}\|^2\}$. An estimation of symbol $\mathbf{s}$ defined by $\hat{\mathbf{s}}$, as seen in

Figure 22, is achieved by means of color calibration to compensate for any impairments induced during the signal propagation, and this is defined by [91]

$$\hat{\mathbf{s}} = \mathscr{R}\mathbf{H}^{-1}\mathbf{r}. \tag{67}$$

For demodulation, having obtained the symbol $\hat{\mathbf{s}}$, the signal is converted back to the xy-chromaticity coordinates, and finally, the decoding module is used to retrieve the binary stream of data $\mathbf{b}$ defined by $\hat{\mathbf{b}}$ as shown in Figure 22. To take full advantage of the modulated information for decoding, the a posteriori probability of each symbol $\hat{\mathbf{s}}_m, \hat{\mathbf{s}}_m \in \mathcal{S}$ must be obtained. This probability may be denoted by [157].

$$\begin{aligned}\Pr\ (\hat{\mathbf{s}}_m \mid \mathbf{r}) &= p\,(\mathbf{r} \mid \hat{\mathbf{s}}_{\mathbf{m}})\,\frac{\Pr\ (\hat{\mathbf{s}}_m)}{p\,(\mathbf{r})} \\ &= \frac{\Pr\ (\hat{\mathbf{s}}_m)}{2\pi\sigma\, p\,(\mathbf{r})}\ \exp\ \left(\frac{-\|\mathbf{r} - \mathscr{R}\mathbf{H}\mathbf{s}\wedge_m\|^2}{2\sigma^2}\right),\end{aligned} \tag{68}$$

where $\Pr\ (\hat{\mathbf{s}}_m)$ is the a priori probability of symbol $\hat{\mathbf{s}}_m$. Equation (68) may be represented in the log domain by

$$lr\,(\hat{\mathbf{s}}_m \mid \mathbf{r}) = A - \left(\frac{\|\mathbf{r} - \mathscr{R}\mathbf{H}\mathbf{s}\wedge_m\|^2}{2\sigma^2}\right), \tag{69}$$

where $A = \ln\,[\ \Pr\ (\hat{\mathbf{s}}_m)] - \ln\,[2\pi\sigma\, p\,(\mathbf{r})]$. If there is no a priori information provided, A is the same for all symbols, and $lr\,(\hat{\mathbf{s}}_m \mid \mathbf{r})$ is defined by $\ln\,[\ \Pr\ (\hat{\mathbf{s}}_m \mid \mathbf{r})]$. Symbol $\hat{\mathbf{s}}_m$ can now be estimated using equation (69) as the maximum-likelihood (ML) function and the maximum a posteriori probability (MAP) estimate defined by the following equation [157].

$$\begin{aligned}\hat{\mathbf{s}} &= \hat{\mathbf{s}}_m \in \mathcal{S}\,[\,lr\,(\hat{\mathbf{s}}_m \mid \mathbf{r})] \\ &= \hat{\mathbf{s}}_m \in \mathcal{S}\,\|\mathbf{r} - \mathscr{R}\mathbf{H}\mathbf{s}\wedge_m\|^2.\end{aligned} \tag{70}$$

The symbol $\hat{\mathbf{s}}_m$, with the least distance from the received symbol $\mathbf{r}$, can now be regarded as the legitimate symbol $\hat{\mathbf{s}}$ which is the result of the MAP detection. The symbol $\hat{\mathbf{s}}$ in the end is then decoded and mapped into data bit $\hat{\mathbf{b}}$.

In CSK, dimming is achieved by employing amplitude control. This technique controls the brightness of the LEDs by modulating the driving forward current of the RGB chips of the multiluminaire light source [91, 98]. In different circumstances when there is an inappropriate control of the forward current for amplitude dimming, the color shift of the light source may arise and become a hindrance in the performance of the system. For any of the appropriate dimmer control setting, the optical power of the optical source is unchanged, which suggest that the color of the band center for the constellations is constant. There are no negative impacts due to flickering in CSK because there is no amplitude variation as opposed to other schemes like OOK [98]. Various researchers in the field have proposed and implemented CSK-based techniques to improve the standardized IEEE 802.15.7 CSK scheme.

6.3.4. Optical Orthogonal Frequency Division Multiplexing. This multicarrier modulation scheme is an up-and-rising modulation scheme for OWC technologies, which facilitate the realization of some high-speed optical systems [160], and it has in the past recent years gained momentum for use in VLC. O-OFMD is an adaptation of the conventional OFDM which is widely used for RF technologies due to its clear-cut benefits. Such benefits include ease of implementation because the scheme takes advantage of digital signal processing techniques, high spectral efficiency, and effective subcarrier allocation which leads to maximized data transfer rates as well as its capability to resist ISI and frequency selective fading [92]. To explain O-OFDM, we will start off by outlining a general description of the principles for conventional OFDM. These principles are with reference to the graphical baseband representation in Figure 23.

In the traditional OFDM, the high-speed serial data streams are converted into relatively low-speed parallel data substreams. The use of parallel substream transmission allows for the extension of the pulse width of the symbol. Also, this kind of transmission considerably enhances the robustness of multipath fading resistance [21, 92] which minimizes the intricacy of the receiver's equalizer. The parallel low-speed substreams are then digitally modulated using quadrature amplitude modulation (QAM) or quadrature phase-shift keying. Output symbols from the QAM process are then split into groups where each group is made up of N modulated symbols. Without the consideration of the group index as a way of simplification, a group is defined by a frequency-domain signal $\mathbf{X} = [X(0), X(1), \cdots, X(N-1)]^{tr}$. The next step entails the loading of each of the individual elements denoted by $X(k)$ into one of the orthogonal subcarriers. There are a total of N subcarriers with each loading only one element of $\mathbf{X}$ per transmission. Each subcarrier has a center frequency defined by $2\,\pi$/kN. Symbols are all transmitted concurrently on their subcarriers. Since the subcarriers are not related in any form due to their orthogonality, they can be overlapped, and this greatly increases the bandwidth efficiency. Symbol loading is basically the transformation of $\mathbf{X}$ using the N point inverse discrete Fourier transform (IDFT) which yields a new signal represented by vector $\mathbf{x} = [x(0), x(1), \cdots, x(N-1)]^{tr}$ which is a time-domain signal representing OFDM symbol is obtained using.

$$x(n) = \frac{1}{\sqrt{N}}\sum_{k=0}^{N-1} X(k)\ \exp\ \left(j\frac{2\pi}{N}kn\right). \tag{71}$$

The final step requires the insertion of a cyclic prefix (CP) to the start of each OFDM symbol, and this intercepts the occurrence of ISI between the adjoining symbols. To ensure that there is no ISI, the length of the CP must be chosen such that it is not less than the length of the multipath channel [92, 161].

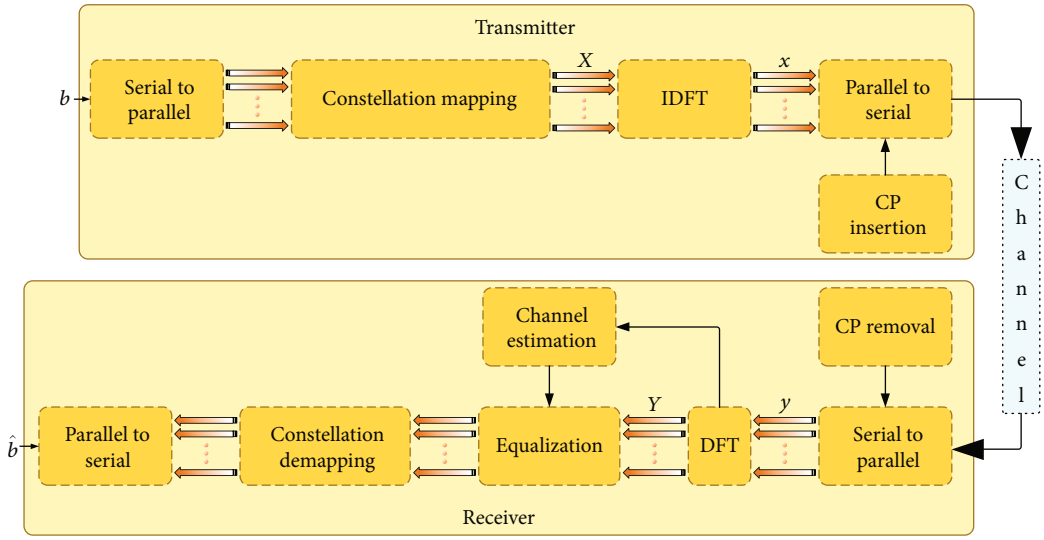

Figure 23: Fundamental OFDM block diagram.

For the process of demodulating the received signal, the modulation process is performed in reverse with an additional process of equalization as seen in Figure 23. Consider a multipath channel with an impulse response expressed as $h = [h(0), h(1), \cdots, h(N-1)]^{tr}$, the received signal of this channel can be denoted by

$$r(n) = h(n) * x_c(n) + z(n), \tag{72}$$

where $*$ represents linear convolution, $x_c(n)$ is the OFDM symbol with the CP, and $z(n)$ is the AWGN with zero mean. The first step in recovering the signal is to remove the appended CP, and this results in vector $\mathbf{y}$ with a length of N and $\mathbf{y}$ is given as

$$y(n) = h(n) \circledast x(n) + z(n). \tag{73}$$

Based on the signal processing theory which states that circular convolution of signals in the time-domain is the same as simply obtaining a product of signals in the frequency-domain, N point discrete Fourier transform (DFT) of $y(n)$, $h(n)$, and $z(n)$ can be defined as $Y(k)$, $H(k)$, and $Z(k)$, respectively. Therefore, the signal can be represented in the frequency-domain by

$$Y(k) = H(k)X(k) + Z(k), \quad k = 0, 1, \cdots, N-1. \tag{74}$$

From equation (74), we can observe that the symbol $X(k)$ is transmitted in a frequency flat channel with an impulse response $H(k)$ in separate subcarriers which do not interfere with one another. This property makes it relatively easier to perform equalization because the recovery of $X(k)$ from each carrier can be performed with either zero forcing (ZF) of minimum mean square error (MMSE), which is a one-tap equalization technique. The recovered signal can be expressed using [161].

$$X(k) = \begin{cases} \dfrac{Y(k)}{H(k)}, & \text{ZF}, \\ \dfrac{H^*(k)Y(k)}{|H(k)|^2 + \sigma^2}, & \text{MMSE}. \end{cases} \tag{75}$$

By reason of the need for real-valued and nonnegative signals for IM/DD, the modulating signal should be a real time-domain signal. Therefore, the depiction in Figure 24 should be altered to make it suitable for VLC adaptation. The alteration involves the inclusion of the Hermitian symmetry module before the IDFT block as well as the clipping module after the parallel-to-serial conversion module or the DC-bias block depending on which mode of obtaining a unipolar signal is used [160]. Obtaining a real time-domain signal is commonly achieved by firstly making the frequency-domain signal $\mathbf{X}$ conform to the Hermitian symmetry constraint. Secondly, the Hermitian-imposed signal is converted to a unipolar signal. This conversion is due to the fact that the conventional OFDM signals are bipolar. There are many ways in which the Hermitian symmetry conforming signals can be converted to unipolar signals and the most prominent are the DC-biased O-OFDM (DCO-OFDM) and asymmetrically clipped O-OFDM (ACO-OFDM) [21, 22, 92, 161]. However, the conversion of signals to unipolar consequently degrades the spectral efficiency since the available bandwidth is reduced by half [162, 163]. In the case of DCO-OFDM, all of the initial OFDM subcarriers are combined with an appropriate positive DC-bias. An appropriate DC bias value would be a value that results in the mean value of the positive signal that lies at the midpoint of the optical source's linear range [161]. The negative part of the combined signal is clipped in order to remain with only the positive unipolar subcarriers [135, 164, 165].

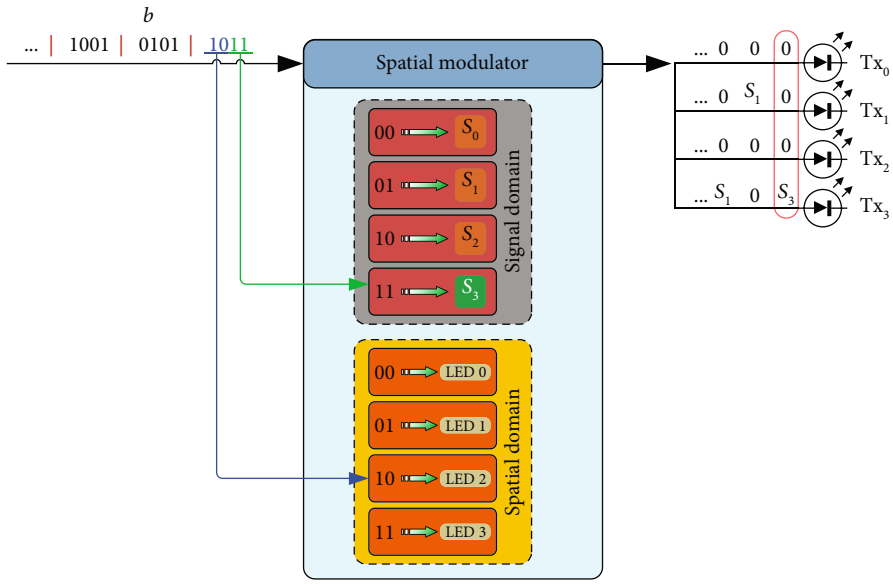

Figure 24: Optical spatial modulation method.

Nonetheless, clipping is known to pose nonlinear distortions which leads to performance degradation as it was investigated in [166]. As an addition, this method is less energy efficient due to its high power consumption at optimal levels which is achieved by bit and power loading [22]. For ACO-OFDM, the even subcarriers are replaced by zeros while only the odd subcarriers are modulated, and this results in antisymmetrical real-valued signals [166]. With this, it is safe to clip the negative part of the OFDM signal without any distortions [162]. Despite the higher energy efficiency of the ACO-OFDM, it has lower spectral efficiency because it uses only half of the subcarriers in comparison with DCO-OFDM which has approximately double the spectral efficiency of the former.

With reference to the conventional frequency division multiplexing, the spectrum of the subcarriers does not overlap with each other. In O-OFDM, however, the subcarriers are overlapped with one another in order to allow for an improved spectral efficiency. For distortion-free recovery, the subcarriers should be orthogonal for the period length of the signal. Nonlinearity of the LED luminaires and the limited availability of dimming support techniques are the two major drawbacks of O-OFDM [21, 160, 167, 168]. The effects of nonlinearity which have been found to most likely affect systems with a higher dynamic range since they have a high peak-to-average power ratio (PAPR) were investigated by various research works like those of [135, 167]. On the other hand, a couple of research works worked on innovating new techniques to enable and improve dimming control in OFDM systems [169, 170]. Higher PAPR has been found to be mitigated in different ways, and these can be found in [167, 168]. In spite of all the challenges, O-OFDM is still a highly regarded modulation scheme with staggering data rates in the range of several Gbps through the use of just a single LED [171–173]. Recently, there are few contributions to the state of the art for high-speed OFDM VLC systems. An experiment to demonstrate a data rate of a 10.72 Gb/s WDM VLC system over a distance of 1 metre through the use of 64-QAM DMT was carried out in [174]. The authors used a commercial single-packaged LED consisting of six LED chips. To enhance the data rate and the performance of BER in this system, preequalisation and postequalisation techniques are used. Other significant and experimental works include those of [175, 176] a VLC system based on the use of phosphor-based white light was demonstrated. The data transmission data rate of 2.705 Gbit/s using 16-QAM OFDM was accomplished over a distance of 1.5 m at an illuminance level of 545 lx. The authors in [175] also used phosphor-based white light to demonstrate a VLC system that produced a data rate of 6.915 Gbit/s using a single channel. This data rate was achievable over a distance of 1.5 m without the use of a blue optical filter. On the receiver side, a beam of white light was measured and found to have a 14 cm diameter and an illuminance level of 795 lx. This system is capable of concurrently providing illumination and data transmission within the stipulated propagation distance. Details of other experimental works of high-speed VLC based on the use of multicolour LEDs and OFDM instead of phosphor-based LEDs can be found in [177, 178].

The three physical layers for VLC are specified in [91] by the IEEE 802.15.7 standard as PHY I, PHY II, and PHY III. PHY I, which typically yields data rates in the range of 11.67 kbps to 266.6 kbps operates at an optical clock rate not exceeding 400 Hz. In addition, PHY I is designed for just one light source which makes it suitable for single-carrier modulation schemes being the OOK and VPPM. PHY I is found mainly in outdoor applications since the light sources switch at a slow rate because of high LED driving currents. On the other hand, PHY II is operational at an optical clock rate of less or equal to 120 MHz yielding data rates of 1.25 Mps to 96 Mbps. Typical applications for PHY II are those of indoor scenery where there are mobile and portable devices that use fast-switching LEDs. Just like the PHY I, PHY II also supports single-carrier modulation schemes

and single light sources. One other physical layer as defined in [91] operates at an optical clock rate of at most 24 MHz. This clock rate happens to be the maximum clock rate for TLED multiluminaire sources [21, 98]. The achievable data rates for PHY III are from approximately 12 Mbps to 96 Mbps. Specific data rates within the specified ranges of the three physical layer modes are determined by four metrics which are optical clock rate, the choice of modulation scheme, the use of the RLL, and the FEC codes [21, 91, 98]. The revision of [90] in [91] resulted in the addition of three more PHY layers for OCC. The said layers are defined as PHY IV, PHY V, and PHY VI. The use case for PHY IV is when discrete light sources are used and the maximum achievable data rate is 22 kbps, depending on the modulation scheme selected as per Table 79 in [91]. The PHY V is developed with the intension of being used in scenarios where there is availability of diffused surface light sources. The maximum achievable data rate is 5.71 kbps, depending on the modulation scheme selected as per Table 79 in [91]. As for the PHYIV, it is intended for use with video displays and with varying data rates in the scale of a few kbps as per the modulation schemes defined in Table 79 by [91]. Owing to the predominance of present day devices, which are equipped with optical cameras and LEDs, the facilitation of OWC implementation becomes seamless. This simplicity is propelled by the fact that in OCC there is already an LED flashlight and imaging sensors of the camera, and these two components forms a transmitter-receiver pair. Different research outputs based on OCC have been and continue to be released and published. For a more detailed discussion on OCC, the reader is referred to some of the notable and experimental research work found in [179, 180].

6.4. MIMO and Multiple Access Schemes. It is conventionally a standard practice to make use multiluminaires for the provision of adequate levels of illuminance for various environments. In most cases, at least as of recent, the luminaires have several LEDs, which have the capability of being used as transmitters to facilitate for the design and implementation of optical MIMO systems for VLC. With a similar objective as in RF MIMO systems, optical MIMO utilizes multiple LEDs to significantly improve the performance of VLC systems from the transmission point of view [12, 22]. Normally, these enhancements come about the utilization of spatial multiplexing which increases the system's throughput or by the use of spatial diversity which decreases the BER [181]. The spectral efficiency is greatly enhanced due to the fact that there is an establishment of a parallel communication platform. This platform is created when transmitters with multiple light sources are used in conjunction with receivers which have multiple detectors [21]. Consequently, this results in augmented data transmission capacity in contrast to when there is a single transmitter-receiver pair. Furthermore, the use of the optical MIMO technique makes it easy to come up with mobile optical wireless schemes where there is no need for stringent alignment of the transmitter and receiver [182, 183]. However, it has been shown in the literature that the use of spatial multiplexing for optical MIMO is not an effective technique for enhancing the data transmission rates for nonimaging receivers [182].

In comparison with RF MIMO, the design and implementation of optical MIMO systems for VLC are not easy by reason of limited spatial diversity [21]. This limitation is mostly prevalent in indoor applications where the paths taken by the impinging signals from the transmitter to the receiver are less diverse as opposed to naturally diverse paths in RF MIMO systems. Works on spatial diversity with reference to optical MIMO are given in [97, 176–179]. Another issue faced in VLC MIMO is attributed to the design of the optical MIMO system receiver which is commonly designed as either nonimaging or imaging receivers [176, 182]. For a nonimaging receiver, a group of PD is arranged without any dependence on each other, and each of the PDs has its own optical concentrator [178]. This kind of receiver is favorable in systems where there is a need for very high gain which can be easily provided because of the narrow FOV of the individual PDs. Nonetheless, this technique comes with a shortfall of a very tight requirement for the alignment of a transmitter-receiver pair on account of the narrow FOV. A slight misalignment of this pair will drastically reduce the spectral capacity of the system [21]. As for imaging receivers, image sensors are employed as constituents of the receiver. An image sensor is basically a composite of an imaging optical device such as a projection lens as well as a large array of PDs. Such a sensor subsequently creates an adequate FOV which greatly reduces the need for the tight alignment of the transmitter-receiver pair [178, 179, 183]. On the other hand, the limitation of such receivers is that there is the need for exceptional image processing for the creation of a MIMO channel that has a high level of efficiency, and as an addition, each of the PDs have a constrained gain. Another factor which reduces the throughput of systems based on imaging sensors is the low sampling rate of the sensors [21].

There are three most common types of algorithms for VLC MIMO, which have been implemented by various researchers in the literature, and these are repetition coding (RC), spatial multiplexing (SMP), and spatial modulation (SM) [184–186]. The most elementary and easy to understand technique is the RC in which all the transmitters are simultaneously transmitting the same data signal. The spectral efficiency and the computational complexity of the RC algorithm are given by $\log_2(M)$ and $M(2N_tN_r + N_r - 1)$, respectively [184]. N_t is the total number of transmitters, and N_r is the total number of photodetectors. This algorithm performs well when designed for FSO schemes due to its transmit diversity [1]. Moreover, the transmitted signals from different transmitters add up constructively on the receiver, and this increases the overall gain of the system. For SMP, all the transmitters are simultaneously transmitting different data signals. The enhanced spectral efficiency (in contrast to RC technique) and the computational complexity of the SMP algorithm are given by $N_t \log_2(M)$bit/s/Hz and $M^{N_t}(2N_tN_r + N_r - 1)$, respectively [184]. In essence, SMP leads to the creation of parallel multiple single-input single-output (SISO) data streams. With this type of transmission, there is a challenge since it is highly mandatory for the transmitter-receiver pair to be accurately aligned with one

another so that interchannel interference (ICI) may be mitigated [21]. One other MIMO technique is the SM where only a single LED of the transmitter array is activated for the entire transmission duration of one data symbol, while all other LEDs are in idle mode. To all intents and purposes, the constellation diagram of the signal is broadened by introducing an extra dimension referred to as the spatial dimension. This additional dimension is for the transmission of auxiliary bits. The individual transmitters of the transmitting array are only activated one at a time when their preassigned unique spatial symbol is harmonious with the random spatial data symbol to be transmitted [97, 184, 187].

On the transmitter side, the data bits are classified into data symbols. Eventually, the bits of each data symbol are delineated into two data-carrying domains being the spatial and signal constellation domains [180, 184]. Both the spatial and signal domains are used to transmit the information at the same time. Thus, SM yields a higher spectral efficiency of $\log_2(MN_t)$/bit/s/Hz with a computational complexity of $MN_t(3N_r - 1)$. The most significant bits of each data symbol are mapped by the spatial modulator into the spatial domain and the point at which the symbol is mapped is the one that decides on which LED is selected. The remaining least significant bits are then mapped into the signal domain, and this symbol dictates the level of the optical intensity that is emitted by the activated LED [180, 184]. The symbol point mapped into the signal domain propagates the channel through any of the digital modulation schemes including PAM, OOFDM, and CSK. However, some modulation schemes such as PAM need to be modified in order to avoid the transmission of signals that have their intensities set to zero as they would lead to the loss of spatial information on the receiver side [184] because none of the transmitters will be activated.

The transmitted signal is then detected on the receiver side by an array of PDs. The path for a specific transmitter-receiver pair is characterized by its channel impulse response as defined by equation (32). The spatial placement of each LED determines the channel conditions of the optical signal which are unique for any given LED [3]. To that end, the receiver estimates the transmitted data symbol based on the channel experiences of each and every propagating signal on the corresponding transmitter-receiver path independently. With that being said, a prior knowledge of $h(t)$ of all the propagation paths for each transmitter-receiver pair is essential on the receiver side. Normally, the ML criterion is exploited for this estimation, and, therefore, the estimation of the received data symbol can be performed in a similar manner as specified in Section 6.3.3 by equation (70). Here, the smallest Euclidean distance is computed between the received signal and a set of all legitimate combinations in the spatial and signal domains [180, 184], hence, enabling the possibility of spatial domain symbol detection. Due to the property of having only one transmitter emission per symbol duration, SM is completely robust to ICI, and this makes it less complex to decode the transmitted symbols in contrast with other techniques used in MIMO [97, 180].

For illustration of SM operation, consider the encoding SM technique using 4-level PAM with constellation size of $M = 4$ and $N_t = 4$ optical transmitters as shown in Figure 25. The data stream **b** is divided into data symbols according to the digital modulation level. These groups are then encoded by the spatial modulator which sequentially maps the bits into their corresponding transmitter index and constellation point. In the case of this example, the first data symbol to be transmitted contains the bit sequence "1011." Therefore, the transmitter being activated for signal emission of these bits is that of LED 2. LED 2 corresponds with the most two significant bits "10" which are mapped into the spatial domain. The least two significant bits, "11," are then mapped into the signal domain at constellation point denoted by $\mathbf{s}_3$.

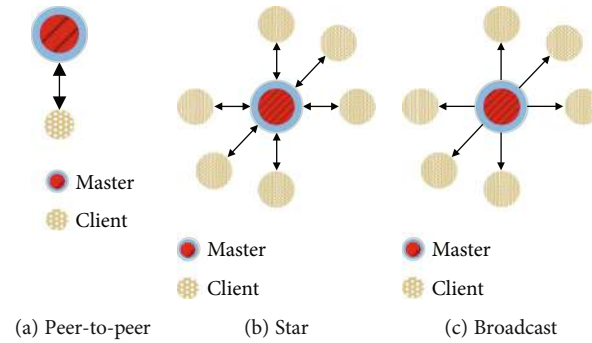

Figure 25: MAC topologies for the VLC link layer.

SM has been explored based on the merit of its performance over other MIMO techniques in order to improve it further. Authors in [188, 189] have demonstrated that the performance of SM can be improved by creating a power imbalance between the LED transmitters in the event that there is a very high correlation between the optical paths. In [190], the authors implemented a technique that can be used to invalidate the high channel correlation caused by power-imbalance in OWC systems. With their proposed technique, the authors optimized the channel parameters in order to maximize the associated capacity constraint. With the consideration of the partial availability of channel state information (CSI), the system performance of SM was investigated in [191]. The investigators concluded that there is a mandatory need for a high degree of accuracy in CSI estimation in order to unleash the full potential of SM. Some researchers have gone further and implemented schemes that allow for the exploitation of activating more than one transmitter per symbol duration instead of just one. Such works can be found in [188, 192]; these schemes are termed generalized spatial modulation techniques. The adaptability of these schemes in activating more than one LED has led to improved spectral efficiency. In spite of that, this adaptability comes at an expense of having to deal with sophisticated design with regards to symbol constellation.

Link layer services such as media access control are vitally important when there are more than one LED transmitters which are radiating and connected to photo-receiver devices. The IEEE standard in [91] details a proposal of VLC link-layer topologies as peer-to-peer topology, star topology, and the broadcast topology. Figure 25 graphically represents the

abovementioned link-layer topologies. The choice of the link layer to be exploited solely depends on the type of VLC application.

In a peer-to-peer topology, one of the devices acts as a master of the channel link between the connected devices being referred to as the clients. Communication between the two connected devices is not restricted due to the availability of the uplink for the client to the master. Such a topology is suitable for applications of contactless communication systems such as near-field communication. When a variety of client devices are connected and communicating to some device which is acting as a master device, the topology is said to be a star topology. Wireless access networks are one of the systems that take advantage of this kind of topology. The fact that the transmission signals are in the same collision domain makes it a challenge is establishing star topologies for VLC MAC layer designs [21]. In a case of broadcast topology, there is a similarity with star topology except that the client devices cannot transmit to the master but only receive since there is no uplink to the transmitter. This property simplifies the MAC layer design as compared to star topology. Application examples for this kind of topology include data broadcasting services to various devices in a wireless network.

From another perspective of the link layers, typical schemes that are used for MAC are described as follows.

6.4.1. Optical Orthogonal Frequency Division Multiple Access (OOFDMA). For OOFDMA, specific groups of subcarriers are allocated to multiple users per time slot [193], and it is merely an extension of OOFDM which is functioning on the physical layer. This innovation has been studied and investigated by various research fields including the works of [193–196]. Duque et al. [193] found out that major problems faced by OOFDMA are decoding complexity and power efficiency faced by VLC technology. An experimental demonstration by [194] showed that using OOFDMA can provide both communication and indoor positioning. The authors exploited QPSK, and the experimental results showed that the developed system yields an error vector magnitude at 15 and a mean positioning error of 1.68. Chen et al. [195] developed a VLC system where they used joint transmission of the signals from multiple LEDs together with OFDMA. It was shown that the signal to interference and noise ratios for users at the edge of a cell can be substantially improved. Additionally, there was an increase in the system throughput of such a VLC system can be higher than that of RF-based systems due to IM which leads to reduced CCI while using coordinated multipoint transmission.

6.4.2. Optical Carrier Sense Multiple Access (OCSMA). In [91], random medium access is defined by two categories where the master can have its beacons activated or deactivated. When the beacons are activated, the entire time slot is divided into intervals that are equivalent to the beacon time length. The frame intervals which are bounded by the beacons are a composite of contention access periods (CAP) and contention-free periods (CFP). Additionally, it contains multiple guaranteed time slots (GTS). For the client to transmit, it first needs to determine the next available "back-off" slot. Once this slot has been located, the client hangs on for a couple of random "back-off" slots, and then it performs the clear channel assessment (CCA). The client will start transmitting in the event that the CCA determines that the channel was not busy, if busy, the clients wait for some extra random buts and then it repeats the CCA. In a scenario where the beacons are disabled, media is accessed by the use of an unslotted random channel access. Transmission takes place only in the event that the client was able to detect that the channel is free during the random "back-off" period; otherwise, the client waits for the next random "back-off" period. Some of the works on CSMA can be found in [197, 198].

6.4.3. Optical Code Division Multiple Access (OCDMA). This scheme has been explained, analyzed, exploited, and implemented for optical systems including VLC in research works such as in [199–202]. Other researchers have implemented novel approaches with an aim of improving the performance of the scheme, and some of the works are in [203, 204]. In OCDMA, access to one channel is facilitated by optically orthogonal codes for multiple users. The idea is that all devices in a network are allocated a unique binary sequence (code) in order to be able to encode information in the time domain by way of switching the LED between high and low states. This scheme can be divided into two methods, and they are synchronous OCDMA [203] and asynchronous OCDMA [205]. The former method uses a set of synchronized codes to decode and distinguish the users; however, this method suffers the effects of multipath reflections and faces challenges when it comes to synchronization [201, 206]. The latter makes use of pseudonoise (PN) codes to identify each user. Using PN codes is able to somewhat solve the synchronization problems for the former method; however, there is an elevated multiple access interference when the number of users increased [201].

7. Open Challenges of VLC

There are a number of challenges that are faced by VLC technology, and these are widespread in various aspects that are crucial for the practical implementation of VLC systems with their full potential of providing high-speed networking. In this treatise, we outline some of the major areas that need more work in order to achieve the ultimate potential that can be offered by VLC.

We have observed that other link configurations have not been given much attention; most works are focused on implementing and evaluating systems that employ LOS links. However, such systems are not suitable for indoor applications by reason of strict alignment and shadowing between the transmitter-receiver pair. A slight misalignment of the receiver-transmitter pair as well as any obstruction between the pair degrades the performance of the system in terms of speed and data transmission. This being said, there is a dire need to invent LOS techniques that are capable of adapting to misalignment, shadowing with negligible system degradation which in-turn will improve mobility and wider coverage of the network. Additionally, very little research efforts in optical MIMO technologies have been directed towards other

link configurations such as non-LOS and diffuse links. Most of the undergoing research is mainly focused on optical MIMO systems that use LOS links. Due to the nature of mobility of multiple users and their network devices, there is a need for new techniques that can allow users to have a higher degree of freedom while moving around the occupied spaces. Based on this, optimization of the link configurations is still an open challenge that requires further investigation to pave way for ease of application.

Another aspect that is still open for exploration is the development of the uplink and downlink for VLC communication with the existing devices. The majority of the literature is focused only on the transmission from the transmitter LED to the receiver PD (downlink). Currently, all of the newly rolled out devices are equipped with economical and competent optical components, for instance, flashlight. Be that as it may, these components are not suitable for being used for VLC systems owing to their capability of reducing efficiency and posing visual distress to users. Frequent flashing of such components waste a lot of energy, and it causes flickering which is perceptible to the human eye during operation. To avoid these problems, the use of complementary technologies viz. RF and IR has been investigated to be used for the development of an uplink in VLC. Anyhow, the use of these technologies, specifically RF, leads to a very complex system design and network management. The complexity is driven by the use of HetNets which have a very low research output in the literature yet it imposes a lot of crucial challenges including link-layer design and reliable data delivery (handover) from one technology to the other.

The use of multiple LEDs results in a very high spectral efficiency. Besides this positive potential, the nature of light signals to be confined within walls makes it easy to mitigate ICI within confined indoor spaces. On the contrary, densely arranged light arrays in the same room may lead to tremendous degradation of the spectral capacity because of low SINR. MIMO systems are generally used for solving this problem as there is coordination between the interfering signals from different LEDs which in turn results in an elevated SINR on the receiver side. Optimization techniques which involve the rearrangement of transmitting LEDs are also one of the schemes used for reducing the mutual interference of the LEDs. Therefore, there is a need for a thorough analysis of different parameters as well as systematic design procedures in this area so that interference management can be performed with ease.

One important question that is of great importance is what happens when the light is switched off since this technology is intended to perform a dual purpose of illumination and data transfer. The literature suggest that in heterogeneous networks, this problem can be addressed easily by switching to either RF of IR technologies in the event that the user only requires to use data services. Although that is the case, the problem persists in the event that the system only uses VLC technology. This poses a very difficult challenge since the transmission of data is dependent on the luminous intensity of the light sources. Some researchers are on the quest of developing techniques that could pave way for communication even when the lights are dimmed to a certain level that will appear to the human eye as if the lights are off. The dimming of lights at different times of the day differs because the amount of ambient light in the room is not constant. As a result, dimming has been found to be one of the major problems that hinder the progressiveness of this technology, and it calls for the need for new innovative methods.

One other research aspect underway is the adaptation of some existing devices with little or no hardware modifications to be used for the VLC application. Since there are a variety of mobile devices such as smartphones, VLC can be integrated with such devices since they already have optical components including cameras and external LEDs [207–210]. Some of the existing hardware, in particular, the LEDs and PDs, have some limitations that are a hindrance in terms of their cut-off frequencies. Therefore, there is a need for a solid research input into this area to evaluate the materials that are being used for the production of illuminating sources and optical detectors to circumvent the bottleneck. Technological advances on these components can be found in [211].

8. Consolidation of VLC with Current and Upcoming Technologies

Most of the ongoing, emerging, and envisaged wireless communication trends including sixth-generation (6G) among others are shifting to the right of the electromagnetic spectrum to employ higher frequency bands. On the right side of the spectrum, there are a variety of transmission media including mm-Wave links, terahertz links, and optical links. The said links are capable of enabling seamless wireless transmission networks boasting high-speed and low-latency [212]. With this, OWC, in particular VLC, is one of the fairly advancing technological trends that has become more relevant for the evolution and establishment of some of the most recent along with pipelined wireless communication developments. Specifically, the properties of VLC and its objectives as well as those of the recently developed and upcoming techniques qualify the amalgamation of VLC with other cutting-edge technologies of the near future [20, 213, 214]. One may argue that most of the techniques that have been proposed for seeing the realization of future networks are inefficient due to their energy consumption, and they are additionally not economical due to high hardware costs [215] with the exception of VLC. Hence, the need for intensive research efforts in the economically cheap and energy-efficient VLC which when properly developed and designed could pave way for cheap future networks capable of meeting the requirements and demands efficiently.

We present and discuss a number of techniques where VLC has the likelihood of being used for the facilitation of various communication services for several technologies in wireless communication. Various research groups and individual researchers are putting in efforts to undertake research on the feasibility of VLC for future wireless networks. Most of the pursued research interests pay particular attention to various VLC aspects with one common goal. This common goal is to realize methods and techniques that will lead to the commissioning of systems that are suited for seaming less

operation wireless communication systems of the future. The following subsections outline a selected number of innovations which could potentially have VLC used in one or several elements of their methods.

8.1. Fifth-Generation (5G) Networks. The aim of 5G networks is to curb the impediments that are being faced by the previous cellular standards. 5G networks have the capability of supporting an enormous amount of data traffic for a very large number of wireless connections with diverse quality of service (QoS) requirements [216]. This generation of mobile networks has enabled the inception of new revolutionized concepts such as the internet of things (IoT), see [217] for the future IoT. A complete 5G system is designed to meet the specifications of three use cases of 5G. These cases are outlined as enhanced massive mobile broadband (eMBB), ultrareliable low latency communications (URLLC), and massive machine-type communications (mMTC) [218, 219].

The eMBB use case is concerned with the transfer of data in magnitudes of multigigabyte for the end-users by providing an increased system capacity owing to the ever-increasing demands for higher data transfer rates. This use case is mainly focused on the enhancement of systems by tapping into the use of the mm-Wave range of the spectrum to allow the allocation of higher bandwidth. The other use case, which is eMBB, looks into the advancement of antenna arrays which entails the use of hundreds of transmitter and receiver antenna elements. The use of many antenna elements paves way for the introduction of massive MIMO and beamforming. URLLC introduces support for requirements of relatively new applications for industries which are mission critical. Such industries are eHealth, which include remote surgery, and automotive industry, in which we find one of its applications in autonomous driving. One other application supported by URLLC is that of cloud robotics which is classified under the fourth industrial revolution. All of the aforementioned applications under URLLC call for enhanced latency, reliability, availability, and security. The mMTC use case is aimed towards the realization of connecting billions of devices using highly cost-effective means without an overload of the network. Critical aspects that determine the success of mMTC include low power consumption, adequate coverage, longtime availability, and cost efficiency [218]. Be that as it may, the simultaneous facilitation of wireless network services for all the three 5G usage cases will be burdensome. This difficulty faced by the simultaneous facilitation is mainly caused by the proliferation of mobile devices which lead to the congestion of the microwave bands in the radio spectrum [29, 30].

During the development of 5G technology, which is as of present being rolled out for commercialized use around the world [220, 221], VLC was and still is anticipated to be a complementary technique to the mm-Wave technique for short-range indoor-based communication in 5G networks. The motivation for this particular application of VLC in 5G is by reason of evidence and mobile data traffic predictions which have been presented by various studies directed towards VLC and 5G [23, 28, 30, 222]. It has been shown that the majority of data traffic in the future will be contributed by indoor networks. In the near future, it is anticipated that most of the users will spend 80% of the time indoors whereas the remaining 20% of the time will be spent outdoors. One other reason is due to the benefits of VLC which include low cost, high energy efficiency, enhanced capacity, and reduced interference.

In 5G, the prime focus is to incorporate VLC with mm-Wave technology [20, 23, 222]. This embarkation is motivated by the skyrocketing amount of devices [30] which will expand the mm-Wave technology to its full capacity in the future and, hence, affect the data rates. Several researchers have proposed a number of novel approaches that could lead to the practical implementation of a mm-Wave system that is complemented by VLC. Authors in [222] proposed the design of a heterogeneous 5G mobile cellular network architecture with three layers where each layer is intended to address a certain range of coverage and communication requirement. The proposed architecture consists of a macrocell layer, picocell layer, and the optical attocell layer which operates within the visible part of the electromagnetic spectrum, while the macrocell and picocell layers operate below 3 and in the mm-Wave part of the electromagnetic spectrum, respectively. The macrocell is used to coordinate both the picocell and attocell. The focus of their architecture is directed mainly towards the technicalities of optical attocells as well as challenges that come with such technicalities. The authors address the communication mechanisms for the downlink, uplink, and backhaul. From the proposed architecture, one of the main benefits of the proposed architecture include elevated system capacity which is made possible by the use of a great number of smaller cells which are being used to offload data traffic from the larger cells. Another benefit is the improved user experience because the network users acquire higher data transfer rates from both the mm-Wave link and the VLC link. In 5G networks, optical attocells are typically implemented for indoor applications. However, the realization of the uplink is one of the main limiting and difficult challenges for VLC systems; therefore, it is considered to be highly competent for downlink communication while the uplink is achieved through the use of other technologies such as RF and IR.

It is worth noting that other OWC technologies including OCC and FSO are regarded to be used in various subsystems of 5G networks. The application of these technologies on a certain 5G subsystem depends on the environmental setup, i.e., indoor, outdoor, or outer space, and this comes with challenges. A recent survey by [223] outlines and presents with clarity the role of OWC technological development in 5G and 6G. The said survey encircles the prospects, directions, and challenges towards the merger of RF and OWC. A comprehensive summary on the development of OWC research with the perspective of 5G systems is also given in [223]. In spite of the substantial research on OWC for 5G systems, VLC is not at a level where it can be commercialized into the world of consumer markets due to the lack of internationally approved practical techniques. This hindrance is caused by most of the challenges as outlined in Section 7. Therefore, it is anticipated that the incorporation of VLC with RF could be more beneficial beyond 5G innovations

with the view that the development of VLC would have advanced very well before the commercialization of 6G which is expected to be deployed to the world markets by the year 2030.

8.2. Sixth-Generation (6G) Networks. Currently, various institutions and organizations are embarking on the task of developing the system requirements and specifications of beyond 5G networks which include 6G. Following the deployment of 5G, it is highly anticipated that the development and standardization of 6G will take place from 2020 and be completed by the year 2030 [213]. Different countries around the globe are setting up research initiatives that will enable the development and inception of 6G. Many of the prominent initiatives towards 6G are the 6G flagship project in Finland [224] and the establishment of a 6G research center by South Korea which are also in partnership with the University of Oulu in Finland with the aim of developing the 6G networking technologies. Japan, United States of America, and China are also embarking on various activities that are directed towards the progression of 6G [221]. Since 6G networks will be expected to operate optimally while accommodating a very huge amount of data traffic, the most feasible way in which this can be achieved is the use of different noncongested frequency bands. Unlike 5G, 6G is expected to concurrently support all of the three use cases as well as adding some additional use cases. The use cases of 6G are shown in Figure 26.

In [221], these use cases are indicated as the enhanced mobile broadband plus (eMBB-Plus), unconventional data communication (UCDC), three-dimensional integrated communications (3D-InteCom), big communications (BigCom), and lastly secure ultrareliable low-latency communications (SURLLC). As a successor of eMBB in 5G, eMBB-Plus is expected to support mobile communication systems which have elevated standards and specific user requirements as compared to the current systems. It is imperative for this use case to be highly competent in the optimization of cellular networks with regard to big data transmission, handover, and interference mitigation. Subscribers will have access to additional eMBB-Plus services at an economical cost. For instance, there will be accurate indoor positioning, which could be provided by the use of VLC which currently has a very high accuracy in the range of under a few centimeters [225–227]. Another additional functionality with affordable costs is the global compatibility of connections between different mobile networks with thoughtfulness of security and privacy. Moreover, cellular coverage using VLC for indoor scenery is one area which could be directed towards 6G development. VLC cellular coverage has not been yet addressed for inclusion into current cellular systems; therefore, proper consideration of this would see VLC a viable solution for indoor cellular networking. More research efforts will be aimed at the development of new hardware, algorithms for NLOS systems when considered for inclusion in beyond 5G technologies [228].

Unlike the case of 5G, the BigCom in 6G considers to offer and deliver a fair service to both dense and remote areas when compared to 5G which is mostly concerned about great

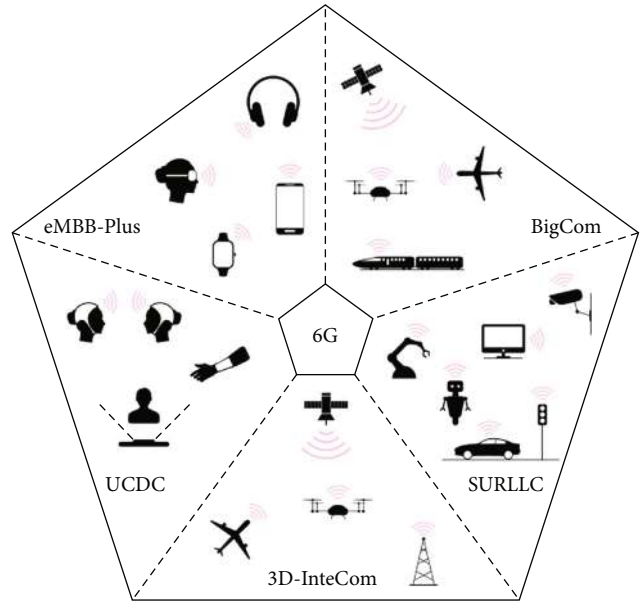

Figure 26: Supported use cases of a 6G network [221].

service delivery for dense areas with less attention to remote areas. However, it should be clearly stated that BigCom in 6G intends to strike a reasonable resource balance between remote and dense areas other than providing equally good service delivery in both areas. The idea with this consideration is to ensure that there is always enough network coverage to allow for the provision of a tolerable service delivery for all subscribers regardless of where they are located. Due to the nature of illumination source positioning for an indoor setup, using VLC for indoor service provision would be relatively easy to determine the fairness of BigCom services within an indoor using fairness techniques such as the Gini coefficient [229] together with the Lorenz curve [230]. SURLLC is a combination of the URLLC and mMTC, this differs from 5G in the sense that the critical reliability requirements are very high at 99.9999999%, and the latency needs not to exceed 0.1. Since the main applications of SURLLC are for industrial and military communications, there is a dire demand for uncompromising precision and security. This being said, future high precision equipment, robots, and vehicular communication will greatly benefit from this use case. Therefore VLC together with its counterpart, being the terahertz communication [231] can be some of the technologies that can enable this in 6G networks.

As for 3D-InteCom, there are motivations that the planning, analysis, and optimization of the network be done in three dimensions instead of two so that there is consideration for the communication nodes at different heights [221]. Such scenarios where the third dimension of height is involved include underwater, satellite, and unmanned aerial vehicle (UAV) communications, and they will greatly benefit from three-dimensional planning, analysis, and optimization. This calls for the amendment and of the analytical framework in [232] based on stochastic geometry and graph theory to bring it up to date so that it fits into 6G technology. Considering the height of the communication node will lead to new

research directions of network optimization such as elevation beamforming for full-dimension MIMO systems [233]. The optimization of OWC networks would be one of the eye-catching technologies on account that it finds application satellite, underwater, and UAV communications. Currently, the UCDC use case does not have a well-defined application framework. However, it is believed to develop into areas such as tactile, holographic, human-bond communications, and other forms of wireless communication that could not be classified into the other four use cases mentioned above [221]. As opposed to the RF technology, which is expensive, heavily regulated, and congested, OWC technologies are capable of meeting the requirements of a wide range of use cases in 6G and the demands from the IoT network. With that being said, different kinds of communications including but not limited to point-to-multipoint, chip-to-chip, point to point, machine-to-machine, and vehicle-to-infrastructure can be supported with ease. The competence of these technologies emanates from the ability to lay out a platform for the setup of small and ultradense networks. Moreover, the power consumption of VLC is very low and this is one of the key requirements for current and upcoming networking generations as well as the IoT paradigm, which boasts a massive connectivity requirement [18]. Since the scope of this work is limited to indoor VLC, which excludes the majority of OWC technologies, the reader is referred to [234] for a detailed role of OWC technologies in 5G/6G and IoT.

8.3. Intelligent Reflective Surfaces (IRSs). The performance of a wireless communication network can be remarkably enhanced by the use of a relatively new technology trend termed IRS [235]. The idea of IRSs is to smartly alter the propagation environment of a message carrying signal by using a large number of passive reflecting elements on a planar surface [236, 237]. The configuration of such a system is illustrated in Figure 27. Each of the reflective elements is capable of controlling the properties such as the phase or the amplitude of the signal by reflecting the incident signal independently. Either the phase or the amplitude (or both) may be considered; for a simple explanation, consider a system where the phase shift is used. The individual phase shifts of each of the reflective elements are altered jointly so that the signal at the receiver may be enhanced or nullified in terms of its energy or maximum achievable data rate. This technique of altering the phase shifts from all paths to the receiver is commonly known as passive beamforming [234, 238].

Due to the nature of VLC channels which suffer from blockages for VLC configurations, the IRSs may be used to combat this challenge of blockage. Just like VLC technology, IRS technology is cheap and is easily adopted for indoor wireless communication systems without altering any communication hardware or habitable spaces owing to their ability to be seamlessly mounted or removed from room planes such as the walls and ceilings. With this, it is highly fitting and desirable to have VLC consolidated with IRSs for application in dense indoor networks including but not limited to shopping centers and airports which are powered by a number of illuminating devices, and in most cases, they have planes which are normally used for advertisements and exhibitions using LED technology. However, despite the efforts of various researchers with the perspective of validating the feasibility of IRS [239–242], there is still a long way to go in terms of design, development, performance analysis, and optimization of IRS-based wireless networks.

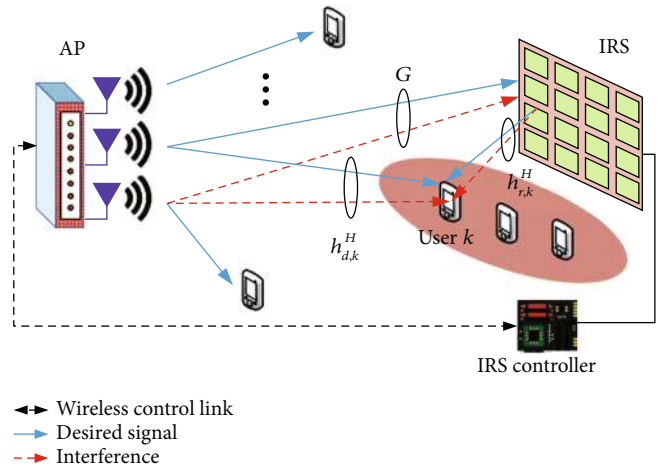

Figure 27: IRS-based wireless communication system [237].

9. Summary and Conclusion

We have provided a relatively understandable and comprehensive tutorial and a survey for indoor VLC. A provision of VLC context within optical wireless communication techniques was laid out to pave way for its use as a complementary technique of RF with efforts to curb the spectrum crunch. The efficiency, in terms of both power and cost-effectiveness of the new solid-state devices used for illumination as well as their ease of adaptation for establishment of communication, is one of the main factors that drive the research on VLC. This paper covers the theory of illumination and optical detection as a means of helping with an elaborate layout of the system architecture as well as the VLC structure. The system architecture helps with the understanding of link configurations, while the structure explains aspects including link characterization. Some of the characterization parameters explained in this paper include modulation techniques, dimming schemes, LED drivers, and link-layer properties for media access control. Additionally, we provide some of the recent developments over the past decade as well as those challenges that are still inhibiting the practicality of VLC. The final section of this paper examines the feasibility of using VLC as one of the enabling technologies for beyond 5G technological trends. Though at an infancy stage, VLC is one of the most eye-catching trends that are capable of delivering highly effective and economical wireless communication services.

In general terms, there is a promising future for this technology in view of the illumination technology which is growing at a very fast pace. With new illumination technologies, we can be able to easily adapt VLC techniques into our daily lives since lighting these days is used in almost every industry, and this will solve many other problems where it is not

feasible to roll out other communication techniques. However, a more intensive research input is needed for the realization of VLC-based future technologies, and the amalgamation with other technologies comes with its own impediments that will have to be addressed before the inception of any practical systems for consumers.

Data Availability

The paper is a review paper. The data sets and codes used in the paper can be found in the relevant references as cited in the manuscript.

Conflicts of Interest

The authors declare that they have no conflicts of interest.

Acknowledgments

We would like to acknowledge the Botswana International University of Science and Technology (BIUST) for research funding. This work was supported by BIUST under grant numbers R00067, R00068 and S00077.

References

[1] M. A. Khalighi and M. Uysal, "Survey on free space optical communication: a communication theory perspective," *IEEE Communications Surveys & Tutorials*, vol. 16, no. 4, pp. 2231–2258, 2014.

[2] M. Uysal and H. Nouri, "Optical wireless communications - an emerging technology," in *2014 16th International Conference on Transparent Optical Networks (ICTON)*, pp. 1–7, Graz, Austria, 2014.

[3] Z. Ghassemlooy, W. Popoola, and S. Rajbhandari, *Optical wireless communications: system and channel modelling with Matlab®*, CRC Press, 2013.

[4] D. Tsonev, S. Videv, and H. Haas, "Light fidelity (Li-Fi): towards all-optical networking," in *Broadband Access Communication Technologies VIII*, San Francisco, California, United States, 2013.

[5] H. Ma, L. Lampe, and S. Hranilovic, "Integration of indoor visible light and power line communication systems," in *2013 IEEE 17th International Symposium on Power Line Communications and Its Applications*, pp. 291–296, Johannesburg, South Africa, 2013.

[6] T. Komine, S. Haruyama, and M. Nakagawa, "Performance evaluation of narrowband OFDM on integrated system of power line communication and visible light wireless communication," in *2006 1st International Symposium on Wireless Pervasive Computing*, pp. 1–6, Phuket, Thailand, 2006.

[7] F. Demers, H. Yanikomeroglu, and M. A. St-Hilaire, "Survey of opportunities for free space optics in next generation cellular networks," in *2011 Ninth Annual Communication Networks and Services Research Conference*, pp. 210–216, Ottawa, ON, Canada, 2011.

[8] F. Khan, S. R. Jan, M. Tahir, and S. Khan, "Applications, limitations, and improvements in visible light communication systems," in *2015 International Conference on Connected Vehicles and Expo (ICCVE)*, pp. 259–262, Shenzhen, China, 2015.

[9] S. Shao, A. Khreishah, M. Ayyash et al., "Design and analysis of a visible-light-communication enhanced WiFi system," *Journal of Optical Communications and Networking*, vol. 7, no. 10, p. 960, 2015.

[10] H. Marshoud, S. Muhaidat, P. C. Sofotasios, S. Hussain, M. A. Imran, and B. S. Sharif, "Optical non-orthogonal multiple access for visible light communication," *IEEE Wireless Communications*, vol. 25, no. 2, pp. 82–88, 2018.

[11] F. Zafar, D. Karunatilaka, and R. Parthiban, "Dimming schemes for visible light communication: the state of research," *IEEE Wireless Communications*, vol. 22, no. 2, pp. 29–35, 2015.

[12] C. W. Hsu, C. W. Chow, I. C. Lu, Y. L. Liu, C. H. Yeh, and Y. Liu, "High speed imaging 3×3 MIMO phosphor white-light LED based visible light communication system," *IEEE Photonics Journal*, vol. 8, no. 6, pp. 1–6, 2016.

[13] X. Huang, J. Shi, J. Li, Y. Wang, and N. Chi, "A Gb/s VLC transmission using hardware preequalization circuit," *IEEE Photonics Technology Letters*, vol. 27, no. 18, pp. 1915–1918, 2015.

[14] S. Nader-Esfahani and M. Afrasiabi, "Simple bit loading algorithm for OFDM-based systems," *IET communications*, vol. 1, no. 3, 2007.

[15] R. Zhang, J. Wang, Z. Wang, Z. Xu, C. Zhao, and L. Hanzo, "Visible light communications in heterogeneous networks: paving the way for user-centric design," *IEEE Wireless Communications*, vol. 22, no. 2, pp. 8–16, 2015.

[16] H. Lee, I. Lee, and S. H. Lee, "Deep learning based transceiver design for multi-colored VLC systems," *Optics Express*, vol. 26, no. 5, pp. 6222–6238, 2018.

[17] L. E. M. Matheus, A. B. Vieira, L. F. Vieira, M. A. Vieira, and O. Gnawali, "Visible light communication: concepts, applications and challenges," *IEEE Communications Surveys & Tutorials*, vol. 21, no. 4, pp. 3204–3237, 2019.

[18] M. Z. Chowdhury, M. T. Hossan, A. Islam, and Y. M. Jang, "A comparative survey of optical wireless technologies: architectures and applications," *IEEE Access*, vol. 6, pp. 9819–9840, 2018.

[19] Y. Zhuang, L. Hua, L. Qi et al., "A survey of positioning systems using visible LED lights," *IEEE Communications Surveys & Tutorials*, vol. 20, no. 3, pp. 1963–1988, 2018.

[20] M. Ayyash, H. Elgala, A. Khreishah et al., "Coexistence of WiFi and LiFi toward 5G: concepts, opportunities, and challenges," *IEEE Communications Magazine*, vol. 54, no. 2, pp. 64–71, 2016.

[21] P. H. Pathak, X. Feng, P. Hu, and P. Mohapatra, "Visible light communication, networking, and sensing: a survey, potential and challenges," *IEEE Communications Surveys & Tutorials*, vol. 17, no. 4, pp. 2047–2077, 2015.

[22] D. Karunatilaka, F. Zafar, V. Kalavally, and R. Parthiban, "LED based indoor visible light communications: state of the art," *IEEE Communications Surveys & Tutorials*, vol. 17, no. 3, pp. 1649–1678, 2015.

[23] S. Wu, H. Wang, and C. H. Youn, "Visible light communications for 5G wireless networking systems: from fixed to mobile communications," *IEEE Network*, vol. 28, no. 6, pp. 41–45, 2014.

[24] A. Sevincer, A. Bhattarai, M. Bilgi, M. Yuksel, and N. Pala, "LIGHTNETs: smart LIGHTing and mobile optical wireless NETworks — a survey," *IEEE Communications Surveys & Tutorials*, vol. 15, no. 4, pp. 1620–1641, 2013.

[25] N. Kumar and N. R. Lourenco, "Led-based visible light communication system: a brief survey and investigation," *Journal of Engineering and Applied Sciences*, vol. 5, no. 4, pp. 296–307, 2010.

[26] D. C. O'Brien, L. Zeng, H. Le-Minh, G. Faulkner, J. W. Walewski, and S. Randel, "Visible light communications: challenges and possibilities," in *2008 IEEE 19th International Symposium on Personal, Indoor and Mobile Radio Communications*, pp. 1–5, Cannes, France, 2008.

[27] S. Cho, G. Chen, and J. P. Coon, "Securing visible light communication systems by beamforming in the presence of randomly distributed eavesdroppers," *IEEE Transactions on Wireless Communications*, vol. 17, no. 5, pp. 2918–2931, 2018.

[28] M. V. Bhalerao and S. S. Sonavane, "Visible light communication: a smart way towards wireless communication," in *2014 International Conference on Advances in Computing, Communications and Informatics (ICACCI)*, pp. 1370–1375, New Delhi, India, 2014.

[29] Cisco, "Cisco Visual Networking Index: Global Mobile Data Traffic Forecast Update, 2016–2021 White Paper," Technical report, Cisco, 2017.

[30] Cisco, "Cisco Visual Networking Index: Global Mobile Data Traffic Forecast Update, 2017–2022 White Paper," Technical report, Cisco, 2019.

[31] I. Filippini, V. Sciancalepore, F. Devoti, and A. Capone, "Fast cell discovery in mm-wave 5G networks with context information," *IEEE Transactions on Mobile Computing*, vol. 17, no. 7, pp. 1538–1552, 2018.

[32] V. Raghavan, A. Partyka, A. Sampath et al., "Millimeter-wave MIMO prototype: measurements and experimental results," *IEEE Communications Magazine*, vol. 56, no. 1, pp. 202–209, 2018.

[33] W. Roh, J. Y. Seol, J. Park et al., "Millimeter-wave beamforming as an enabling technology for 5G cellular communications: theoretical feasibility and prototype results," *IEEE Communications Magazine*, vol. 52, no. 2, pp. 106–113, 2014.

[34] J. Hasch, E. Topak, R. Schnabel, T. Zwick, R. Weigel, and C. Waldschmidt, "Millimeter-wave technology for automotive radar sensors in the 77 GHz frequency band," *IEEE Transactions on Microwave Theory and Techniques*, vol. 60, no. 3, pp. 845–860, 2012.

[35] L. Lu, G. Y. Li, A. L. Swindlehurst, A. Ashikhmin, and R. Zhang, "An overview of massive MIMO: benefits and challenges," *IEEE Journal of Selected Topics in Signal Processing*, vol. 8, no. 5, pp. 742–758, 2014.

[36] E. Björnson, E. G. Larsson, and T. L. Marzetta, "Massive MIMO: ten myths and one critical question," *IEEE Communications Magazine*, vol. 54, no. 2, pp. 114–123, 2016.

[37] E. G. Larsson, O. Edfors, F. Tufvesson, and T. L. Marzetta, "Massive MIMO for next generation wireless systems," *IEEE Communications Magazine*, vol. 52, no. 2, pp. 186–195, 2014.

[38] C. Han, J. M. Jornet, and I. Akyildiz, "Ultra-massive MIMO channel modeling for graphene-enabled terahertz-band communications," in *2018 IEEE 87th Vehicular Technology Conference (VTC Spring)*, pp. 1–5, Porto, Portugal, 2018.

[39] A. Garcia-Rodriguez, G. Geraci, L. G. Giordano, A. Bonfante, M. Ding, and D. Lopez-Perez, "Massive MIMO unlicensed: a new approach to dynamic spectrum access," *IEEE Communications Magazine*, vol. 56, no. 6, pp. 186–192, 2018.

[40] V. Jungnickel, K. Manolakis, W. Zirwas et al., "The role of small cells, coordinated multipoint, and massive MIMO in 5G," *IEEE Communications Magazine*, vol. 52, no. 5, pp. 44–51, 2014.

[41] S. M. R. Islam, M. Zeng, and O. A. Dobre, "NOMA in 5G systems: exciting possibilities for enhancing spectral efficiency," *Computer Repos*, vol. 1, no. 2, 2017, https://arxiv.org/abs/1706.08215.

[42] L. Dai, B. Wang, Y. Yuan, S. Han, I. Chih-lin, and Z. Wang, "Non-orthogonal multiple access for 5G: solutions, challenges, opportunities, and future research trends," *IEEE Communications Magazine*, vol. 53, no. 9, pp. 74–81, 2015.

[43] Z. Ding, M. Peng, and H. V. Poor, "Cooperative non-orthogonal multiple access in 5G systems," *IEEE Communications Letters*, vol. 19, no. 8, pp. 1462–1465, 2015.

[44] T. Cevik and S. Yilmaz, "An overview of visible light communication systems," *International journal of Computer Networks & Communications*, vol. 7, no. 6, pp. 139–150, 2015.

[45] M. L. Pall, "Wi-Fi is an important threat to human health," *Environmental Research*, vol. 164, pp. 405–416, 2018.

[46] ICNIRP (International Commission for Non-Ionizing Radiation Protection) Standing Committee on Epidemiology, A. Ahlbom, A. Green, L. Kheifets, D. Savitz, and A. Swerdlow, "Epidemiology of health effects of radiofrequency exposure," *Environmental Health Perspectives*, vol. 112, no. 17, pp. 1741–1754, 2004.

[47] P. M. Mariappan, D. R. Raghavan, S. H. Abdel Aleem, and A. F. Zobaa, "Effects of electromagnetic interference on the functional usage of medical equipment by 2G/3G/4G cellular phones: a review," *Journal of Advanced Research*, vol. 7, no. 5, pp. 727–738, 2016.

[48] H. I. Bassen, "RF interference (RFI) of medical devices by mobile communications transmitters," in *Mobile Communications Safety*, pp. 65–94, Springer US, Boston, MA, 1997.

[49] M. Iqbal-Faruque, N. Aisyah-Husni, M. Ikbal-Hossain, M. Tariqul-Islam, and N. Misran, "Effects of mobile phone radiation onto human head with variation of holding cheek and tilt positions," *Journal of Applied Research and Technology*, vol. 12, no. 5, pp. 871–876, 2014.

[50] A. Jovicic, J. Li, and T. Richardson, "Visible light communication: opportunities, challenges and the path to market," *IEEE Communications Magazine*, vol. 51, no. 12, pp. 26–32, 2013.

[51] L. Grobe, A. Paraskevopoulos, J. Hilt et al., "High-speed visible light communication systems," *IEEE Communications Magazine*, vol. 51, no. 12, pp. 60–66, 2013.

[52] R. Perez-Jimenez, J. Rufo, C. Quintana, J. Rabadan, and F. J. Lopez-Hernandez, "Visible light communication systems for passenger in-flight data networking," in *2011 IEEE International Conference on Consumer Electronics (ICCE)*, pp. 445-446, Las Vegas, NV, USA, 2011.

[53] M. Kavehrad, Z. Hajjarian, and A. Enteshari, "Energy-efficient broadband data communications using white LEDs on aircraft powerlines," in *2008 Integrated Communications, Navigation and Surveillance Conference*, pp. 1–8, Bethesda, MD, USA, 2008.

[54] F. Ahmed-Zaid, F. Bai, S. Bai et al., "Vehicle safety communications-applications (VSC-A) final report," Technical report, U.S. Department of Transportations (DOT) National Highway Traffic Safety Administration (NHTSA, 2011.

[55] World Economic Forum, "Connected world transforming travel, transportation and supply chains insight report,"

Technical report, World Economic Forum In collaboration with The Boston Consulting Group, 2013.

[56] V. Rajkumar and P. Bhattacharjee, "Risk assessment of RF radiation ignition hazard," in *2015 4th International Conference on Reliability, Infocom Technologies and Optimization (ICRITO) (Trends and Future Directions)*, pp. 1–3, Noida, India, 2015.

[57] W. D. Rawle, "Conditions for remote detonation of explosive initiators using RF energy," Technical report, Smiths Aerospace, 2005.

[58] J. Hartley, "Making safe waves in hazardous areas a wireless white paper," Technical report, Extronics Ltd, 2014.

[59] S. O. Makgetho, G. A. Mapunda, B. Basutli, A. M. Zungeru, K. Koodirile, and J. M. Chuma, "Leaky wave and slot antennas: a survey and comparison," *International Journal on Communications Antenna and Propagation (IRECAP)*, vol. 9, no. 1, p. 1, 2019.

[60] "Atrius™ IoT Retail Solutions".

[61] J. Boyd, "Fujitsu forges Li-Fi-like QR code replacement," *IEEE Spectrum*, 2014, https://spectrum.ieee.org/tech-talk/telecom/wireless/fujitsu-forges-lifilike-qr-code.

[62] "How lighting evolved over the years? - @zodhyatech - Medium," 2017.

[63] M. Crawford, "LEDs for solid-state lighting: performance challenges and recent advances," *IEEE Journal of Selected Topics in Quantum Electronics*, vol. 15, no. 4, pp. 1028–1040, 2009.

[64] S. M. Sze and K. K. Ng, *Physics of Semiconductor Devices*, John wiley & sons, New Jersey, 3 edition, 2007.

[65] E. F. Schubert, *Light-Emitting Diodes*, Cambridge University Press, Cambridge, 3rd edition, 2018.

[66] C. Kottke, J. Hilt, K. Habel, J. Vučić, and K.-D. Langer, "1.25 Gbit/s visible light WDM link based on DMT modulation of a single RGB LED luminary," in *European Conference and Exhibition on Optical Communication*, America, 2012.

[67] G. Cossu, A. M. Khalid, P. Choudhury, R. Corsini, and E. Ciaramella, "3.4 Gbit/s visible optical wireless transmission based on RGB LED," *Optics express*, vol. 20, no. 26, pp. B501–B506, 2012.

[68] S. Muthu, F. J. Schuurmans, and M. D. Pashley, "Red, green, and blue LEDs for white light illumination," *IEEE Journal of Selected Topics in Quantum Electronics*, vol. 8, no. 2, pp. 333–338, 2002.

[69] M. Bass, V. N. Mahajan, and E. W. Van Stryland, *Handbook of Optics. Volume II, Design, Fabrication and Testing, Sources and Detectors, Radiometry and Photometry*, McGraw-Hill, New York, 3rd edition, 2010.

[70] E. E. Miller, F. L. Roesler, and M. A. Thompson, *Applied Optics*, John Wiley & Sons Inc, New York, 1999.

[71] J. Kahn and J. Barry, "Wireless infrared communications," *Proceedings of the IEEE*, vol. 85, no. 2, pp. 265–298, 1997.

[72] Y. Qiu, H. H. Chen, and W. X. Meng, "Channel modeling for visible light communications-a survey," *Wireless Communications and Mobile Computing*, vol. 16, no. 14, 2034 pages, 2016.

[73] J. Barry, J. Kahn, W. Krause, E. Lee, and D. Messerschmitt, "Simulation of multipath impulse response for indoor wireless optical channels," *IEEE Journal on Selected Areas in Communications*, vol. 11, no. 3, pp. 367–379, 1993.

[74] C. C. Davis, *Lasers and electro-optics: fundamentals and engineering*, Cambridge University Press, Cambridge, 2 edition, 2013.

[75] S. Demiguel, Ning Li, Xiaowei Li et al., "Very high-responsivity evanescently coupled photodiodes integrating a short planar multimode waveguide for high-speed applications," *IEEE Photonics Technology Letters*, vol. 15, no. 12, pp. 1761–1763, 2003.

[76] K. Kato, A. Kozen, Y. Muramoto, Y. Itaya, T. Nagatsuma, and M. Yaita, "110-GHz, 50%-efficiency mushroom-mesa waveguide p-i-n photodiode for a 1.55-/spl mu/m wavelength," *IEEE Photonics Technology Letters*, vol. 6, no. 6, pp. 719–721, 1994.

[77] K. Kishino, M. Unlu, J. I. Chyi, J. Reed, L. Arsenault, and H. Morkoc, "Resonant cavity-enhanced (RCE) photodetectors," *IEEE Journal of Quantum Electronics*, vol. 27, no. 8, pp. 2025–2034, 1991.

[78] Yih-Guei Wey, K. S. Giboney, J. E. Bowers et al., "108-GHz GaInAs/InP p-i-n photodiodes with integrated bias tees and matched resistors," *IEEE Photonics Technology Letters*, vol. 5, no. 11, pp. 1310–1312, 1993.

[79] K. Kato, "Ultrawide-band/high-frequency photodetectors," *IEEE Transactions on Microwave Theory and Techniques*, vol. 47, no. 7, pp. 1265–1281, 1999.

[80] K. Kato, S. Hata, A. Kozen, J. I. Yoshida, and K. Kawano, "High-efficiency waveguide InGaAs pin photodiode with bandwidth of over 40 GHz," *IEEE Photonics Technology Letters*, vol. 3, no. 5, pp. 473-474, 1991.

[81] H. Ito, T. Furuta, S. Kodama, and T. Ishibashi, "InP/InGaAs uni-travelling-carrier photodiode with 310 GHz bandwidth," *Electronics Letters*, vol. 36, no. 21, p. 1809, 2000.

[82] K. Shiba, T. Nakata, T. Takeuchi, T. Sasaki, and K. Makita, "10 Gbit/s asymmetric waveguide APD with high sensitivity of -30 dBm," *Electronics Letters*, vol. 42, no. 20, pp. 1177-1178, 2006.

[83] G. P. Agrawal, *Fiber-optic communication systems*, Wiley, 4 ed edition, 2010.

[84] X. Li and C. Patrick Yue, "3 GHz, 1 mW inverter-based TIA with capacitive feedback for enhanced gain and sensitivity in VLC applications," *Electronics Letters*, vol. 55, no. 8, pp. 469–471, 2019.

[85] S. Fuada, A. P. Putra, Y. Aska, and T. Adiono, "Trans-impedance amplifier (HA) design for Visible Light Communication (VLC) using commercially available OP-AMP," in *2016 3rd International Conference on Information Technology, Computer, and Electrical Engineering (ICITACEE)*, pp. 31–36, Semarang, Indonesia, 2016.

[86] X. X. Wang, Z. G. Wang, J. S. Liu, and X. M. Lei, "10-Gb/s high-density trans-impedance amplifier in 0.18-mm CMOS," in *2009 International Conference on Wireless Communications & Signal Processing*, Nanjing, China, 2009.

[87] "Visible light communications consotium (VLCC)".

[88] "JEITA/JEITA Standards/AV&IT Technology Standardization/Visible Light Communications".

[89] "OMEGA - Home Gigabit Access - Communication Technology Institute".

[90] "IEEE 802.15.7-2011 - IEEE standard for local and metropolitan area networks–Part 15.7: short-range wireless optical communication using visible light," 2011.

[91] "IEEE 802.15.7-2018 - IEEE standard for local and metropolitan area networks–Part 15.7: short-range optical wireless communications - IEEE Standard," 2018.

[92] N. Chi, *LED-based visible light communications*, Signals and Communication Technology, Springer, Berlin, Heidelberg, 2018.

[93] P. Huynh and M. Yoo, "VLC-based positioning system for an indoor environment using an image sensor and an accelerometer sensor," *Sensors*, vol. 16, no. 6, 2016.

[94] B. Siddiqui, M. A. Pasha, A. Naeem, N. U. Hassan, and T. Jadoon, "LED-based visible light communication system for low data rate point-and-grab applications," in *2015 13th International Conference on Frontiers of Information Technology (FIT)*, pp. 258–263, Islamabad, Pakistan, 2015.

[95] R. Mesleh, R. Mehmood, H. Elgala, and H. Haas, "Indoor MIMO optical wireless communication using spatial modulation," in *2010 IEEE International Conference on Communications*, pp. 1–5, Cape Town, South Africa, 2010.

[96] H. Tabassum and E. Hossain, "Coverage and rate analysis for co-existing RF/VLC downlink cellular networks," *IEEE Transactions on Wireless Communications*, vol. 17, no. 4, pp. 2588–2601, 2018.

[97] R. Mesleh, H. Elgala, and H. Haas, "Optical spatial modulation," *Journal of Optical Communications and Networking*, vol. 3, no. 3, 2011.

[98] S. Rajagopal, R. Roberts, and S. K. Lim, "IEEE 802.15.7 visible light communication: modulation schemes and dimming support," *IEEE Communications Magazine*, vol. 50, no. 3, pp. 72–82, 2012.

[99] C. Medina, M. Zambrano Nuñez, M. Zambrano, and K. Navarro, "Led based visible light communication: technology, applications and challenges-a survey," *International Journal of Advances in Engineering & Technology*, vol. 8, pp. 482–495, 2015.

[100] G. J. Foschini, "Layered space-time architecture for wireless communication in a fading environment when using multi-element antennas," *Bell Labs Technical Journal*, vol. 1, no. 2, pp. 41–59, 1996.

[101] F. Gfeller and U. Bapst, "Wireless in-house data communication via diffuse infrared radiation," *Proceedings of the IEEE*, vol. 67, no. 11, pp. 1474–1486, 1979.

[102] D. J. Brady, "Multiplex sensors and the constant radiance theorem," *Optics Letters*, vol. 27, no. 1, pp. 16–18, 2002.

[103] X. Zhang, K. Cui, M. Yao, H. Zhang, and Z. Xu, "Experimental characterization of indoor visible light communication channels," in *2012 8th International Symposium on Communication Systems, Networks & Digital Signal Processing (CSNDSP)*, pp. 1–5, Poznan, Poland, 2012.

[104] J. Rufo, J. Rabadan, V. Guerra, and R. Perez-Jimenez, "BRDF models for the impulse response estimation in indoor optical wireless channels," *IEEE Photonics Technology Letters*, vol. 29, no. 17, pp. 1431–1434, 2017.

[105] A. Al-Kinani, C. X. Wang, H. Haas, and Y. Yang, "Characterization and modeling of visible light communication channels," in *2016 IEEE 83rd Vehicular Technology Conference (VTC Spring)*, pp. 1–5, Nanjing, China, 2016.

[106] A. Yesilkaya, F. Miramirkhani, E. Basar, E. Panayirci, and M. Uysal, "Performance of MIMO enhanced unipolar OFDM with realistic indoor visible light channel models," in *2016 IEEE Wireless Communications and Networking Conference*, pp. 1–6, Doha, Qatar, 2016.

[107] C. Chen, D. Basnayaka, and H. Haas, "Non-line-of-sight channel impulse response characterisation in visible light communications," in *2016 IEEE International Conference on Communications (ICC)*, pp. 1–6, Kuala Lumpur, Malaysia, 2016.

[108] I. Raza, S. Jabeen, F. Shabbir, M. Abbasi, S. Chaudhry, and S. A. Hussain, "Optical wireless channel characterization for indoor visible light communications," *Indian Journal of Science and Technology*, vol. 8, no. 22, 2015.

[109] Z. Vatansever and M. Brandt-Pearce, "Visible light positioning with diffusing lamps using an extended Kalman filter," in *2017 IEEE Wireless Communications and Networking Conference (WCNC)*, San Francisco, CA, USA, 2017.

[110] O. Gonzalez, S. Rodriguez, R. Perez-Jimenez, B. Mendoza, and A. Ayala, "Error analysis of the simulated impulse response on indoor wireless optical channels using a Monte Carlo-based ray-tracing algorithm," *IEEE Transactions on Communications*, vol. 53, no. 1, pp. 124–130, 2005.

[111] S. Arumugam and J. John, "Effect of transmitter positions on received power and bandwidth in diffuse indoor optical wireless systems," *Optical and Quantum Electronics*, vol. 39, no. 1, pp. 1–14, 2007.

[112] J. Kahn, W. Krause, and J. Carruthers, "Experimental characterization of non-directed indoor infrared channels," *IEEE Transactions on Communications*, vol. 43, no. 2/3/4, pp. 1613–1623, 1995.

[113] P. Kannan, S. M. Carroll, and J. B. Carruthers, "Propagation modelling for indoor optical wireless communications using fast multi-receiver channel estimation," *IEEE Proceedings-Optoelectronics*, vol. 150, no. 5, pp. 473–481, 2003.

[114] J. B. Carruthers and S. M. Carroll, "Statistical impulse response models for indoor optical wireless channels," *International Journal of Communication Systems*, vol. 18, no. 3, pp. 267–284, 2005.

[115] N. Hayasaka and T. Ito, "Channel modeling of nondirected wireless infrared indoor diffuse link," *Electronics and Communications in Japan (Part I: Communications)*, vol. 90, no. 6, pp. 9–19, 2007.

[116] C. R. Lomba, R. T. Valadas, and A. M. de Oliveira Duarte, "Efficient simulation of the impulse response of the indoor wireless optical channel," *International Journal of Communication Systems*, vol. 13, no. 7-8, pp. 537–549, 2000.

[117] M. Abtahi and H. Hashemi, "Simulation of indoor propagation channel at infrared frequencies in furnished office environments," in *Proceedings of 6th International Symposium on Personal, Indoor and Mobile Radio Communications*, vol. 1, pp. 306–310, Toronto, Ontario, Canada, Canada, 1995.

[118] M. Pakravan and M. Kavehrad, "Indoor wireless infrared channel characterization by measurements," *IEEE Transactions on Vehicular Technology*, vol. 50, no. 4, pp. 1053–1073, 2001.

[119] C. R. A. T. Lomba, R. T. Valadas, and A. M. Oliveira Duarte, "Propagation losses and impulse response of the indoor optical channel: a simulation package," in *Mobile Communications Advanced Systems and Components*, C. G. Günther, Ed., pp. 285–297, Springer, Berlin, Heidelberg, 1994.

[120] M. Uysal, F. Miramirkhani, T. Baykas, N. Serafimovski, and V. Jungnickel, "IEEE 802.11bb reference channel models for indoor environments," Technical report, 2018.

[121] V. Jungnickel, V. Pohl, S. Nonnig, and C. von Helmolt, "A physical model of the wireless infrared communication channel," *IEEE Journal on Selected Areas in Communications*, vol. 20, no. 3, pp. 631–640, 2002.

[122] F. J. López-Hernández, R. Pérez-Jiménez, and A. Santamaría, "Monte Carlo calculation of impulse response on diffuse IR wireless indoor channels," *Electronics Letters*, vol. 34, no. 12, pp. 1260–1262, 1998.

[123] H. Hashemi, Y. Gang, M. Kavehrad, F. Behbahani, and P. Galko, "Indoor propagation measurements at infrared frequencies for wireless local area networks applications," *IEEE Transactions on Vehicular Technology*, vol. 43, no. 3, pp. 562–576, 1994.

[124] S. Li, S.-C. Tan, C. K. Lee, E. Waffenschmidt, S. Y. Hui, and C. K. Tse, "A survey, classification, and critical review of light-emitting diode drivers," *IEEE Transactions on Power Electronics*, vol. 31, no. 2, pp. 1503–1516, 2016.

[125] Y. Qin and S. Hui, "Comparative study on the structural designs of LED devices and systems based on the general photo-electro-thermal theory," *IEEE Transactions on Power Electronics*, vol. 25, no. 2, pp. 507–513, 2010.

[126] S. Y. Hui and Y. X. Qin, "A general photo-electro-thermal theory for light emitting diode (LED) systems," *IEEE Transactions on Power Electronics*, vol. 24, no. 8, pp. 1967–1976, 2009.

[127] H. T. Chen, X. H. Tao, and S. Y. Ron Hui, "Estimation of optical power and heat-dissipation coefficient for the photo-electro-thermal theory for LED systems," *IEEE Transactions on Power Electronics*, vol. 27, no. 4, pp. 2176–2183, 2012.

[128] H. T. Chen, W. C. Choy, and S. Y. Hui, "Characterization, modeling, and analysis of organic light-emitting diodes with different structures," *IEEE Transactions on Power Electronics*, vol. 31, no. 1, pp. 581–592, 2016.

[129] A. Mirvakili and V. J. Koomson, "High efficiency LED driver design for concurrent data transmission and PWM dimming control for indoor visible light communication," in *2012 IEEE Photonics Society Summer Topical Meeting Series*, Seattle, WA, USA, 2012.

[130] M. S. Rea, *The IESNA Lighting Handbook: Reference and Application*, Illuminating Engineering Society of North America (IESNA), New York, 9 edition, 2000.

[131] K. Modepalli and L. Parsa, "Lighting up with a dual-purpose driver: a viable option for a light-emitting diode driver for visible light communication," *IEEE Industry Applications Magazine*, vol. 23, no. 2, pp. 51–61, 2017.

[132] Y.-C. Lee, J.-L. Lai, and C.-H. Yu, "The LED driver IC of visible light communication with high data rate and high efficiency," in *2016 International Symposium on VLSI Design, Automation and Test (VLSI-DAT)*, Hsinchu, Taiwan, 2016.

[133] A. V. N. Jalajakumari, D. Tsonev, K. Cameron, H. Haas, and R. Henderson, "An energy efficient high-speed digital LED driver for visible light communications," in *2015 IEEE International Conference on Communications (ICC)*, pp. 5054–5059, London, UK, 2015.

[134] A. Mirvakili and V. Joyner, "A digitally-controlled, bi-level CMOS LED driver circuit combiningPWM dimming and data transmission for visible light networks," in *2010 IEEE Globecom Workshops*, pp. 1067–1071, Miami, FL, USA, 2010.

[135] H. Elgala, R. Mesleh, and H. A. Haas, "Study of led nonlinearity effects on optical wireless transmission using OFDM," in *2009 IFIP International Conference on Wireless and Optical Communications Networks*, Cairo, Egypt, 2009.

[136] H. Chowdhury, *Data Download on the Move in Visible Light Communications: Design and Analysis [Ph.D. thesis]*, University of Oulu, 2016.

[137] S. H. Lee, S. Y. Jung, and J. K. Kwon, "Modulation and coding for dimmable visible light communication," *IEEE Communications Magazine*, vol. 53, no. 2, pp. 136–143, 2015.

[138] S. Park, D. K. Jung, H. S. Shin et al., "Information broadcasting system based on visible light signboard," in *7th, IASTED international conference on wireless and optical communications*, pp. 311–313, Montreal, Canada, 2007.

[139] J. Grubor, S. Lee, K. D. Langer, A. Koonen, and J. Walewski, "Wireless high-speed data transmission with phosphorescent white-light LEDs," in *33rd European Conference and Exhibition of Optical Communication-Post-Deadline Papers (published 2008)*, pp. 1-2, Berlin, Germany, 2007.

[140] H. le Minh, D. O'Brien, G. Faulkner et al., "High-speed visible light communications using multiple-resonant equalization," *IEEE Photonics Technology Letters*, vol. 20, no. 14, pp. 1243–1245, 2008.

[141] J. Vucic, C. Kottke, S. Nerreter et al., "125 Mbit/s over 5 m wireless distance by use of OOK-modulated phosphorescent white LEDs," in *2009 35th European Conference on Optical Communication*, pp. 1-2, Vienna, Austria, 2009.

[142] J. Vucic, C. Kottke, S. Nerreter et al., "230 Mbit/s via a wireless visible-light link based on OOK modulation of phosphorescent white LEDs," in *Optical Fiber Communication Conference*, pp. 1–3, San Diego, CA, USA, 2010.

[143] N. Fujimoto and H. Mochizuki, "477 Mbit/s visible light transmission based on OOK-NRZ modulation using a single commercially available visible LED and a practical LED driver with a pre-emphasis circuit," in *Optical Fiber Communication Conference/National Fiber Optic Engineers Conference 2013*, pp. 1–3, Anaheim, CA, USA, 2013.

[144] N. Fujimoto and H. Mochizuki, "614 Mbit/s OOK-based transmission by the duobinary technique using a single commercially available visible LED for high-speed visible light communications," in *European Conference and Exhibition on Optical Communication*, pp. 1–3, Amsterdam, Netherlands, 2012.

[145] H. Li, X. Chen, B. Huang, D. Tang, and H. Chen, "High bandwidth visible light communications based on a post-equalization circuit," *IEEE Photonics Technology Letters*, vol. 26, no. 2, pp. 119–122, 2014.

[146] H. Li, X. Chen, J. Guo, and H. Chen, "A 550 Mbit/s real-time visible light communication system based on phosphorescent white light LED for practical high-speed low-complexity application," *Optics Express*, vol. 22, no. 22, pp. 27203–27213, 2014.

[147] P. A. Haigh, Z. Ghassemlooy, S. Rajbhandari, and I. Papakonstantinou, "Visible light communications using organic light emitting diodes," *IEEE Communications Magazine*, vol. 51, no. 8, pp. 148–154, 2013.

[148] S. Zhang, S. Watson, J. J. D. McKendry et al., "1.5 Gbit/s multi-channel visible light communications using CMOS-controlled GaN-based LEDs," *Journal of lightwave technology*, vol. 31, no. 8, pp. 1211–1216, 2013.

[149] C. H. Yeh, C. W. Chow, and L. Y. Wei, "1250 Mbit/s OOK wireless white-light VLC transmission based on phosphor laser diode," *IEEE Photonics Journal*, vol. 11, no. 3, pp. 1–5, 2019.

[150] S. Zhao, J. Xu, and O. Trescases, "A dimmable LED driver for visible light communication (VLC) based on LLC resonant DC-DC converter operating in burst mode," in *2013 Twenty-Eighth Annual IEEE Applied Power Electronics Conference and Exposition (APEC)*, Long Beach, CA, USA, 2013.

[151] K. Modepalli and L. Parsa, "Dual purpose HB-LED driver for illumination and visible light communication," in *2013 Twenty-Eighth Annual IEEE Applied Power Electronics*

Conference and Exposition (APEC), pp. 875–880, Long Beach, CA, USA, 2013.

[152] K. Lee and H. Park, "Modulations for visible light communications with dimming control," *IEEE photonics technology letters*, vol. 23, no. 16, pp. 1136–1138, 2011.

[153] CIE, "International Commission on Illumination, Colorimetry-Part 3: CIE Tristimulus Values, ISO 11664-3 : 2012(E)/CIE S014-3/E:2011," 1931.

[154] E. Monteiro and S. Hranilovic, "Design and implementation of color-shift keying for visible light communications," *Journal of Lightwave Technology*, vol. 32, no. 10, pp. 2053–2060, 2014.

[155] X. Liang, M. Yuan, J. Wang, Z. Ding, M. Jiang, and C. Zhao, "Constellation design enhancement for color-shift keying modulation of quadrichromatic LEDs in visible light communications," *Journal of Lightwave Technology*, vol. 35, no. 17, pp. 3650–3663, 2017.

[156] R. Singh, T. OFarrell, and J. P. David, "An enhanced color shift keying modulation scheme for high-speed wireless visible light communications," *Journal of Lightwave Technology*, vol. 32, no. 14, pp. 2582–2592, 2014.

[157] C. Zhu, Y. Huo, J. Jiang et al., "Hierarchical colour-shift-keying aided layered video streaming for the visible light downlink," *IEEE Access*, vol. 4, pp. 3127–3152, 2016.

[158] J. Luna-Rivera, R. Perez-Jimenez, J. Rabadan-Borjes, J. Rufo-Torres, V. Guerra, and C. Suarez-Rodriguez, "Multiuser CSK scheme for indoor visible light communications," *Optics express*, vol. 22, no. 20, article 24256, 2014.

[159] J. Jiang, R. Zhang, and L. Hanzo, "Analysis and design of three-stage concatenated color-shift keying," *IEEE Transactions on Vehicular Technology*, vol. 64, no. 11, pp. 5126–5136, 2015.

[160] J. Armstrong, "OFDM for optical communications," *Journal of lightwave technology*, vol. 27, no. 3, pp. 189–204, 2009.

[161] J. Dang, L. Wu, and Z. Zhang, "OFDM systems for optical communication with intensity modulation and direct detection," in *Optical fiber and wireless communications*, vol. 5, pp. 85–103, Intech Open, 2017.

[162] J. Armstrong and B. J. Schmidt, "Comparison of asymmetrically clipped optical OFDM and DC-biased optical OFDM in AWGN," *IEEE Communications Letters*, vol. 12, no. 5, pp. 343–345, 2008.

[163] D. Tsonev, S. Sinanovic, and H. Haas, "Novel unipolar orthogonal frequency division multiplexing (U-OFDM) for optical wireless," in *2012 IEEE 75th Vehicular Technology Conference (VTC Spring)*, Yokohama, Japan, 2012.

[164] M. Z. Afgani, H. Haas, H. Elgala, and D. Knipp, "Visible light communication using OFDM," in *2nd International Conference on Testbeds and Research Infrastructures for the Development of Networks and Communities, 2006. TRIDENTCOM 2006*, vol. 2006, pp. 129–134, Barcelona, Spain, 2006.

[165] H. Elgala, R. Mesleh, H. Haas, and B. Pricope, "OFDM visible light wireless communication based on white LEDs," in *2007 IEEE 65th Vehicular Technology Conference - VTC2007-Spring*, pp. 2185–2189, Dublin, Ireland, 2007.

[166] S. Dimitrov, S. Sinanovic, and H. Haas, "Clipping noise in OFDM-based optical wireless communication systems," *IEEE Transactions on Communication*, vol. 60, no. 4, pp. 1072–1081, 2012.

[167] H. Zhang, Y. Yuan, and W. Xu, "PAPR reduction for DCO-OFDM visible light communications via semidefinite relaxation," *IEEE Photonics Technology Letters*, vol. 26, no. 17, pp. 1718–1721, 2014.

[168] M. S. Mossaad and S. Hranilovic, "Practical OFDM signalling for visible light communications using spatial summation," in *2014 27th Biennial Symposium on Communications (QBSC)*, pp. 5–9, Kingston, ON, Canada, 2014.

[169] F. Yang and J. Gao, "Dimming control scheme with high power and spectrum efficiency for visible light communications," *IEEE Photonics Journal*, vol. 9, no. 6, pp. 1–12, 2017.

[170] Q. Wang, Z. Wang, and L. Dai, "Asymmetrical hybrid optical OFDM for visible light communications with dimming control," *IEEE Photonics Technology Letters*, vol. 27, no. 9, pp. 974–977, 2015.

[171] J. R. D. Retamal, H. M. Oubei, B. Janjua et al., "4-Gbit/s visible light communication link based on 16-QAM OFDM transmission over remote phosphor-film converted white light by using blue laser diode," *Optics express*, vol. 23, no. 26, pp. 33656–33666, 2015.

[172] D. Tsonev, H. Chun, S. Rajbhandari et al., "A 3-Gb/s single-LED OFDM-based wireless VLC link using a gallium nitride μLED," *IEEE Photonics Technology Letters*, vol. 26, no. 7, pp. 637–640, 2014.

[173] Y. Wang, Y. Wang, and N. Chi, "Experimental verification of performance improvement for a gigabit wavelength division multiplexing visible light communication system utilizing asymmetrically clipped optical orthogonal frequency division multiplexing," *Photonics Research*, vol. 2, no. 5, pp. 138–142, 2014.

[174] E. Xie, X. He, M. S. Islim et al., "High-speed visible light communication based on a III-nitride series-biased micro-LED array," *Journal of Lightwave Technology*, vol. 37, no. 4, pp. 1180–1186, 2019.

[175] M. D. Mohamed and S. Hranilovic, "Spatial multiplexing and diversity techniques for multiple-element optical wireless links," in *2009 Conference Record of the Forty-Third Asilomar Conference on Signals, Systems and Computers*, pp. 1626–1630, Pacific Grove, CA, USA, 2009.

[176] Y.-Y. Zhang, H.-Y. Yu, J.-K. Zhang, Y.-J. Zhu, J.-L. Wang, and T. Wang, "Full large-scale diversity space codes for MIMO optical wireless communications," in *2015 IEEE International Symposium on Information Theory (ISIT)*, vol. 2015, pp. 1671–1675, Hong Kong, China, 2015.

[177] T. Komine and M. Nakagawa, "Fundamental analysis for visible-light communication system using LED lights," *IEEE Transactions on Consumer Electronics*, vol. 50, no. 1, pp. 100–107, 2004.

[178] J. M. Kahn, R. You, P. Djahani, A. G. Weisbin, Beh Kian Teik, and A. Tang, "Imaging diversity receivers for high-speed infrared wireless communication," *IEEE Communications Magazine*, vol. 36, no. 12, pp. 88–94, 1998.

[179] J. Vucic, C. Kottke, S. Nerreter, K. D. Langer, and J. W. Walewski, "513 Mbit/s visible light communications link based on DMT-modulation of a white LED," *Journal of Lightwave Technology*, vol. 28, no. 24, pp. 3512–3518, 2010.

[180] H. G. Olanrewaju, F. B. Ogunkoya, and W. O. Popoola, "Spatial modulation – a low complexity modulation technique for visible light communications," in *Visible Light Communications*, vol. 1, pp. 1–22, IntechOpen, 2017.

[181] P. Saengudomlert, "Transmit beamforming for line-of-sight MIMO VLC with IM/DD under illumination constraints," in *2015 12th International Conference on Electrical Engineering/Electronics, Computer, Telecommunications and*

Information Technology (ECTI-CON), pp. 1–4, Hua Hin, Thailand, 2015.

[182] L. Zeng, D. O'Brien, H. Le Minh et al., "High data rate multiple input multiple output (MIMO) optical wireless communications using white LED lighting," *IEEE Journal on Selected Areas in Communications*, vol. 27, no. 9, pp. 1654–1662, 2009.

[183] A. H. Azhar, T. A. Tran, and D. O'Brien, "A gigabit/s indoor wireless transmission using MIMO-OFDM visible-light communications," *IEEE Photonics Technology Letters*, vol. 25, no. 2, pp. 171–174, 2013.

[184] T. Fath and H. Haas, "Performance comparison of MIMO techniques for optical wireless communications in indoor environments," *IEEE Transactions on Communications*, vol. 61, no. 2, pp. 733–742, 2013.

[185] Y.-J. Zhu, W.-F. Liang, J.-K. Zhang, and Y.-Y. Zhang, "Space-collaborative constellation designs for MIMO indoor visible light communications," *IEEE Photonics Technology Letters*, vol. 27, no. 15, pp. 1667–1670, 2015.

[186] A. Khalid, H. M. Asif, S. Mumtaz, S. Al Otaibi, and K. Konstantin, "Design of MIMO-visible light communication transceiver using maximum rank distance codes," *IEEE Access*, vol. 7, pp. 89128–89140, 2019.

[187] Y. A. Chau and S. H. Yu, "Space modulation on wireless fading channels," in *IEEE 54th Vehicular Technology Conference. VTC Fall 2001. Proceedings (Cat. No.01CH37211)*, vol. 3, pp. 1668–1671, Atlantic City, NJ, USA, USA, 2001.

[188] T. Fath, M. Di Renzo, and H. Haas, "On the performance of space shift keying for optical wireless communications," in *2010 IEEE Globecom Workshops*, pp. 990–994, Miami, FL, USA, 2010.

[189] M. D. Renzo and H. Haas, "Space shift keying (SSK) MIMO over correlated rician fading channels: performance analysis and a new method for transmit-diversity," *IEEE Transactions on Communications*, vol. 59, no. 1, pp. 116–129, 2011.

[190] N. Ishikawa and S. Sugiura, "Maximizing constrained capacity of power-imbalanced optical wireless MIMO communications using spatial modulation," *Journal of Lightwave Technology*, vol. 33, no. 2, pp. 519–527, 2015.

[191] M. di Renzo and H. Haas, "Space shift keying (SSK) modulation with partial channel state information: optimal detector and performance analysis over fading channels," *IEEE Transactions on Communications*, vol. 58, no. 11, pp. 3196–3210, 2010.

[192] S. P. Alaka, T. L. Narasimhan, and A. Chockalingam, "Generalized spatial modulation in indoor wireless visible light communication," in *2015 IEEE Global Communications Conference (GLOBECOM)*, pp. 1–7, San Diego, CA, USA, 2015.

[193] J. Dang and Z. Zhang, "Comparison of optical OFDM-IDMA and optical OFDMA for uplink visible light communications," in *2012 International Conference on Wireless Communications and Signal Processing (WCSP)*, Huangshan, China, 2012.

[194] B. Lin, X. Tang, Z. Ghassemlooy, C. Lin, and Y. Li, "Experimental demonstration of an indoor VLC positioning system based on OFDMA," *IEEE Photonics Journal*, vol. 9, no. 2, pp. 1–9, 2017.

[195] C. Chen, D. Tsonev, and H. Haas, "Joint transmission in indoor visible light communication downlink cellular networks," in *2013 IEEE Globecom Workshops (GC Wkshps)*, pp. 1127–1132, Atlanta, GA, USA, 2013.

[196] J. Y. Sung, C. H. Yeh, C. W. Chow, W. F. Lin, and Y. Liu, "Orthogonal frequency-division multiplexing access (OFDMA) based wireless visible light communication (VLC) system," *Optics Communications*, vol. 355, pp. 261–268, 2015.

[197] V. V. Mai, T. C. Thang, and A. T. Pham, "CSMA/CA-based uplink MAC protocol design and analysis for hybrid VLC/Wifi networks," in *2017 IEEE International Conference on Communications Workshops (ICC Workshops)*, pp. 457–462, Paris, France, 2017.

[198] V. V. Huynh and Y. M. Jang, "Fairness CSMA/CA MAC protocol for VLC networks," *International journal of advanced smart convergence*, vol. 1, no. 1, pp. 14–18, 2012.

[199] M. E. Marhic, "Coherent optical CDMA networks," *Journal of Lightwave Technology*, vol. 11, no. 5/6, pp. 854–864, 1993.

[200] H. Ghafouri-Shiraz and M. M. Karbassian, "Optical CDMA networks principles," in *Analysis and Applications*, John Wiley & Sons, 2012.

[201] T. C. Schenk, L. Feri, H. Yang, and J. P. M. Linnartz, "Optical wireless CDMA employing solid state lighting LEDs," in *2009 IEEE/LEOS Summer Topical Meeting*, pp. 23-24, Newport Beach, CA, USA, 2009.

[202] A. Stok and E. H. Sargent, "The role of optical CDMA in access networks," *IEEE Communications Magazine*, vol. 40, no. 9, pp. 83–87, 2002.

[203] M. M. Karbassian and F. Kueppers, "Synchronous optical CDMA networks capacity increase using transposed modified prime codes," *Journal of Lightwave Technology*, vol. 28, no. 17, pp. 2603–2610, 2010.

[204] K. Cui, *Physical Layer Characteristics and Techniques for Visible Light Communications [Ph.D thesis]*, University of California Riverside, 2012.

[205] S. A. Khan and J. Bajcsy, "Chip-asynchronous binary optical CDMA: an optimum signaling scheme for random delays," *IEEE Photonics Journal*, vol. 5, no. 2, 2013.

[206] J. Liu, Z. Pan, W. Noonpakdee, and S. Shimamoto, "Impact of light reflection on indoor wireless optical CDMA systems," *Journal of Optical Communications and Networking*, vol. 4, no. 12, pp. 989–996, 2012.

[207] A. Duque, R. Stanica, H. Rivano, and A. Desportes, "Unleashing the power of LED-to-camera communications for IoT devices," in *Proceedings of the 3rd Workshop on Visible Light Communication Systems - VLCS '16*, pp. 55–60, New York City, New York, 2016.

[208] S. Schmid, L. Arquint, and T. R. Gross, "Using smartphones as continuous receivers in a visible light communication system," in *Proceedings of the 3rd Workshop on Visible Light Communication Systems - VLCS '16*, pp. 61–66, New York City, New York, 2016.

[209] N. Rajagopal, P. Lazik, and A. Rowe, "Hybrid visible light communication for cameras and low-power embedded devices," in *Proceedings of the 1st ACM MobiCom workshop on Visible light communication systems - VLCS '14*, pp. 33–38, Maui, Hawaii, USA, 2014.

[210] M. Haus, A. Y. Ding, and J. Ott, "LocalVLC: augmenting smart IoT services with practical visible light communication," in *2019 IEEE 20th International Symposium on "A World of Wireless, Mobile and Multimedia Networks" (WoWMoM)*, Washington, DC, USA, USA, 2019.

[211] Y. Zhang, L. Wang, K. Wang, K. S. Wong, and K. Wu, "Recent advances in the hardware of visible light communication," *IEEE Access*, vol. 7, pp. 91093–91104, 2019.

[212] T. Kawanishi, "THz and photonic seamless communications," *Journal of Lightwave Technology*, vol. 37, no. 7, pp. 1671–1679, 2019.

[213] M. Katz, P. Pirinen, and H. Posti, "Towards 6G: getting ready for the next decade," in *2019 16th International Symposium on Wireless Communication Systems (ISWCS)*, vol. 2019, pp. 714–718, Oulu, Finland, Finland, 2019-Augus.

[214] T. Huang, W. Yang, J. Wu, J. Ma, X. Zhang, and D. Zhang, "A survey on green 6G network: architecture and technologies," *IEEE Access*, vol. 7, pp. 175758–175768, 2019.

[215] S. Zhang, Q. Wu, S. Xu, and G. Y. Li, "Fundamental green tradeoffs: progresses, challenges, and impacts on 5G networks," *IEEE Communications Surveys & Tutorials*, vol. 19, no. 1, pp. 33–56, 2017.

[216] Y. Zikria, S. Kim, M. Afzal, H. Wang, and M. Rehmani, "5G mobile services and scenarios: challenges and solutions," *Sustainability*, vol. 10, no. 10, article 3626, 2018.

[217] F. Cirillo, F. J. Wu, G. Solmaz, and E. Kovacs, "Embracing the future internet of things," *Sensors*, vol. 19, no. 2, 2019.

[218] S. Redana and Ö. Bulakci, "5GPPP architecture working group view on 5G architecture," in *The 5G Infrastructure Public Private Partnership*, Technical report, 2017.

[219] L. Wan, Z. Guo, Y. Wu et al., "4G/5G spectrum sharing: efficient 5G deployment to serve enhanced mobile broadband and internet of things applications," *IEEE Vehicular Technology Magazine*, vol. 13, no. 4, pp. 28–39, 2018.

[220] M. Shafi, A. F. Molisch, P. J. Smith et al., "5G: a tutorial overview of standards, trials, challenges, deployment, and practice," *IEEE Journal on Selected Areas in Communications*, vol. 35, no. 6, pp. 1201–1221, 2017.

[221] S. Dang, O. Amin, B. Shihada, and M. S. Alouini, "What should 6G be?," *Nature Electronics*, vol. 3, no. 1, pp. 20–29, 2020.

[222] L. Feng, R. Q. Hu, J. Wang, P. Xu, and Y. Qian, "Applying VLC in 5G networks: architectures and key technologies," *IEEE Network*, vol. 30, no. 6, pp. 77–83, 2016.

[223] M. Z. Chowdhury, M. Shahjalal, M. K. Hasan, and Y. M. Jang, "The role of optical wireless communication technologies in 5G/6G and IoT solutions: prospects, directions, and challenges," *Applied Sciences*, vol. 9, no. 20, article 4367, 2019.

[224] M. Katz, M. Matinmikko-Blue, and M. Latva-Aho, "6Genesis flagship program: building the bridges towards 6G-enabled wireless smart society and ecosystem," in *2018 IEEE 10th Latin-American Conference on Communications (LATINCOM)*, Guadalajara, Mexico, 2018.

[225] S. Y. Jung, S. R. Lee, and C. S. Park, "Indoor location awareness based on received signal strength ratio and time division multiplexing using light-emitting diode light," *Optical Engineering*, vol. 53, no. 1, article 016106, 2014.

[226] S. Hann, J. H. Kim, S. Y. Jung, and C. S. Park, "White LED ceiling lights positioning systems for optical wireless indoor applications," in *36th European Conference and Exhibition on Optical Communication*, pp. 1-2, Torino, Italy, 2010.

[227] K. Gligoric, M. Ajmani, D. Vukobratovic, and S. Sinanovic, "Visible light communications-based indoor positioning via compressed sensing," *IEEE Communications Letters*, vol. 22, no. 7, pp. 1410–1413, 2018.

[228] M. Giordani, M. Polese, M. Mezzavilla, S. Rangan, and M. Zorzi, "Towards 6G networks: use cases and technologies," 2019, https://arxiv.org/abs/1903.12216.

[229] L. Ceriani and P. Verme, "The origins of the Gini index: extracts from Variabilità e Mutabilità (1912) by Corrado Gini," *The Journal of Economic Inequality*, vol. 10, no. 3, pp. 421–443, 2012.

[230] M. O. Lorenz, "Methods of measuring the concentration of wealth," *Publications of the American Statistical Association*, vol. 9, no. 70, 1905.

[231] T. S. Rappaport, Y. Xing, O. Kanhere et al., "Wireless communications and applications above 100 GHz: opportunities and challenges for 6G and beyond," *IEEE Access*, vol. 7, pp. 78729–78757, 2019.

[232] M. Haenggi, J. G. Andrews, F. Baccelli, O. Dousse, and M. Franceschetti, "Stochastic geometry and random graphs for the analysis and design of wireless networks," *IEEE Journal on Selected Areas in Communications*, vol. 27, no. 7, pp. 1029–1046, 2009.

[233] Q. U. A. Nadeem, A. Kammoun, and M. S. Alouini, "Elevation beamforming with full dimension MIMO architectures in 5G systems: a tutorial," *IEEE Communications Surveys & Tutorials*, vol. 21, no. 4, pp. 3238–3273, 2019.

[234] Q. Wu and R. Zhang, "Intelligent reflecting surface enhanced wireless network via joint active and passive beamforming," *IEEE Transactions on Wireless Communications*, vol. 18, no. 11, pp. 5394–5409, 2019.

[235] E. Basar, M. Di Renzo, J. De Rosny, M. Debbah, M. S. Alouini, and R. Zhang, "Wireless communications through reconfigurable intelligent surfaces," *IEEE Access*, vol. 7, pp. 116753–116773, 2019.

[236] Q. Wu and R. Zhang, "Towards smart and reconfigurable environment: intelligent reflecting surface aided wireless network," *IEEE Communications Magazine*, vol. 58, no. 1, pp. 106–112, 2020.

[237] S. Li, B. Duo, X. Yuan, Y. C. Liang, and M. Di Renzo, "Reconfigurable intelligent surface assisted UAV communication: joint trajectory design and passive beamforming," *IEEE Wireless Communications Letters*, vol. 9, no. 5, pp. 716–720, 2020.

[238] J. Gao, C. Zhong, X. Chen, H. Lin, and Z. Zhang, "Unsupervised learning for passive beamforming," *IEEE Communications Letters*, vol. 24, no. 5, pp. 1052–1056, 2020.

[239] S. Nie, J. M. Jornet, and I. F. Akyildiz, "Intelligent environments based on ultra-massive Mimo platforms for wireless communication in millimeter wave and terahertz bands," in *ICASSP 2019 - 2019 IEEE International Conference on Acoustics, Speech and Signal Processing (ICASSP)*, pp. 7849–7853, Brighton, United Kingdom, United Kingdom, 2019-May.

[240] S. Hu, F. Rusek, and O. Edfors, "Beyond massive MIMO: the potential of data transmission with large intelligent surfaces," *IEEE Transactions on Signal Processing*, vol. 66, no. 10, pp. 2746–2758, 2018.

[241] X. Tan, Z. Sun, J. M. Jornet, and D. Pados, "Increasing indoor spectrum sharing capacity using smart reflect-array," in *2016 IEEE International Conference on Communications (ICC)*, Kuala Lumpur, Malaysia, 2016.

[242] L. Subrt and P. Pechac, "Intelligent walls as autonomous parts of smart indoor environments," *IET Communications*, vol. 6, no. 8, pp. 1004–1010, 2012.